Biodegradable Hyperbranched Polyglycerol Copolymers as Responsive Drug Delivery Systems

Inaugural-Dissertation

to obtain the academic degree

Doctor rerum naturalium (Dr. rer. nat.)

submitted to

the Department of Biology, Chemistry, Pharmacy

of Freie Universität Berlin

by

Mariam Cherri

From Beirut, Lebanon

Berlin 2024

This doctoral dissertation was completed under the supervision of Prof. Dr. Rainer Haag at the Institute of Chemistry and Biochemistry, Freie Universität Berlin, from June 2020 to February 2024.

1. Reviewer: Prof. Dr. Rainer Haag, Freie Universität Berlin

2. Reviewer: Prof. Dr. Marie Weinhart, Freie Universität Berlin, Leibniz Universität Hannover

Date of defense: 30.05.2024

Declaration of independence

Herewith I certify that I have prepared and written my thesis independently and that I have not used any sources and aids other than those indicated by me. This dissertation has not yet been presented to any other examination authority in the same or a similar form and has not yet been published.

Berlin, April 2024 ---(Mariam Cherri)

Acknowledgments

I would love to first thank Prof. Dr. Rainer Haag for providing me with a safe space, time, and knowledge that allowed me to carry on with this journey. The core of his supervision was the trust and the deconstruction of the "management" concept as we are used to it. He gave me the space to be creative, take my own decisions and come up with new ideas, while being a great inspiration and had the right advice and solution whenever I looked for it. Thank you for the care and support.

Second, I would like to thank my second supervisor Prof. Dr. Marie Weinhart for being the inspiration for me to continue in this field since I joined the Macromolecular Chemistry, she taught more than four years ago. Thank you for all the shared knowledge, I aspire to you on so many different aspects.

I am certainly very grateful to Dr. Ehsan Mohammadifar, who was my direct supervisor since I conducted my master thesis project. I learned a lot from you, whether in lab practice, theory, critical thinking and how to address problem solving. You were the most help, and nothing could have been achieved without your support. I also found a brother in you, someone who understands where I come from, my sense of humor and is there for me whenever I needed him. I found harmony and comprehension in the way we worked together that only lead to great accomplishment.

The thesis projects would not have made it without my two students Fernanda Romero and Paraskevi Stergiou that worked intensely on the projects as if they were their own. It brings so much joy to my heart to watch you work and grow and become better at what you do every single day, you make me very proud. You only made this journey more wholesome for me especially that our relationship developed way beyond our shared work and will stay with me forever. Thank you for the love, shared meals, shared struggles, hugs and laughter for you and the friendships I developed during these years especially with Obida Bawadkji, Andrea Cosimi, Taylor Page, Dr. Olaf Wagner, Dr. Vahid Ahmadi, Dr. Abhishek Singh, Guoxin Ma and Peng Tang.

Thank you to everyone I collaborated with on projects whether at Freie Universität within different departments: Dr. Michael Schirner, Dr. Fatemeh Zabihi, Luca Steiner, Prof. Dr. Beate Paulus, Dr. Fabian Schumacher and Prof. Dr. Wolfgang Bäumer or at Charité: Maren Witt, Prof. Dr. Kerstin Danker and Prof. Dr. Henrik Dommisch. It was such an enriching experience to gather all this diverse knowledge to bring projects to life.

Thanks to Dr. Wiebke Fisher for always being there to give me support and encouragement and to comfort any doubt and uncertainty I was having; you have no idea how

To the liberation of people
& the occupied land

Table of content

1 Introduction

1.1 Challenges in Drug Delivery

Early chemotherapy which can be practically viewed as dye therapy, since the first promising chemotherapeutical experiments used dyes like methylene blue and trypan red aid the foundational groundwork for Paul Ehrlich's theory.[1, 2] This theory posited that the biological efficacy of chemical compounds is intrinsically linked to their molecular structure and the histological and cell structures, hence a specific biological targets they interact with.[1-3] In the second stage of his research, Ehrlich conceptualized about the existence of receptors that are associated with the cells or distributed more abundantly in the blood stream and are responsible for the interaction with antigens or toxins.[4] Later, his immunological theory was further shifted from interactions with antigens to binding to drugs that will differ in structures and legends.[5, 6] Eventually and in 1910, the magic bullet concept was born. The theory of drugs that go straight to their intended cell-structural targets efficaciously attacking pathogens but remaining harmless to healthy tissues which will reduce the possibility of side-effects in patients. His scientific revolution was based on the postulate "we have to learn how to aim chemically". Ehrlich hypothesized that the essence of synthetic chemistry lay in the modification of a primary substance through diverse chemical processes, followed by an evaluation of the resultant compounds for their therapeutic efficacy.[7-9]

It has been more than a century since Paul Ehrlich conceptualized the "Magic Bullet"[9] and still the primary obstacles in pharmacological delivery have persisted, specifically: (i) regulating the elimination of drugs from the bloodstream, (ii) enhancing the solubility of compounds with limited water solubility, and (iii) achieving precise targeting of specific biological tissues. Although numerous artificial delivery mechanisms have successfully addressed the first two challenges and have been integrated into clinical settings, a synthetic drug delivery system (DDS) that address all three challenges has yet to be commercialized.

1.1.1 The Challenge of Drug Solubilization: Classic polymer solubilizers

Other than targetability, the solubilization of poorly water-soluble drugs remains a paramount challenge, dictating the success of therapeutic efficacy and patient compliance. The advent of polymer solubilizers such as Cremophor-EL, Tween-80 and Tween-20 (Structures in Figure 1) has been pivotal in revolutionizing DDSs.[10, 11] These agents, through their unique physicochemical properties, have significantly enhanced the solubility, stability, and bioavailability of a broad spectrum of pharmacological compounds. Cremophor-EL, a non-ionic surfactant derived from castor oil, is renowned for its efficacy in solubilizing hydrophobic drugs, especially in oncological therapies.[12, 13] Similarly, Tween-80 and Tween-20, members of

the polysorbate family, have garnered widespread use due to their safety, biocompatibility, and versatility in various formulations, ranging from oral to parenteral administration. These surfactants, by reducing surface tension, facilitate the formation of micelles, encapsulating the hydrophobic drug molecules and enhancing their aqueous solubility.[14-16] Despite these advantages, the use of these solubilizers is not without limitations. Cremophor-EL has been associated with hypersensitivity reactions and alterations in drug pharmacokinetics.[12, 13] Tween-80 and Tween-20, while generally considered safe, are susceptible to oxidative degradation and may interact with certain proteins, potentially affecting the stability and activity of biologic drugs. [14-16] Given that biocompatibility is a critical determinant of the success or failure of these systems *in vivo*, it is imperative to thoroughly examine the factors that confer biocompatibility.
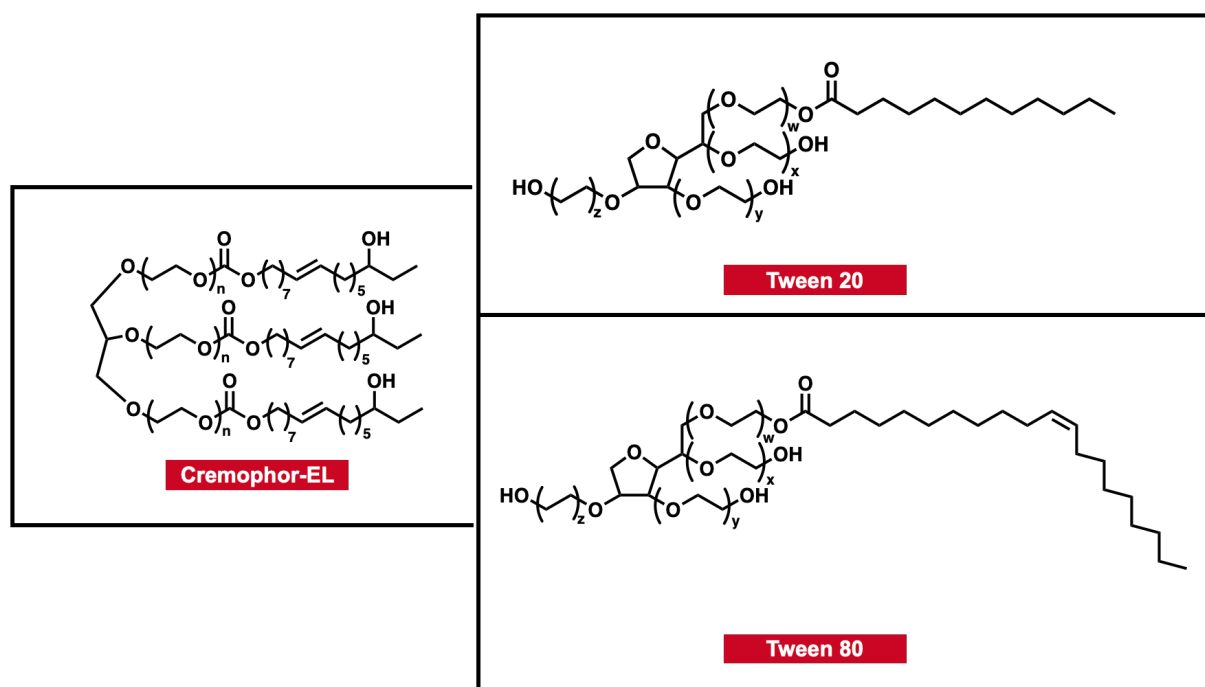
Figure 1. The classic polymer solubilizers: Cremophor-EL, Tween 20, and Tween 80.

1.2 Biophysicochemical Interactions at Nano-Bio-Interfaces

To achieve a compatible design of biomaterials with biological systems the understanding of the biophysicochemical interactions at the interface between the biomaterials and the biological entities at the nano-level is crucial. This will demand the identifications of the main forces that governs the interactions at the interface to further identify the factors that makes a biomaterial compatible *in vivo*.

1.2.1 The interfacial interactions between nanomaterials and biological systems

The forces that embody the interactions of nanoparticles and cells are mainly: Van der Waals (VDW), electrostatic, solvation, solvophobic and depletion (Figure 2, Table 1).[17-20] The

VDW force of interaction is highly dependent on the positioning of the surface atoms and their standard bulk permittivity functions for which its complexity increases on the interface between nanomaterials and biological systems.[19] Another consideration is the ionic strength that is often about 150 mM in biological fluids. This will result in the screening of electrostatic interactions within few nanometers of the surface. The elevated ionic strength effectively diminishes the contribution of VDW forces at zero frequency, while the dispersion interactions at higher frequencies continue to be influential. Additionally, the process of solvation emerges as a critical factor, particularly for inorganic and other hydrophilic nanoparticles, water molecules, are capable of adhering to particle surfaces, possessing adequate energy, thereby forming steric barrier layers. These layers act as physical impediments, obstructing proximity and interaction between adjacent particles and thereby hindering their contact or adhesion. Therefore, particle stability is augmented by solvation forces through mechanisms termed 'hydration pressure' or 'hydrophilic repulsion'. In instances where the relative affinity of two interacting surfaces for water molecules is significantly lower compared to the affinity amongst the water molecules themselves, rapid dehydration and aggregation ensue. This phenomenon is known as 'hydrophobic attraction' or the 'hydrophobic effect'.[19]
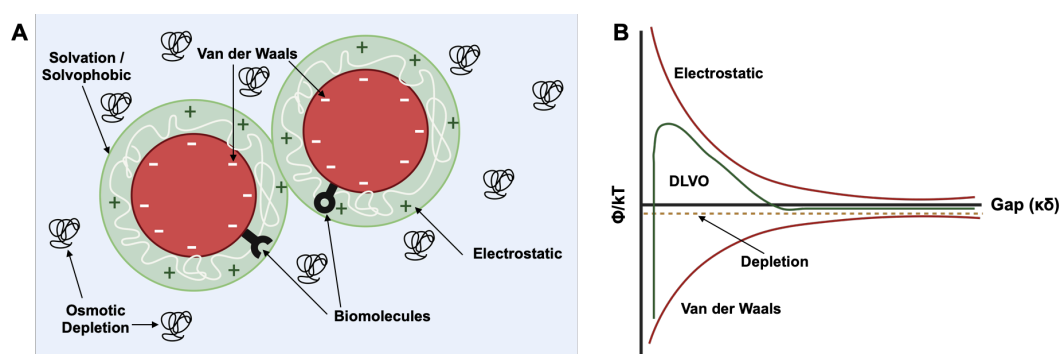
Figure 2. A) Traditional forces for colloidal fabrication (electrostatic and VDW) and other important interactions (solvation, solvophobic, biomolecular and depletion) that occur when particles are suspended in biological media or encounter cells. B) VDW and depletion forces are attractive whereas the electrostatic forces are repulsive over a typical length scale. The DLVO theory[21-23] defines the stabilization mechanism of colloidal dispersions through the interplay between van der Waals and electrostatic forces, in contrast to the steric repulsions induced by polymeric solubilizers. This theory, formulated in the 1940s by Derjaguin and Landau[24], as well as by Verwey and Overbeek[25], highlights the crucial role of two interactions in determining the stability of colloidal systems: attractive van der Waals forces between colloidal particles and repulsive electrostatic Coulomb interactions. The DLVO theory in colloid science considers the sum of these forces. Φ, interaction potential; k, Boltzmann

constant; T, absolute temperature; κ, inverse Debye length and δ, separation distance. Reproduced with permission from ref. [20].

Although the mentioned forces are still valid when particle approaches a surface membrane, other differences can rise.[20] This is due to the nature of the cell membrane that is non-rigid and can deform because of its fluidity and thermodynamics bringing new layers of complexity. Second complexity is the patchiness of the cell surface, charges can be non-uniform and will alter the energy of interparticle interactions. A third layer of complexity emerges from the active nature of cells. Through ion transport or secretion of proteins and other biomolecules, cells alter the surface properties of particles, thereby transforming them into entities vastly different from their original form in the system. This process introduces the notion of a time-dependent, dynamic interface.[26, 27] Additionally, the potential for endocytosis - the process by which surface-bound nanoparticles are internalized by cellular membrane invagination - adds further intricacy to these interactions, complicating their theoretical prediction. For the process of particle phagocytosis, wherein professional phagocytes like macrophages and dendritic cells actively engulf particulates[28, 29], models have been developed considering receptor-ligand interactions, electrostatic forces, steric repulsion, and VDW attractions between the particle surface and the phagocyte membrane.[30] These models acknowledge that interaction dynamics are influenced by variables such as cell type, differentiation stage, culture medium composition, and cellular processing pathways. Furthermore, envision a theoretically infinite array of nanoparticles characterized by: (i) a diversity of external morphologies, including spherical, cubic, triangular, tubular, hyperbranched, and needle-like shapes; (ii) internal crystallinity designed to yield pronounced photonic, electronic, semiconducting, transport, sorption, and catalytic properties; and (iii) surface chemistries conducive to selective binding, temperature or pH-dependent amphoteric or amphiphilic behavior, and antimicrobial functionality.[20]

Table 1. Main Forces Governing the Interfacial Interactions Between Nanomaterials and Biological Systems. Adapted with Permission from ref.[20]

Force	origin and nature	range (nm)	Possible impact on the interface
Hydrodynamic interactions	Convective drag, shear, lift, and Brownian diffusion are often hindered or enhanced at nanoscale separations between interacting interfaces	10^2 to 10^6	Increase the frequency of collisions between nanoparticles and other surfaces responsible for transport
Electrodynamic interactions	VDW interactions arising from each of the interacting materials and the intervening media	1 to 100	Universally attractive in aqueous media; substantially smaller for biological media and cells owing to high water content
Electrostatic interactions	Charged interfaces attract counter-ions and repel co-ions through Coulombic forces, giving rise to the formation of an electrostatic double layer	1 to 100	Overlapping double layers are generally repulsive as most materials acquire negative charge in aqueous media, but can be attractive for oppositely charged materials

Solvent interactions	Lyophilic materials interact favorably with solvent molecules Lyophobic materials interact unfavorably with solvent molecules	1 to 10	Lyophilic materials are thermodynamically stable in the solvent and do not aggregate Lyophobic materials are spontaneously expelled from the bulk of the solvent and forced to aggregate or accumulate at an interface
Steric interactions	Polymeric species adsorbed to inorganic particles or biopolymers expressed at the surfaces of cells give rise to spring-like repulsive interactions with other interfaces	1 to 100[a]	Generally, increase stability of individual particles but can interfere in cellular uptake, especially when surface polymers are highly water-soluble
Polymer bridging interactions	Polymeric species adsorbed to inorganic particles or biopolymers expressed at the surfaces of cells containing charged functional groups can be attracted by oppositely charged moieties on a substrate surface	1 to 100	Generally, promote aggregation or deposition, particularly when charge functionality is carboxylic acid and dispersed in aqueous media containing calcium ions

[a]Depending on the length of adsorbed or expressed polymeric species.

1.2.2   Determination of in vivo biocompatibility
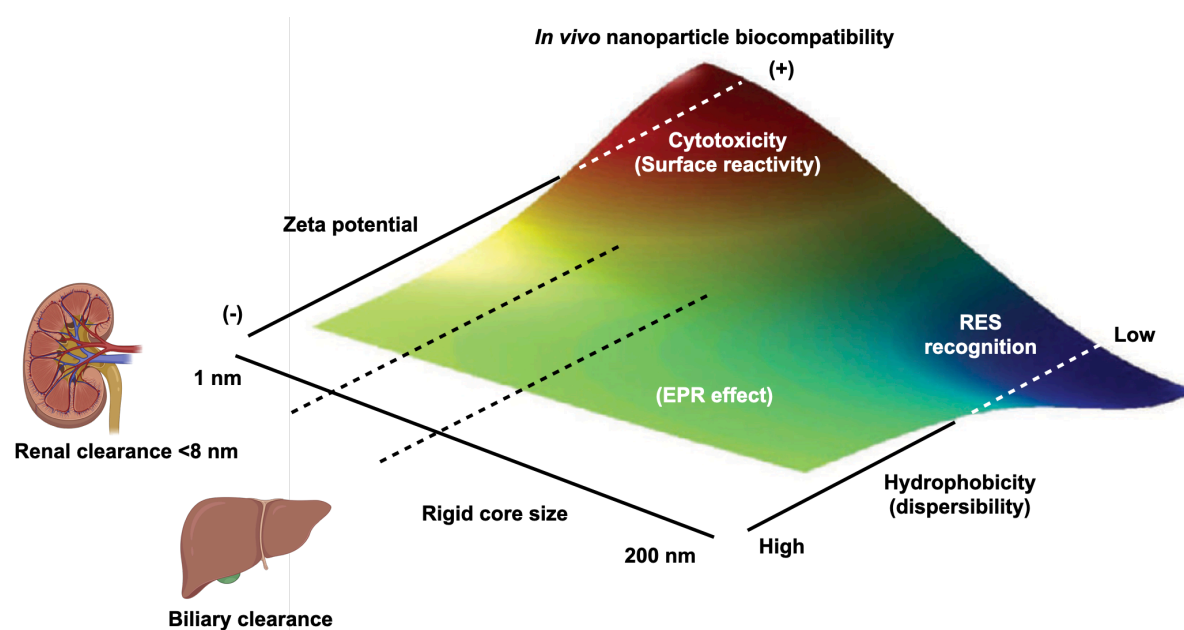
Figure 3. The three-dimensional phase diagram illustrates key biocompatibility trends identified from *in vivo* testing of approximately 130 nanoparticles designed for therapeutic purposes.[31] This diagram highlights how *in vivo* biocompatibility (indicated by a color spectrum) depends on factors like particle size, surface charge (zeta potential), and dispersibility, notably influenced by hydrophobicity. The color spectrum represents biocompatibility levels: red for probable toxicity, blue for likely safety, and a gradient of blue-green-yellow for varying safety levels. Particles with positive charge or high surface reactivity tend to be toxic (shown in red), in contrast to larger, hydrophobic, or less dispersed particles which are quickly and safely (indicated in blue) cleared by the reticuloendothelial system (RES). Particles facilitating enhanced EPR effects, ideal for delivering chemotherapy drugs to cancers, are usually medium-sized and have relatively neutral surface charges. The figure is credited to Scott McNeil. Reproduced with permission from ref. [20].

The complexity of the interactions between biomaterials and biological systems makes it hard to assess the biophysiochemical characteristics that determines the *in vivo* biocompatibility of nanoparticles. The

Nanotechnology Characterization Laboratory (NCL) at the National Cancer Institute in Maryland looked at 130 different nanoparticle types, including fullerenes, metal oxides, polymers, liposomes, dendrimers, quantum dots and gold colloids and deducted that hydrophobicity, size and surface charge are the main parameters influencing nanoparticle biocompatibility.[31] Hydrophobic nanoparticles typically exhibit brief *in vivo* half-lives, ranging from seconds to minutes, primarily due to their rapid clearance from circulation by the reticuloendothelial system's cellular components, especially within the liver and spleen. The significance of nanoparticle size is further evidenced by studies showing that the lungs, gastrointestinal tract, and skin act as robust barriers against nanoparticle uptake and dissemination. Conversely, when directly injected into the bloodstream, the size of nanoparticles critically influences their clearance rates and pathways from the body. Particles under 8 nm, for example, can be excreted by the kidneys, whereas particles over 200 nm are typically trapped by the liver and spleen; the liver can clear particles larger than approximately 200 nm, but clearance does not always equate to excretion given the bile duct's mere ~30 nm diameter. Kupffer cells retain these particles until they are degraded by the liver. Nanoparticles ranging from 30–40 nm to several hundred nanometers can passively accumulate at tumor sites via the enhanced permeation and retention (EPR) effect (see Section 1.3.1), attributed to the increased permeability of tumor vasculature and reduced lymphatic drainage. The impact of particle charge is also highlighted by the NCL studies examining the safety of nanomaterials *in vivo* and *in vitro*, using nanoparticles of relatively consistent size but varying zeta potentials.[31] Cationic particles have shown higher cytotoxicity and a greater propensity to induce hemolysis and platelet aggregation compared to neutral or anionic particles[32], a trend corroborated by studies on cationic polystyrene beads, which have been found to induce cytotoxicity, vascular leakage, and inflammatory infiltrates in the lungs of exposed rats and mice.[33] This toxicity mechanism might also elucidate the occurrence of acute pulmonary edema and bronchiolitis obliterans observed in humans exposed to cationic spray paint particles. These findings are summarized in a three-dimensional phase diagram that illustrates the qualitative biocompatibility trends (Figure 3). The biocompatibility scale is represented through a color gradient, where red signifies potential toxicity, blue indicates likely safety, and the blue-green-yellow transition reflects varying intermediate safety levels. Cationic particles or those with high surface reactivity tend to exhibit more toxic (red-toned) characteristics compared to larger, relatively hydrophobic, or poorly dispersed particles. The latter are quickly and safely (blue-toned) cleared by the RES. Particles facilitating the EPR effect, which is advantageous for chemotherapeutic drug delivery to cancerous tissues, typically possess mid-range sizes and relatively neutral surface charges.

1.3 Targeted Drug Delivery
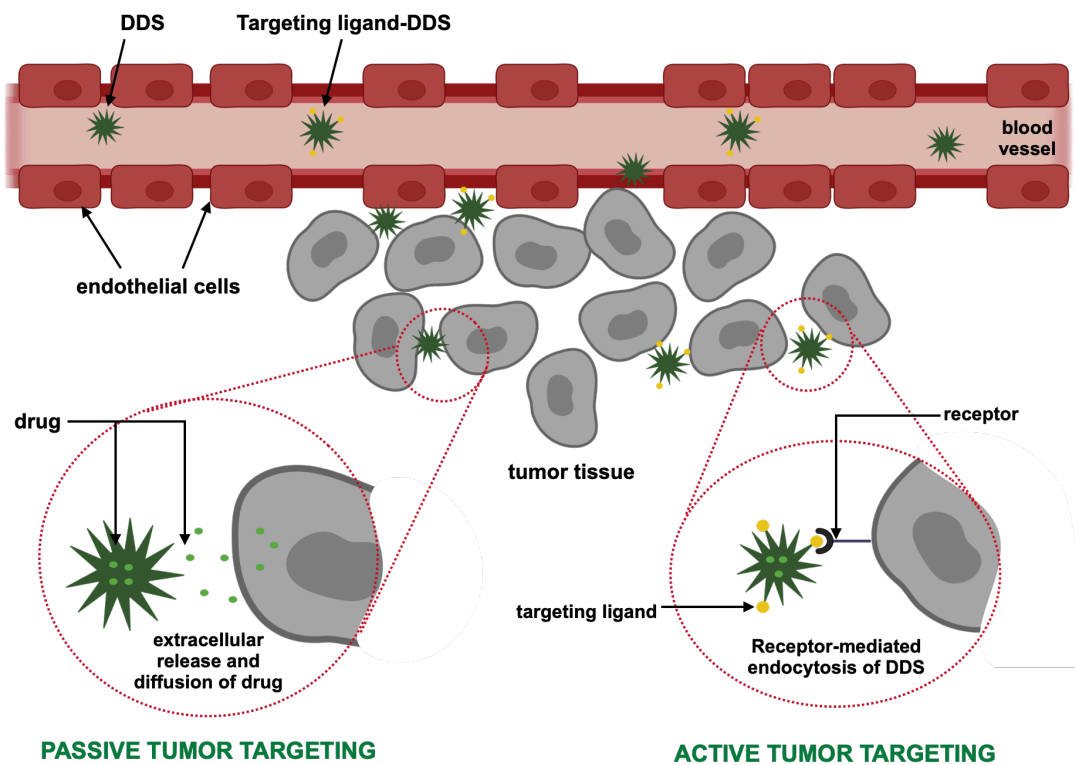
Figure 4. From passive to active targeting of drug delivery systems (DDS).

1.3.1 Passive targeting

Loaded drug delivery systems (DDSs) of nanometric scale can traverse the bloodstream and preferentially accumulate at tumor sites, leveraging the EPR effect.[34-36] This passive targeting approach benefits from extended circulation time in the bloodstream and the distinct physiological differences between tumor and healthy tissues, such as more developed vasculature and larger endothelial gap junctions in tumors (up to 1 μm). Notably, very small carriers are swiftly eliminated by the kidneys (e.g., renal clearance threshold for nano-objects with a hydrodynamic diameter of 6 nm)[37-39], while larger ones predominantly accumulate in the liver and spleen (sizes exceeding a few hundred nanometers).[40] In contrast, nanocarriers with diameters ranging from 20 to 200 nm can effectively erupt into tumor tissues.[41] Given the essential role of carrier size in facilitating low accumulation in healthy tissues and high accumulation in tumor tissues via the EPR effect, this parameter was considered critical in the design of polymer-based drug delivery systems (Figure 4).[42]

Even though the EPR effect was noted as a huge breakthrough when it was discovered by Maeda in the late 80s, nowadays, the approach is regarded as a too simplistic as it cannot be the only fit for all existing tumor microenvironments. The new approach is to move towards methods that can be more individualized and result in an improved nanomedicine treatment.

Parameters to be taken into consideration are the nature, the complexity and the heterogeneity of the EPR effect and to come up with systems and strategies to be able to image and visualize the EPR-based tumor targeting.[43] In a recent publication, Sindhwani *et al*. reported new findings that the transport of nanoparticles into solid tumors, contrary to prior assumptions, is not primarily facilitated by inter-endothelial gaps. Their research indicates that up to 97% of nanoparticles enter tumors through an active process involving endothelial cells.[44] This conclusion is derived from comprehensive analyses involving four distinct mouse models, three types of human tumors, mathematical simulations, and modeling, as well as two different imaging techniques.[44] These findings challenge the existing foundation of cancer nanomedicine development, suggesting that a deeper understanding of these active pathways may be crucial in enhancing tumor accumulation of nanoparticles.[44]

1.3.2 Active targeting

The aim of active targeting is to increase the cellular uptake of DDSs for the effective transport of the cargo to a specific cell or site of action. In practice, active targeting is the insertion of a targeting moiety or a legend that is covalently bonded to the surface of the DDS or nanoparticle (Figure 4). These targeting legends engage in specific interactions with receptors found on cancerous or angiogenic endothelial cells, thereby augmenting the binding and internalization of the DDS. Numerous targeting agents have been explored, encompassing a range of aptamers, which can be peptides[45-47] or oligonucleotides[48-50], as well as folic acid[51, 52] (Figure 5).[42] The Haag group has been exploring targeting moieties that are based on polyanions, precisely sulfate groups that will be discussed in detail in Section 1.6.6.
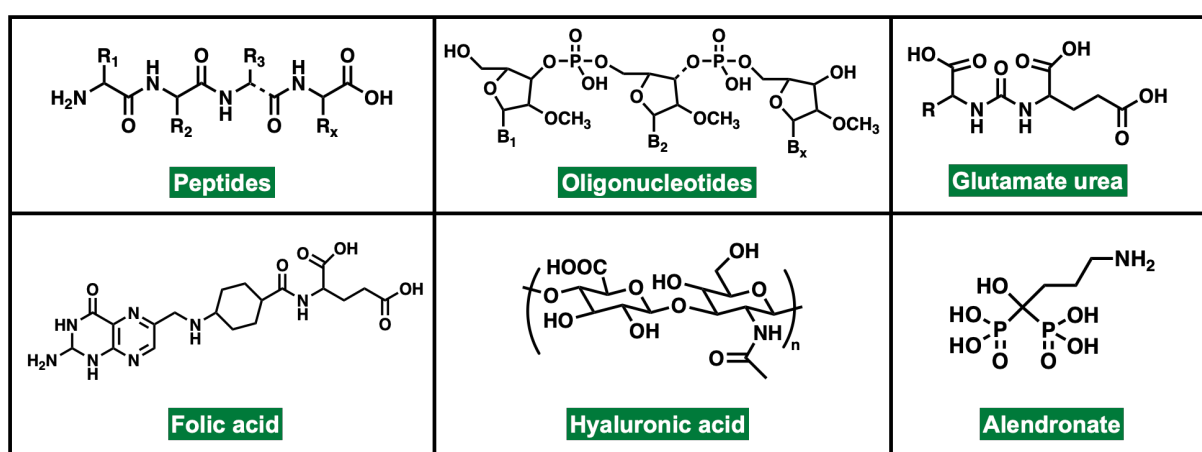
Figure 5. Targeting ligands to enhance recognition and cell uptake in cancer cells.

1.4 Drug Release through Biological Stimuli

1.4.1 Systemic release

In conjunction with the imperative properties of drug solubilization, biocompatibility, and targeting efficacy inherent to a DDS, the release mechanism of the therapeutic agent at a targeted site should be responsive to specific stimuli characteristic of that target. This stimulus-responsive release is a critical factor in ensuring the precise and controlled delivery of the drug to the intended biological environment. These systems are designed to undergo physical or chemical alterations in response to external (exogenous) stimuli: light, ultrasound, magnetic fields, and temperature, or internal (endogenous) stimuli: pH gradients, redox potential, overexpression of enzymes and marker molecules, and variations in ionic strength.[53, 54] This responsiveness facilitates controlled spatio-temporal drug release, modulates tissue accessibility, and promotes cellular uptake (Figure 6).[55, 56]
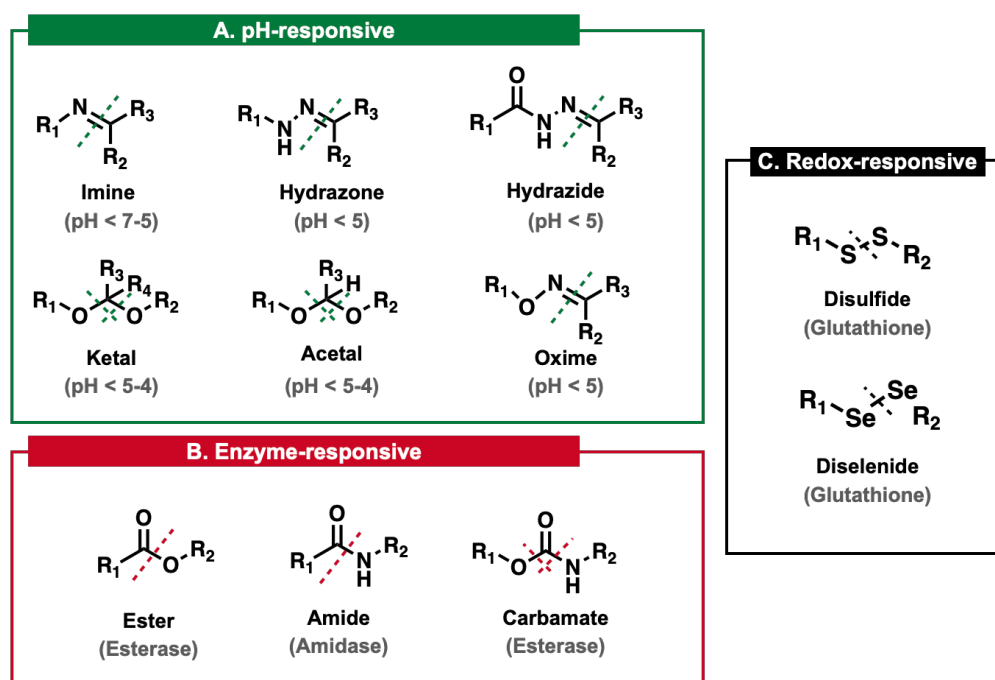
Figure 6. A) pH, B) enzyme and C) redox-responsive bonds used in DDS for biological degradation.

The degradation of the DDS can be realized through the employment of biodegradable polymer systems, as detailed later in section 1.6.4, or by utilizing crosslinks that are sensitive to external or internal stimuli. With research increasingly targeting these triggers, strategies have been developed that involve the integration of labile bonds into the polymer network or the drug linker, thereby instilling responsive characteristics in the DDS (Figure 7).[53] The human body typically maintains a neutral pH, with certain exceptions in specific organs that perform distinct functions. For example, the stomach requires an acidic pH to digest food, while the

intestine, particularly the colon, maintains a more alkaline pH, reaching up to 8. However, in pathological conditions, a decrease in pH is often observed due to abnormal metabolic processes. This results in inflamed and tumoral tissues typically exhibiting an acidic extracellular environment. Additionally, a pH gradient is observed within cellular compartments; early endosomes have a near-neutral pH (6-7), but a significant drop to 4-5 is noted in late endosomes and lysosomes.[57] Since basic pH conditions are rare in disease states, carriers responsive to stimuli are predominantly designed to react to acidic environments. To achieve pH responsiveness, hydrolytically cleavable moieties are utilized. When it comes to enzymatic degradation, the overexpression of certain enzymes in cancerous tissues can be utilized as trigger for carrier degradation or drug release notable among these are proteases, glucuronidases, and carboxylesterases, which are recognized for their elevated presence in cancerous cells.[58] As for the redox potential, numerous redox couples exist within the human body, among which the glutathione (GSH)/glutathione disulfide (GSSG) couple stands out as particularly significant, serving as one of the primary redox buffers.[59] Elevated concentrations of glutathione are typically found in the cytoplasm and within cancer cells; the concentration of intracellular GSH is around 2–10 mM, which is about 1000 folds higher than that in extracellular environment (2–10 μM).[60] This heightened presence has been extensively explored as a trigger for the cleavage of disulfide bonds in therapeutic applications.[61, 62]

Figure 7. Release of cargo from the drug delivery system through A) degradation of the linker, B) degradation of the carrier, and C) release of the cargo upon change in carrier polarity.

1.4.2 Overcoming the skin barrier

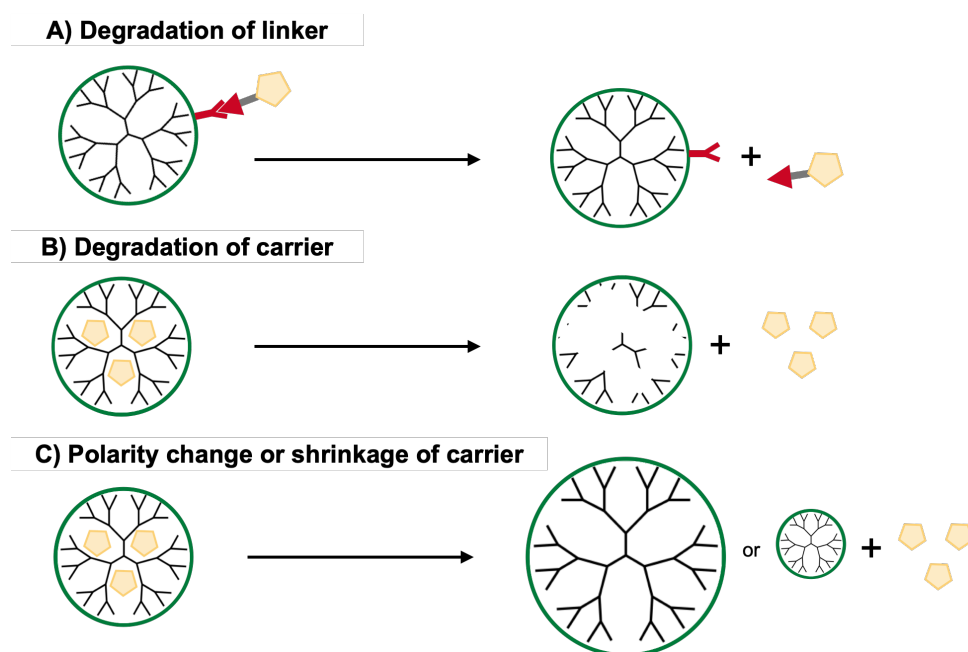The skin, as the body's largest and most accessible organ, covers a surface area of approximately 2 square meters and constitutes about 15% of the total body weight. It functions as a crucial physical barrier, safeguarding the body against external environmental factors and playing a vital role in maintaining homeostasis.[63, 64] Additionally, about one-third of the body's blood circulation takes place through the skin. The human skin comprises three distinct layers: the epidermis, dermis, and hypodermis. The epidermis itself is further divided into two main layers: the nonviable epidermis (stratum corneum) and the viable epidermis, which includes the stratum lucidum, stratum granulosum, stratum spinosum, and stratum basale.[65] The stratum corneum, also referred to as the nonviable epidermis, forms a significant barrier to the transdermal penetration of most drugs and foreign substances. This barrier efficacy is due to a specialized arrangement of hydrophilic keratin proteins tightly interlaced with hydrophobic lamellar lipids.[66] The epidermal layer's thickness varies from 0.5 to 1.0 mm across different body regions[67], with its hydrophobic nature being primarily attributed to components like ceramides (50%), cholesterol (25%), and fatty acids. This layer also contains densely packed, dead corneocytes filled with keratin.[68] Due to the characteristics of the stratum corneum (SC), it poses a significant obstacle to the permeation of substances through the skin.[69] Nonetheless, specific mechanisms exist that enable active compounds to traverse these barriers. These include transcellular (intracellular) permeation through the corneocytes of the SC, intercellular penetration through the spaces in the SC, follicular penetration through hair follicles, and passage through sebaceous or sweat glands (Figure 8).[70, 71] Furthermore, certain transporter proteins, such as efflux transporters, facilitate the absorption of large molecules like P-glycoprotein.[63] The second physical barrier in skin permeation is the viable epidermis, characterized by adhesive membrane proteins forming tight junctions within this layer.[68] The transdermal drug delivery system (TDDS) is a method of administering drugs through the skin directly into systemic circulation, offering a non-invasive and painless approach to systemic drug delivery. This system distinguishes itself from topical drug delivery by its ability to transport drugs through the skin at a controlled and predetermined rate, directly into the systemic circulation.[72] TDDS presents a viable alternative to oral and parenteral routes, effectively circumventing their drawbacks. Oral and parenteral methods are often plagued by the 'peak and valley' phenomenon, resulting in fluctuating plasma drug levels that can lead to unpredictable and erratic therapeutic responses.[73] In contrast, TDDS provides sustained drug release, maintaining drug concentrations above the minimum therapeutic level and thereby reducing the risk of side effects. As a controlled delivery system, TDDS offers significant

convenience for patients. It also allows for straightforward discontinuation in cases of necessity, such as systemic toxicity, while minimizing sensations of pain.[74]
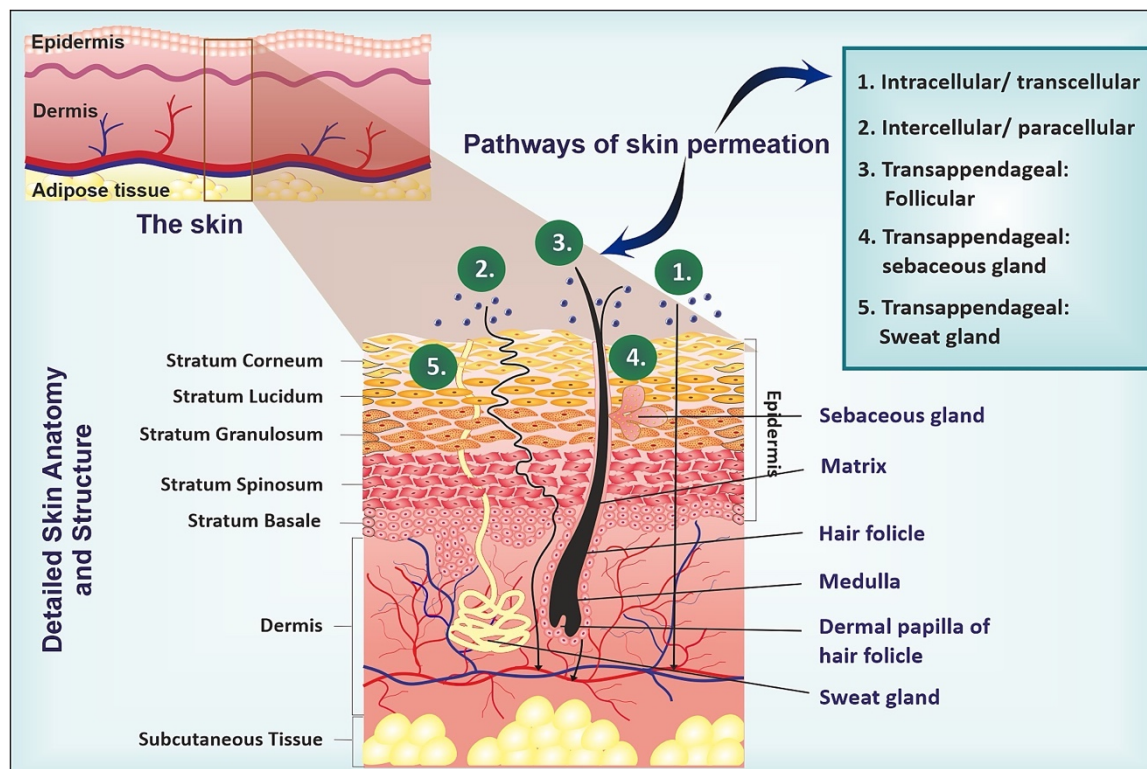
Figure 8. Anatomy of skin along with skin permeation pathways including transcellular, paracellular and transappendageal. Reprinted with permission from ref .[71].

1.5 Design of Polymer-based Drug Delivery Systems

The focus of drug delivery research that has been carried out since the early 1950's is to improve the therapeutic effect and the drug bioavailability at the specific organ of action.[75-77] Polymer-based DDSs are three-dimensional, possessing surface and bulk properties. Through the design of these properties drug loading, release, and pharmacokinetic properties is formulated.[78] The first example of employing a synthetic copolymer for drug delivery was reported by Horst Jatzkewitz in 1954 observing the prolonged residence time of mescaline by conjugating it to N-vinylpyrrolidone and acrylic acid via a dipeptidic linker.[79] In the late 90s, a new method of entrapment of small drug molecule into a polymeric system was reported by Meijer *et al.*[80, 81] In this model, the interactions depended on the molecular size of the guest molecule and the physical size of the dendrimer cavities. The "dendritic box" is a modified G5-PPI with Boc-protected phenylalanine which were able to encapsulate guest molecules of different sizes. In this model, the interactions depended on the molecular size of the guest molecule and the size of the cavities of the dendrimer.[80, 81] This section will discuss first

polymer-drug conjugates and the emergent of supramolecular DDSs that are polymeric based, focusing in detail on the unimolecular systems.

1.5.1.1 Polymer-drug conjugates

Polymeric drug conjugates (PDCs), also known as polymeric prodrugs, represent a fundamental DDS in the field of nanomedicine. These systems involve the covalent attachment of one or more therapeutic agents to a polymer carrier. The conjugation of drugs to polymers offers numerous benefits, such as prolonged circulation time in the bloodstream, regulated drug release, and enhanced pharmacokinetic profiles. Additionally, this approach significantly improves water solubility, minimizes toxicity, and facilitates intracellular delivery of the drugs. Primarily, this strategy of conjugation has been extensively utilized for potent anti-cancer agents characterized by high cytotoxicity and limited solubility. In 1975, Ringsdorf introduced a theoretical model delineating the ideal characteristics of a PDC. According to this framework, an optimal PDC is characterized by the attachment of an active pharmaceutical ingredient (API) to a biocompatible polymer, as depicted in Figure 9. Within this model, the polymeric backbone may also be modified with additional targeting elements and water-solubilizing groups to enhance the therapeutic efficacy of the conjugate.[82] The polymeric backbone can have linear or dendritic architectures. This section will cover dendritic architectures as part of the scope of this work.
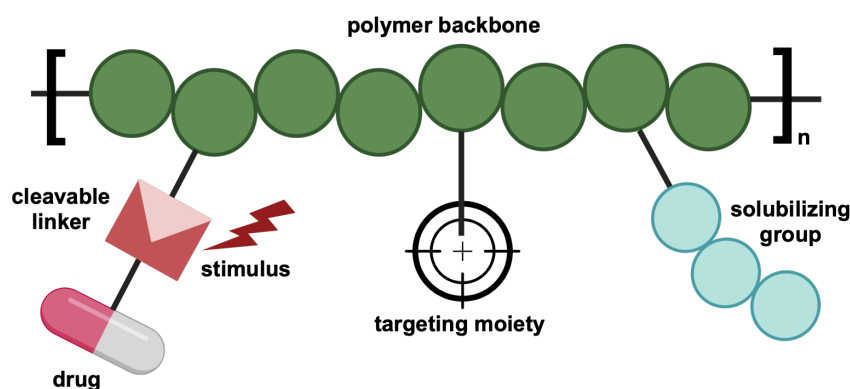
Figure 9. Conceptual scheme of the Ringsdorf model.

Dendrimer-drug conjugates

Dendrimers, distinct from linear polymers, are a class of macromolecules noted for their highly branched and precisely defined structures. The key components of a dendrimer include (i) an initiating core, (ii) successive generations of repeating units branching out from this core, and (iii) terminal functional groups located on the outermost generation.[83, 84] Their suitability

for DDSs is attributed to their spherical conformation, high functional capacity, and uniform size range. Additionally, dendrimers are advantageous due to their efficient cellular uptake, ability to traverse endothelial linings and capillary walls, permeation through biological barriers, targetability, and their capacity to enhance the solubility of hydrophobic drugs.[85, 86] Currently, the dendritic structures that have successfully progressed through clinical trials and entered the market are poly-L-lysine (PLL) dendrimers and their derivatives (www.starpharma.com, refer to Table 2). However, the polyamidoamine (PAMAM) dendrimer also exhibits significant potential for use in dendrimer-drug conjugate systems. It is important to note, though, that the stability of PAMAM dendrimers can be compromised, as they are prone to retro-Michael reactions (β-eliminations) under conditions of elevated temperatures or pH, which might be necessary during their synthesis process.[87]

Table 2. Overview of Dendrimer-drug Conjugates

Trade Name	API	Dendritic structure	Indication	Trial Phase
Vivagel®	-	PEGylated PLL	Antiviral activity	Marketed
DEP® docetaxel	Docetaxel	PEGylated PLL	Lung, prostate cancer	II
DEP®CABAZITAXEL	Cabazitaxel	PEGylated PLL	Prostate, ovarian cancer	I/II
DEP®IRINOTECAN	Irinotecan	PEGylated PLL	Colorectal, pancreatic cancer	I/II
AZD0466	AZD4320	PEGylated PLL	Dual Bcl2/xL inhibitor	II
DEP®GEMCITABINE	Gemcitabine	PEGylated PLL	Pancreatic, lung cancer	Preclinical

DEP® docetaxel, a dendrimer-drug conjugate, has advanced the furthest in clinical trials, presently in phase II (EudraCT number: 2016-000877-19). Clinical trials have indicated that DEP® docetaxel causes less neutropenia and exhibits lower toxicity related to excipients compared to Taxotere®.[88] Starpharma's first commercial dendrimer, SPL7013 (Vivagel®), is designed for the prevention of HIV and herpes simplex virus (HSV) infections. SPL7013 is a fourth-generation poly-L-lysine dendrimer featuring a divalent benzhydrylamine (BHA) core and 32 surface naphthalene disulfonic acid groups, with a molecular weight of 16.581 kDa.[89, 90] The terminal groups confer a high anionic charge and increase hydrophobicity on the dendrimer surface.[91] SPL7013 has demonstrated in-vitro effectiveness against various HIV-1 clades and HIV-2, inhibiting viral attachment and entry, while also showing low toxicity in cervical and colorectal epithelial cell lines and not disrupting the intercellular tight junctions in polarized epithelial cells.[92, 93] Patterson *et al.* developed a dendrimer-drug conjugate in which AZD4320 was chemically attached to the free lysines of a PEGylated fifth-generation poly-L-lysine dendrimer using glutarate, thiol diglycolate, and diglycolate as linkers, as shown in

Figure 10. The molecular weight of this dendrimer is approximately 105 kDa, with a loading capacity of 24-30 wt.% (equivalent to 25-42 AZD4320 molecules). Its solubility in aqueous buffer exceeds 100 mg/ml, and it has a hydrodynamic diameter of about 10 nm (PDI <0.2).[94] The conjugation with AZD4320 significantly enhances the drug's solubility, facilitating intravenous administration. AZD4320, a potent inhibitor of both Bcl-2 and Bcl-xL, has shown promising efficacy. However, its cardiovascular toxicity hindered its standalone clinical development. The dendrimer-drug conjugate, displaying efficacy and cardiovascular tolerability in preclinical models, is poised for clinical advancement.[94]
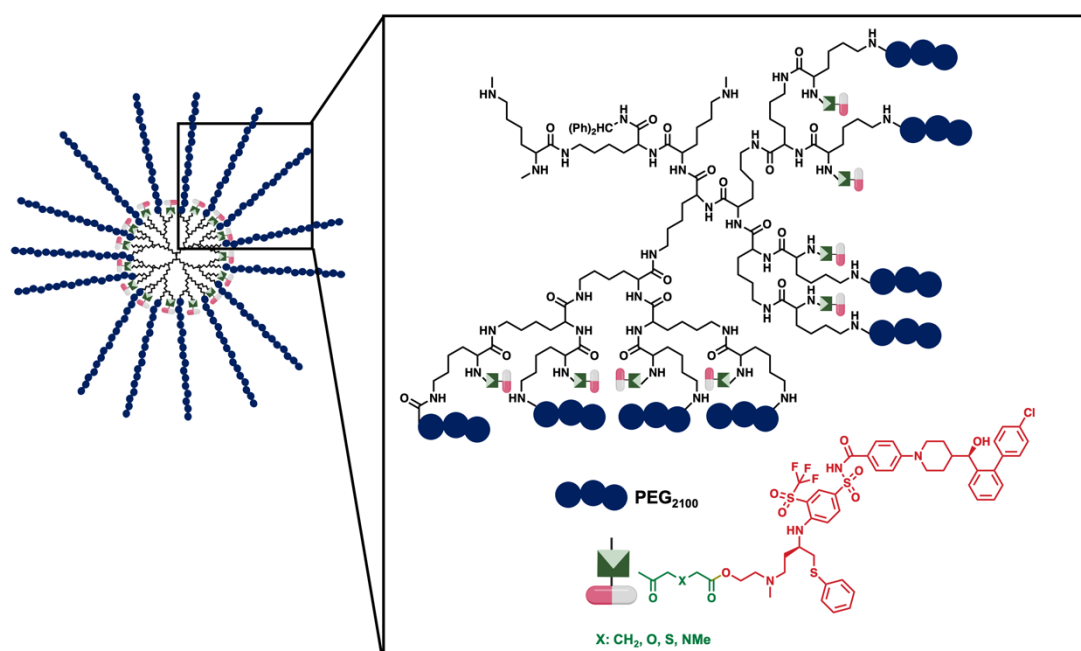
Figure 10. Chemical structure of AZD0466 and dendrimer-AZD4320 conjugates showing the dendrimer structure of PEGylated PLL, and the linkers used. Adapted from ref. [94].

1.5.1.2 Supramolecular drug delivery systems

The aim of a DDSs is to improve the protection, transport and eventually release of its sensitive cargo. This will require and depending on the application the modification and tuning of surface area, physio-chemical and mechanical properties. Consequently, a diverse range of DDSs that are not only limited to conjugation of the API to the polymer has emerged and vary in complexity including: unimolecular and polymeric micelles, liposomes and polymersomes, nanocapsules and nanogels (Figure 11).[95] This work covers the design of supramolecular DDSs on both ends of these systems' spectrum based on size and complexity. The following two sections will describe unimolecular micelles and hydrogels.
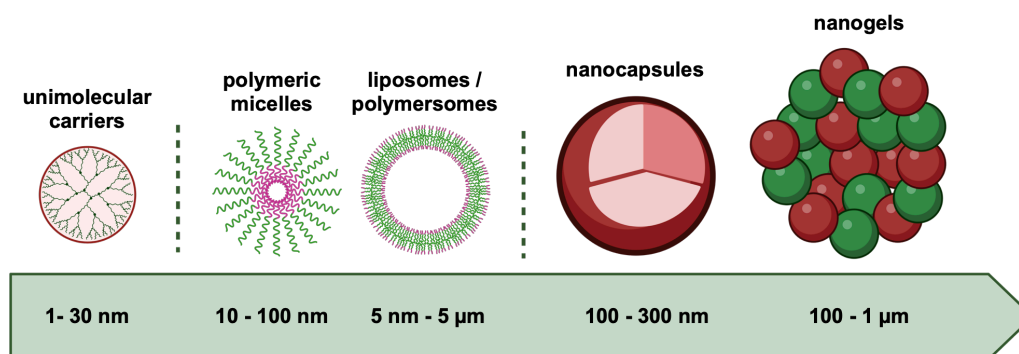
Figure 11. Architectures and categories of supramolecular drug delivery systems.

Unimolecular micelles – beyond covalent bonding

Unimolecular systems, characterized as singular-molecule micelles, exhibit distinct compartments - a core and a shell - that are covalently interconnected.[96] Their structural design encompasses an array of architectures including dendrimers, dendrimer-like star polymers, hyperbranched polymers, and dendronized polymers (Section 1.4.1.2). These unimolecular systems have garnered significant attention in targeted drug delivery research due to their exceptional stability and responsiveness to microenvironmental variations, such as changes in temperature, pH, and ionic strength. Unlike typical amphiphilic micelles, unimolecular carriers are stable upon dilution since their assembly does not depend on a critical micellar concentration (CMC) for when it is not achieved the system can disassemble (Figure 12).[97] The dendritic architectures of unimolecular micelles, characterized by their internal voids and surface functional groups, render them suitable for drug delivery applications. Depending on their structural attributes, active pharmaceutical agents can be non-covalently encapsulated within these systems. This encapsulation can occur either within the internal cavities of the dendritic core, functioning as endoreceptors[80], or at the multivalent surfaces of the system, serving as exoreceptors[98].
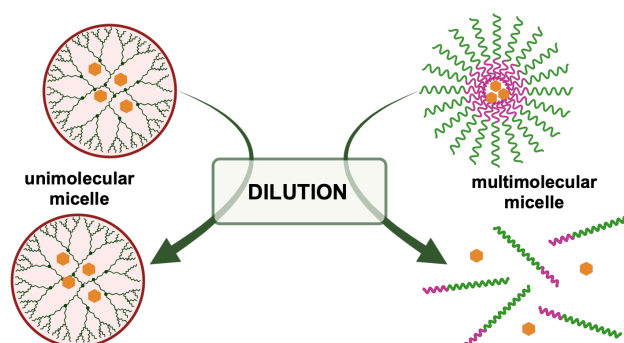
Figure 12. The different physical behavior of unimolecular and multimolecular micelles upon dilution.

The loading of guest molecules in the dendrimer core can be facilitated through hydrophobic, electrostatic, or hydrogen-hydrogen interactions. Fréchet and colleagues developed a unimolecular micelle composed of a dendritic polyaryl ether network with carboxylate surface groups. This system demonstrated the ability to solubilize pyrene, a hydrophobic molecule, in aqueous environments.[99] In this example, the ratio of dendrimers to solubilized pyrene was directly proportional, with the host-guest interactions mediated by π–π interactions between the electron-rich aryl ether and the aromatic guest molecule.[100] The Diederich group introduced a dendrimer variant, named "dendrophane," designed to encapsulate hydrophobic guests within its core. These dendrophanes, soluble in water, possess a cyclophane interior capable of binding aromatic compounds via π–π interactions, demonstrating efficacy in steroid encapsulation.[101, 102] Mitchell and colleagues pioneered a methodology for encapsulating acidic aromatic antibacterial agents, responsive to lower pH levels. These dendrimers, derived from PAMAM, were modified at the surface with a glycerol derivative to yield a water-soluble compound. It is postulated that the host-guest complex forms through acid-base interactions and hydrogen bonding between the internal tertiary amine core and the acidic agent.[103]

1.6   Hyperbranched Polyglycerols – Biodegradability through Copolymerization

This section will detail the emergence of hyperbranched polyglycerols (hPGs) as responsive DDSs, emphasizing their biodegradability achieved through copolymerization. This approach not only enhances their responsiveness but also mitigates *in vivo* accumulation. The narrative will commence with an overview of dendritic polymers, with a special emphasis on hyperbranched variants, then transition to exploring polyglycerols, copolymerization methods, and structural identification. The culmination of this discussion will be an explanation of how biodegradability is incorporated into the hPGs' structural backbone.

1.6.1   *Dendritic polymers*

"Life is branched"[104] was the motto of *Macromolecular Chemistry and Physics* in their special issue in 2007 on Branched Polymers. The purpose was to emphasize the profound influence of branching in synthetic macromolecules and to explore how researchers have adopted these naturally occurring characteristics to design branched polymers.[105] The dendritic family of polymers include different architectures: dendrimers, hyperbranched polymers, dendrigrafts and dendronized polymers (Figure 13).[106, 107] The structure of dendritic polymers differs from the classic cross-linked polymer network, branched and linear polymeric architectures that are shown in Figure 14.
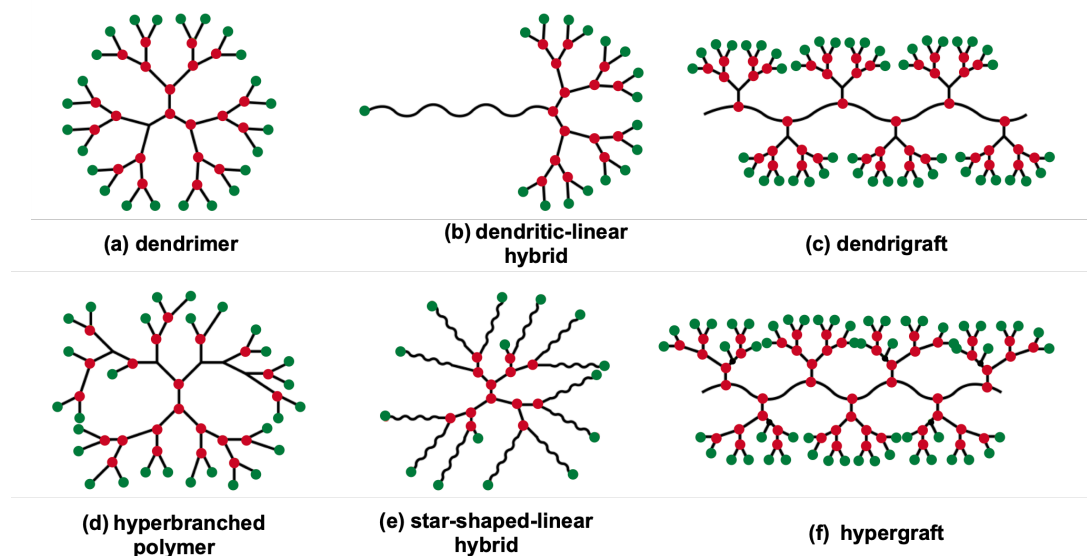
Figure 13. Schematic overview of the subclasses of dendritic polymer architectures: (a) dendrimer, (b) dendritic–linear hybrid, (c) dendrigraft/dendrigrafted polymer, (d) hyperbranched polymer, (e) star-shaped–linear hybrid, (f) hypergraft/hypergrafted polymer. Branching (red) and terminal groups (green) are indicated.

A dendrimer is distinguished by its monodispersity and a "tree-like" configuration, exhibiting a branching symmetry across three dimensions, which leads to a globular architectural structure.[108] Although dendrimers are ideal for various applications including targeted drug delivery, catalysis, sensors, surface engineering, and biomimetic materials,[107] only a limited number of structurally uniform dendrimers have reached the market. The production of these dendritic materials is often labor-intensive and time-consuming, necessitating complex work-up procedures for precise structural definition, which hampers their scalability for large-scale use.[109]
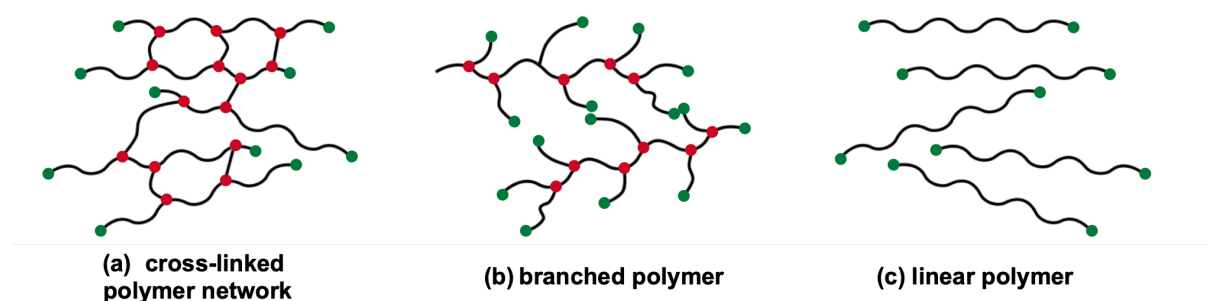
Figure 14. Schematic representation of classical polymer structures with (a) cross-linked polymer network, (b) branched polymer, and (c) linear polymer structures. Net points (red) and terminal groups (green) are indicated.

As an alternative to dendrimers, hyperbranched polymers have been developed. These polymers, in addition to dendritic and terminal units, incorporate linear segments. Their branched structure, which is less uniform compared to dendrimers, results from a typical one-pot synthesis approach that does not require the protection/deprotection steps that are vital in dendrimer synthesis.[105] This one-pot method limits control over molecular weight and branching precision, leading to hyperbranched polymers having polydisperse molecular weights and a degree of branching (DB) less than 1.[105] Despite this, these polymers retain dendritic characteristics such as high branching, numerous terminal functional groups, globular structure, and narrow molecular weight distribution. They exhibit lower solution and melt viscosities due to reduced entanglement and have enhanced solubility compared to linear analogs, attributable to the numerous terminal groups.[107] The degree of branching in hyperbranched polymers is a critical factor that influences their properties, with higher DB values resulting in behavior more akin to dendrimers.[110] Common synthesis methods for hyperbranched polymers involve the use of ABx type monomers (as per Flory's approach[111]) with prevalent polymerization techniques including condensation, cationic, anionic, and ring-opening polymerizations.[107]

1.6.2 Polyglycerol – a multifunctional platform

The structure of polyglycerols (PGs) consists of ether linkages, which support a high density of peripheral hydroxyl groups. Their appeal is attributed to a variety of properties such as chemical stability, outstanding biocompatibility, minimal toxicity, adjustable blood circulation time, low intrinsic viscosity, compact structure, multi-functionality, and straightforward synthesis processes.[108, 112, 113] PG can be synthesized into various structures (linear, hyperbranched, dendronized brush-type and dendrimers) using cationic, anionic, or coordination-based ring-opening polymerization techniques with glycidol as the monomer. This polymer is characterized by its high solubility in water and biocompatibility. Additionally, the presence of hydroxy groups on each repeating unit of PG allows for a wide range of subsequent chemical modifications.[114] The excellent biological and chemical properties of PGs put them in the front line for applications such as carriers of APIs[115], protein conjugation[116-118], or as platform for virus inhibition.[119, 120]

1.6.2.1 Linear polyglycerol

Linear polyglycerol (LPG) consists of a polyether backbone with methyl hydroxy groups as side chains. The synthesis of LPG involves a three-step procedure: (1) protecting the glycidol monomer, (2) conducting anionic ring-opening polymerization (AROP), and (3) implementing acid deprotection (Figure 15).[121] The monomer hydroxyl groups are protected prior to

polymerization to prevent any intramolecular proton exchange during the propagation phase and branching.[121] This approach offers a versatile toolkit for creating diverse compositions and structures using various protected glycidol monomers.[113, 122, 123] The multifunctional backbone of LPG enables a broad spectrum of substitution reactions, facilitating high levels of functionalization.[122] Commercially available monomers like tert-butyl glycidyl ether (tBGE) and allyl glycidyl ether (AGE) are used, but ethoxyethyl glycidyl ether (EEGE) is the most employed protected glycidol in LPG synthesis. This preference is due to its straightforward synthesis and the ease of acidic deprotection of its acetal protecting groups.[113, 123] EEGE was initially synthesized by Fitton et al., in 1987[124], prepared through the reaction of ethyl vinyl ether with glycidol, catalyzed by p-toluenesulfonic acid.[125, 126] In 1994, Taton et al. were the first to report successful polymerization of EEGE using cesium hydroxide as an initiator in bulk polymerization, producing poly(ethoxyethyl glycidyl ether) (PEEGE) with molecular weights around 30 kDa and a relatively broad polydispersity index (Đ=1.5).[125] Modifying the initiator to potassium or cesium alkoxide led to the synthesis of polymers with narrower molecular weight distributions.[127] Various initiators have been effectively used for controlled polymerization of EEGE, including potassium tert-butoxide (t-BuOK)[128, 129], potassium 3-phenyl propanolate (PPOK)[130, 131], alkoxy ethanolates[132], potassium methoxide (MeOK)[133], and BuLi/phosphazene base (Li$^+$/t-BuP$_4$).[130, 134] However, alkali metal-based initiators in EEGE polymerization typically yield molecular weights capped at around 3 kDa or a degree of polymerization (DP$_n$) of approximately 300.[126, 135] Möller et al. attributed this limitation to chain transfer reactions occurring either from the active chain-end or the oxyanion initiator.[129] Similar chain transfer reactions have been reported in the polymerization of other monosubstituted epoxides like propylene oxide (PO) or phenyl glycidyl ether.[136] The process involves proton substitution from the group adjacent to the epoxide ring, leading to the formation of an unsaturated allyl alkoxide.[129]
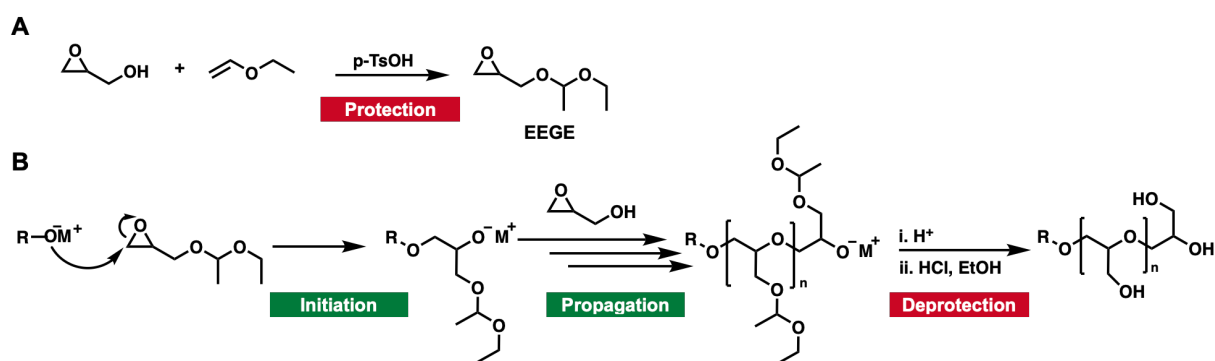

Figure 15. A) Protection of glycidol, and B) polymerization of EEGE, and acidic deprotection of acetal groups.

1.6.2.2 Hyperbranched polyglycerol

In comparison to LPG, hPG possesses a more compact and globular branched structure. These polymers comprise three distinct units: linear, dendritic, and terminal. They typically exhibit a degree of branching that ranges from 0.5 to 0.6.[137] Moreover, they possess a high degree of hydrophilicity, with water solubility exceeding 400 mg/mL. Their molecular weight varies, spanning from a few hundred Daltons to approximately one million Daltons, and they are characterized by a low polydispersity index, ranging from 1.05 to 1.5.[108]

The first polymerization of glycidol was documented in 1966 when Sandler and Berg polymerized the AB_2 type monomer (as theoretically conceptualized by Flory[111]) at ambient temperature using a variety of catalysts. Following this, Dworak *et al.* introduced the concept of glycidol's ring-opening polymerization through a cationic pathway.[138] They outlined two potential mechanisms: the active chain (AC) and activated monomer (AM). Common initiators for this process included Lewis acids (BF_3OEt_2 or $SnCl_4$) and Brønsted acids (CF_3COOH or CF_3SO_3H).[138, 139] A significant challenge in this method was managing reaction kinetics, as numerous side reactions could impede propagation, often resulting in hyperbranched polyglycerols (hPGs) with low molecular weights (below 10 kDa) and wide dispersity.[138] Despite these limitations, the simplicity of this approach continues to attract research into novel hPG architectures using cationic ring-opening polymerization. Mohammadifar *et al.* introduced a green synthesis pathway for hPG, utilizing citric acid as an initiator.[140] They demonstrated that citric acid not only initiates the polymer chain but also integrates into the polymeric structure, acting as a proton donor.[140] The proposed mechanism involved AM cationic ring-opening polymerization.[140] Incorporating citric acid in the backbone rendered the hPG degradable under neutral and acidic conditions.[140] While the polymerization process did not yield molecular weights exceeding 1.5 kDa, the environmentally friendly synthesis and purity of the resulting polymers positioned it as a viable option for biomedical applications.[140] More recently, Kim *et al.* developed a recyclable, metal-free catalytic system for the cationic ring-opening polymerization of glycidol under ambient conditions, using tris(pentafluorophenyl)borane as a catalyst.[141] This method enabled the formation and precipitation of higher molecular weight hPG (1–4 kDa) in nonpolar solvents, facilitating the recycling of both the catalyst and solvent through a straightforward decantation process of the hPG.[141]

The limitations of the cationic ring-opening polymerization of glycidol are overcome by employing a combination of an anionic ring-opening multibranching polymerization (ROMBP) and a slow monomer addition.[137, 142] The process used a partially deprotonated 111-

tris(hydroxymethyl)propane (TMP) as the initiator and was conducted at temperatures between 90–100 °C. The slow addition of glycidol facilitated controlled polymer chain growth and prevented the formation of low molecular weight polymers by limiting oligomer intracyclization. This methodology yielded a medium-sized hyperbranched polyglycerol (hPG) with relatively narrow dispersity (Đ < 1.5).[137] However, the technique introduced by Sunder *et al.*[137], while enabling controlled polymer growth and a defined end product, still encounters challenges in achieving molecular weights exceeding 6.5 kDa. This is attributed to the solvent-free nature of the process, where increasing viscosity eventually leads to suboptimal mixing.[108, 137] Thus, synthesizing high molecular weight polyglycerol becomes crucial, especially for drug delivery applications, as higher molecular weights provide larger hydrodynamic sizes, improved vascular retention, and a greater number of functional groups.[108] Schmitt *et al.* highlighted the correlation between the molecular weight of hPGs and the blood circulation time of the DDS.[143] They evaluated various molecular weights of hPG carriers (ranging from 25–500 kDa) conjugated to the chelator desferrioxamine (DFO) and labeled with the gamma emitter [67]Ga.[143] Through qSPECT/CT imaging in Rag2m mice, they demonstrated that the blood circulation half-lives of the ^{67}Ga-labeled hPGs extended from 9.9 to 47.8 hours as the molecular weight increased.[143] Various methodologies for synthesizing high molecular weight hPGs have been proposed. An initial method, reported by Frey and colleagues, involved modifying stirring intensity, stirrer geometry, monomer addition rate, and incorporating an inert emulsifying agent (Figure 16A). These adjustments led to the production of hPG with a molecular weight up to 20 kDa.[144] More recently, Haag's group introduced an automated solvent-free polymerization technique for hPGs, ensuring high reproducibility and traceability due to automation.[145] They established a linear relationship between torque and polymerization degree, which can be used to monitor molecular weight during polymerization.[145]

The second strategy is the macroinitiator method, wherein the reaction propagates by gradually introducing glycidol to a low molecular weight hPG that has been partially deprotonated, serving as a macroinitiator. Wilms *et al.* used hPG macroinitiators of 0.5 and 1 kDa to synthesize hPGs with molecular weights reaching up to 24 kDa[146], while Moore *et al.* began with a larger hPG macroinitiator (2 kDa), leading to the formation of high molecular weight hPGs of up to 100 kDa (Figure 16B).[147] The third method incorporates a solvent acting as an emulsifying agent, adding another variable to the reaction process. Various solvents were tested, including dioxane[148], 1,4-dioxane, tetrahydropyran, ethylene glycol diethyl ether, and decane (Figure 16C).[149] It was found that the choice of solvent neither compromised the properties nor the degree of branching in the resulting hPG.[148] Furthermore, the type of solvent

influences the exchange of counter ions with the propagating species, which in turn can impact the final molecular weight.[149] Most recently, Kizhakkedathu's group reported a large-scale synthesis of mega hyperbranched polyglycerols (mega hPGs) with molecular weights in the range of millions of Daltons, reaching up to 9.3 MDa, and a polydispersity index as narrow as 1.2.[150] The group combined the macroinitiator and solvent-based methods in their ROMBP reaction. The macroinitiator, a 10% deprotonated 840 kDa hPG using KH in DMF, was utilized, and a slow addition of glycidol was followed to produce the mega HPGs. This macroinitiator was initially synthesized using partially deprotonated TMP in dioxane at 90 °C with a gradual introduction of glycidol.[150] The resulting mega hPGs maintained their characteristics of high water solubility, low intrinsic viscosity, and globular structure.[150]
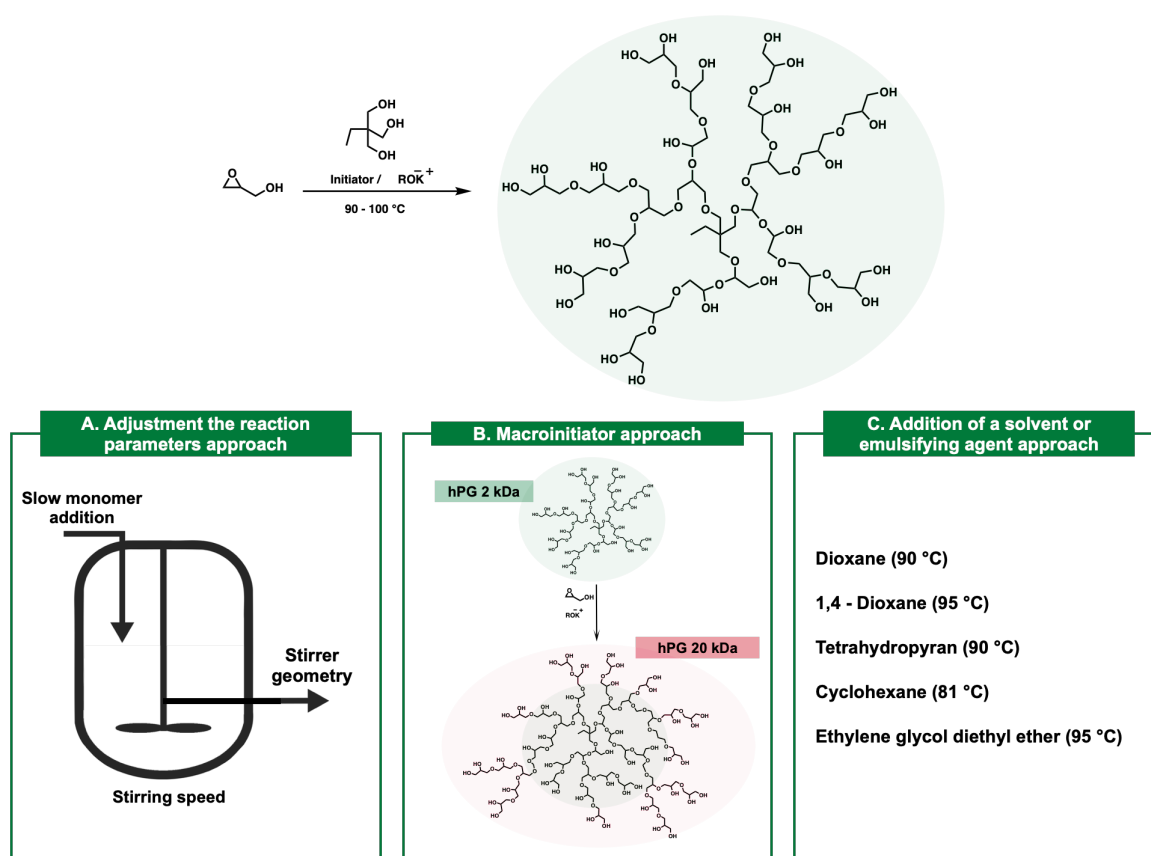
Figure 16. Synthesis of hPG through ROMBP reaction mechanism using TMP as an initiator. A higher molecular weight can be obtained by A) adjusting the reaction parameter, B) using a macroinitiator and C) the addition of a solvent emulsifying agent.

1.6.3 Copolymerization – methods and structures

Copolymerization of two different monomers M_1 and M_2 consists of incorporating both monomers in the final product covalently in opposition to dealing with the mixture of the two homopolymers. The synthesis of copolymers allows for the modification of homopolymer

characteristics by incorporating a suitably selected second monomer unit. As the homopolymers are integrated within the same molecular structure, the resulting copolymer exhibits attributes of both individual homopolymers. This approach enables the alteration of properties like crystallinity, flexibility, as well as melting temperature (T_m) and glass transition temperatures (T_g), through the formation of copolymers.[151] The process of copolymerization offers a significant benefit in that it allows for the strategic incorporation of the characteristics of different homopolymers. Consider the case of polystyrene: inherently brittle, hard, and with only modest solvent resistance. By introducing different comonomers into its structure, the utility spectrum of styrene-based polymers can be significantly broadened. Copolymers incorporating styrene as a comonomer can form either thermoplasts [e.g., poly(styrene-co-acrylonitrile), SAN] or elastomers [e.g., poly(styrene-co-butadiene), SBR, and poly(styrene-block-butadiene-block-styrene), SBS. For instance, integrating acrylonitrile into the polymer enhances the strength and ductility of SAN-polymers and improves their resistance to aliphatic hydrocarbons and mineral oils compared to polystyrene alone. Upon copolymerization, the combination of the two building blocks, the two different monomers, can end up in a virtually infinite number of different products. However, the kinetics of reaction between the homopolymerization and the copolymerization of the monomers (relative reactivity ratios) can result in a defined structure of the end-copolymer. These structures can be a random, alternating, block or two separated homopolymers (Figure 17A).
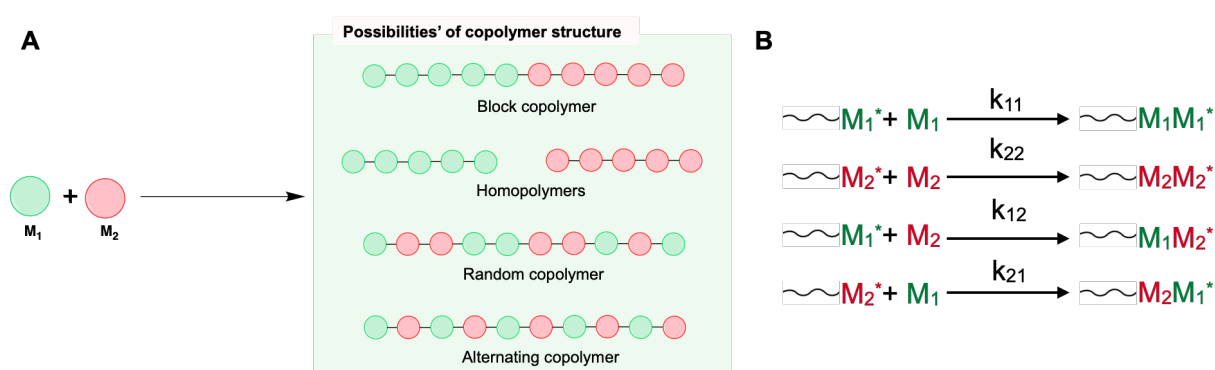
Figure 17. A) The possibilities of copolymer structure of the copolymerization of monomer M_1 and monomer M_2; the obtained copolymer is either a block, random alternating copolymer or two distinct homopolymers. B) The four different reactions that might occur when copolymerizing M_1 and M_2 and the four kinetic constants that can be derived from the reactions.

Mayo-Lewis developed an equation to determine the relative reactivity ratios of comonomers, based on their consumption rates in relation to the ongoing polymerization reactions. A chain growth reaction can propagate through a radical, an anion, a cation or

catalyst-driven. In this context, four distinct reactions are possible (Figure 17B). The formulated equations that describe the consumption rates of the monomers are presented in Equations 1 and 2.

$$-\frac{d[M_1]}{dt} = k_{11}[\sim M_1^*][M_1] + k_{21}[\sim M_2^*][M_1] \tag{1}$$

$$-\frac{d[M_2]}{dt} = k_{22}[\sim M_2^*][M_2] + k_{12}[\sim M_1^*][M_2] \tag{2}$$

Assuming a steady-state condition regarding the number of activated monomers, Equations 1 and 2 can be reformulated as follows:

$$k_{12}[\sim M_1^*][M_2] = k_{21}[\sim M_2^*][M_1] \tag{3}$$

$$[\sim M_1^*] = \frac{k_{21}[\sim M_2^*][M_1]}{k_{12}[M_2]} t \tag{4}$$

Dividing Equation 1 by Equation 2, Equation 5 can be obtained:

$$\frac{d[M_1]}{d[M_2]} = \frac{[M_1]}{[M_2]} \cdot \frac{k_{11}[\sim M_1^*] + k_{21}[\sim M_2^*]}{k_{22}[\sim M_2^*] + k_{12}[\sim M_1^*]} \tag{5}$$

The formulation presented in this equation characterizes the chemical composition of the copolymers generated at any given time point.[152] By incorporating Equation 4 into Equation 5 and subsequently simplifying the resultant expression, Equation 6 is derived:

$$\frac{d[M_1]}{d[M_2]} = \frac{[M_1]}{[M_2]} \cdot \frac{\frac{k_{11}}{k_{12}} \cdot [M_1] + [M_2]}{\frac{k_{22}}{k_{21}} \cdot [M_2] + [M_1]} \tag{6}$$

r_1 and r_2 are defined as the copolymerization parameters, representing the relative reactivity ratios of the comonomers. These are calculated as follows:

$$r_1 = \frac{k_{11}}{k_{12}} \tag{7}$$

$$r_2 = \frac{k_{22}}{k_{21}} \tag{8}$$

The final Mayo-Lewis copolymerization equation is obtained as Equation 9:

$$\frac{d[M_1]}{d[M_2]} = \frac{m_1}{m_2} = \frac{[M_1]}{[M_2]} \cdot \frac{r_1[M_1] + [M_2]}{r_2[M_2] + [M_1]} \tag{9}$$

In this context, m_1 and m_2 denote the concentrations of monomers M_1 and M_2, respectively, within the newly synthesized polymer, while $[M_1]$ and $[M_2]$ denote the initial concentrations of M_1 and M_2 in the reaction mixture. The terms r_1 and r_2 refer to the copolymerization parameters. It should be noted that the assumption of constant relative monomer concentrations is valid only at very low conversion rates (below 10%). Therefore, this assumption allows for only an approximate first estimation of the copolymer's composition.

Based on the values of the relative reactivity ratios, r_1 and r_2, the type of polymerization can be determined. These values and their corresponding polymerization types are summarized in Table 3.[153]

Table 3. Copolymerization Parameters and the Corresponding Molecular Structure

Copolymerization parameter values	Molecular structure
$r_1 > 1$ and $r_2 > 1$	Block copolymer
$r_1 \approx r_2 \approx 0$	Alternating copolymer
$r_1 \approx r_2 \approx 1$	Statistical/random copolymer
$r_1 > 1$, $r_2 < 1$ and $r_1 \cdot r_2 = 1$	Ideal random copolymer
$r_1 \gg 1$ and $r_2 \gg 1$	Homopolymers

Mayo-Lewis approach.[152] In the Mayo-Lewis approach, experimental determination of copolymerization parameters can be achieved by modifying the Mayo-Lewis equation into a function where r_2 is expressed as a function of r_1. This is achieved by altering the initial monomer ratio $\frac{[M_1]}{[M_2]}$ and measuring the resulting m_2/m_1 ratio at a conversion rate below 10%. rearranging Equation 9 to express r_2 as a function of r_1 ($r_2 = f(r_1)$) results in the following formulation:

$$r_2 = \frac{[M_1]^2}{[M_2]^2} \cdot \frac{m_2}{m_1} \cdot r_1 + \frac{[M_1]}{[M_2]} \cdot \frac{m_2}{m_1} - \frac{[M_1]}{[M_2]} \tag{10}$$

$$a = \frac{[M_1]}{[M_2]} \tag{11}$$

$$b = \frac{m_2}{m_1} \tag{12}$$

Resulting in the Equation 13:

$$r_2 = a^2 \cdot b \cdot r_1 + a \cdot b - a \tag{13}$$

Given that $[M_1]$ and $[M_2]$ are the initial concentrations of the monomers and m_1 and m_2 are the concentrations of the remaining monomers at a specific conversion rate (less than 10%), these values can be empirically determined (for instance, using 1H NMR). $r_2 = f(r_1)$ can be graphically represented as a linear equation (Equation 13), where the slope is given by $a^2 \cdot b$ and the intercept by $a \cdot b - a$. Altering the initial monomer concentrations results in varying linear equations; the point where these linear equations from different experiments intersect provides the values for r_1 and r_2. Conducting a greater number of experiments leads to a more

accurate estimation of the copolymerization parameters. Figure 18B illustrates the method of determining the reactivity ratios through the Mayo-Lewis approach.
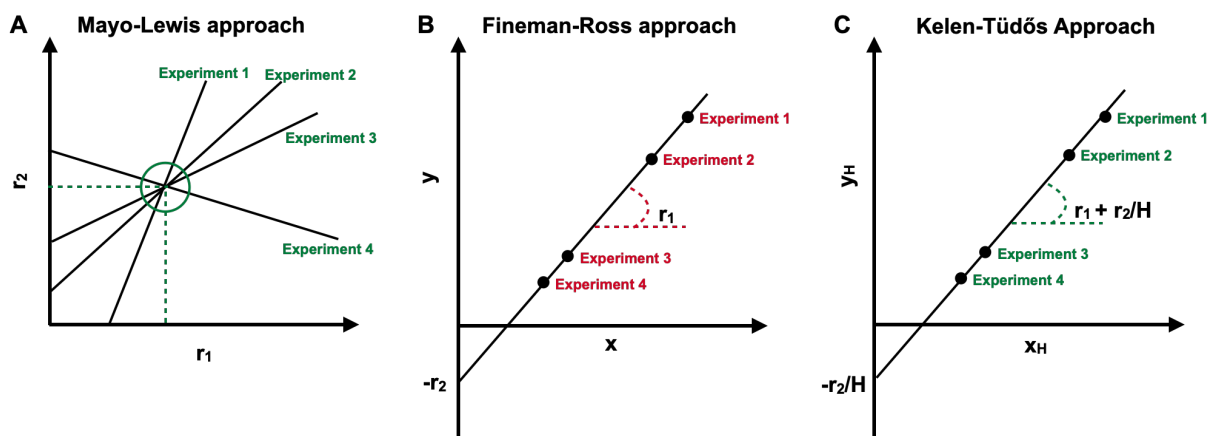
Figure 18. Experimental reactivity ratios' calculations based on the Mayo-Lewis equation, using the three different approaches: A) Mayo-Lewis, B) Fineman-Ross, and C) Kelen Tüdős.

Fineman-Ross Approach.[152] Fineman and Ross adapted the Mayo-Lewis method to account for potential deviations from the point of intersection. In their approach, r_1 is represented as the gradient of the linear function, while $-r_2$ is denoted as the y-intercept, as described in the following Equation:

$$y = r_1 x - r_2 \tag{14}$$

In relation to the Mayo-Lewis equation, the variables y and x can be redefined as follows:

$$y = \frac{[M_1]}{[M_2]} \cdot \frac{m_2}{m_1} \cdot \left(\frac{m_2}{m_1} - 1\right) \tag{15}$$

$$x = \left(\frac{[M_1]}{[M_2]}\right)^2 \cdot \frac{m_2}{m_1} \tag{16}$$

In a series of experiments, where the initial concentrations of monomers vary, a set of y and x values are generated. From these values, a linear fit can be constructed. The slope of this linear fit represents r_1, and the y-intercept corresponds to $-r_2$ (Figure 18B).

Kelen-Tüdős Approach.[152] In this third approach, Kelen and Tüdős developed a mathematical equation incorporating a scaling factor H, as shown in Equation 17:

$$H = \frac{F_{min}}{F_{max}} \tag{17}$$

In this equation, F_{min} and F_{max} signify the minimum and maximum monomer ratios, respectively, within the Fineman-Ross method, aimed at augmenting the reliability of the

copolymerization parameters derived. Thus, by dividing Equation 6 by H + x, the formulation for the Kelen-Tüdős approach is derived, as presented in Equation 20 and Figure 18C:

$$\frac{y}{H+x} = \frac{r_1\,x - r_2}{H+x} \tag{18}$$
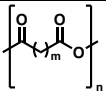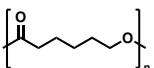
$$\frac{y}{H+x} = -\frac{r_2}{H} + \left(r_1 + \frac{r_2}{H}\right)\cdot\frac{x}{H+x} \tag{19}$$

$$y_H = -\frac{r_2}{H} + \left(r_1 + \frac{r_2}{H}\right)\cdot x_H \tag{20}$$

1.6.4   Synthetic biodegradable polymers

Biodegradable polymers are gaining increasing focus in contemporary medical applications. They are primarily utilized in surgical sutures, implants, and DDSs. Key characteristics to consider for these polymers include their non-inflammatory nature, a degradation timeline aligned with their intended function, suitable mechanical properties, and the generation of non-toxic by-products upon degradation. Table 4 presents a comprehensive overview of various biodegradable polymeric families, outlining their specific applications, benefits, drawbacks, and molecular structures.[154, 155]

Table 4. Biodegradable Polymers and their Applications, Advantages, Disadvantages and Structures

Polymer	Applications	Advantages	Disadvantages	Structure
Polyanhydrides	Drug delivery Tissue engineering	+ Significant monomer flexibility + Controllable degradation rates	– Low molecular weights – Week mechanical properties	
Polyacetals	Drug delivery	+ Mild pH degradation products + pH sensitive degradation	– Low molecular weights – Complex synthesis	
Polycaprolactone	Drug delivery Tissue engineering	+ Highly processable + Many commercial vendors available	– Limited degradation	
Polylactide	Drug delivery Tissue engineering	+ Highly processable + Many commercial vendors available	– Limited degradation – Highly acidic degradation products	
Polyamides	Drug delivery	+ Conjugatable side group + Highly biocompatible degradation products	– very limited degradation – Charge-induced toxicity	

The polyesters, polyglycolide (PGA), polylactide (PLA), and polycaprolactone (PCL) are all approved by the FDA and are among the most extensively documented biodegradable polymers for biomedical use.[156-158] These polymers can be synthesized via ring-opening polymerizations of their respective monomers: glycolide for PGA, lactide for PLA, and ε-caprolactone for PCL. Polyanhydrides represent another category of FDA-approved,

biodegradable polymers. They degrade gradually into their respective diacids. Although they can be synthesized cost-effectively with customizable properties, their quick degradation rate necessitates storage at low temperatures.[159]

1.6.5 Biodegradable dendritic polyglycerols

While high molecular weight hPGs display beneficial properties, previous studies have highlighted a significant limitation in their *in vivo* application: the potential for bioaccumulation in the liver due to a lack of biodegradability.[160] As a result, creating biocompatible and physiologically degradable polymers remains a challenge in this field. For hPGs, various strategies have been employed to introduce degradable elements into the polymer's backbone or initiator. One approach is the copolymerization of cyclic esters with glycidol using a catalytic process and a coordination-insertion ring-opening polymerization mechanism, or an anionic pathway for ring opening. The degradable groups incorporated include acetals[161, 162] or ketals[143, 163], which enable pH-responsive degradation of hPG. Ester linkages, capable of degrading under physiological enzymatic conditions, are another type of degradable bond.[164, 165] Additionally, the differential reduction potential of biological systems, characterized by higher GSH concentrations in the cytosol (2-10 mM) compared to extracellular fluids (<10 μM),[166-168] can be leveraged. One approach is to develop redox-sensitive hPGs by incorporating disulfide bonds in the backbone, allowing degradation in the reductive environment of the cytosol. However, the synthesis of disulfide-bond-containing polymers typically involves condensation polymerization of monomers pre-loaded with disulfide bonds,[169] copolymerization of dihalide-containing monomers with sodium disulfide,[170] or the oxidative coupling of sulfhydryl monomers,[171] making the process somewhat limited due to the sensitivity of disulfide bonds to many polymerization conditions. Son *et al.* was the first to overcome this limitation by developing a novel hPG architecture with disulfide bonds, synthesized via ring-opening polymerization of an epoxide monomer like glycidol but containing a disulfide bond. These disulfides can be reduced to thiols in a GSH-rich environment.[172] Concurrently, Kizhakkedathu *et al.* developed high molecular weight bioreducible hPGs by copolymerizing glycidol with the same monomer used by Son *et al.*, employing 1,4-dioxane as a solvent.[173] Figure 19 shows the copolymerization of glycidol with different comonomers containing a degradable moiety and the degradation of the polymer upon the interaction with a stimuli.
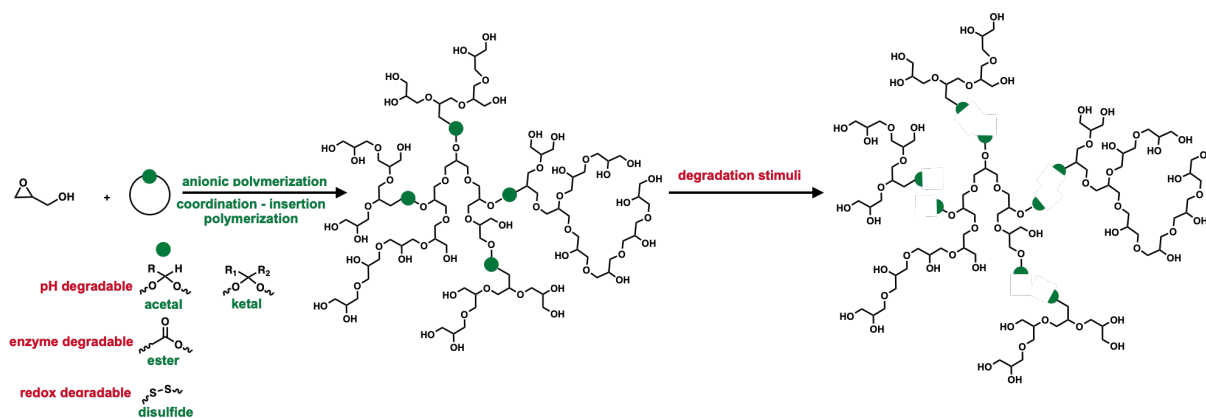
Figure 19. The polymerization of glycidol with another cyclic monomer containing a degradable moiety (acetal, ketal, ester, or disulfide) will result in a degradable copolymer where these moieties can be cleaved when subjected to a degradation stimuli (pH, enzyme or redox).

1.6.6 Dendritic polyglycerols sulfates – as active targeting groups
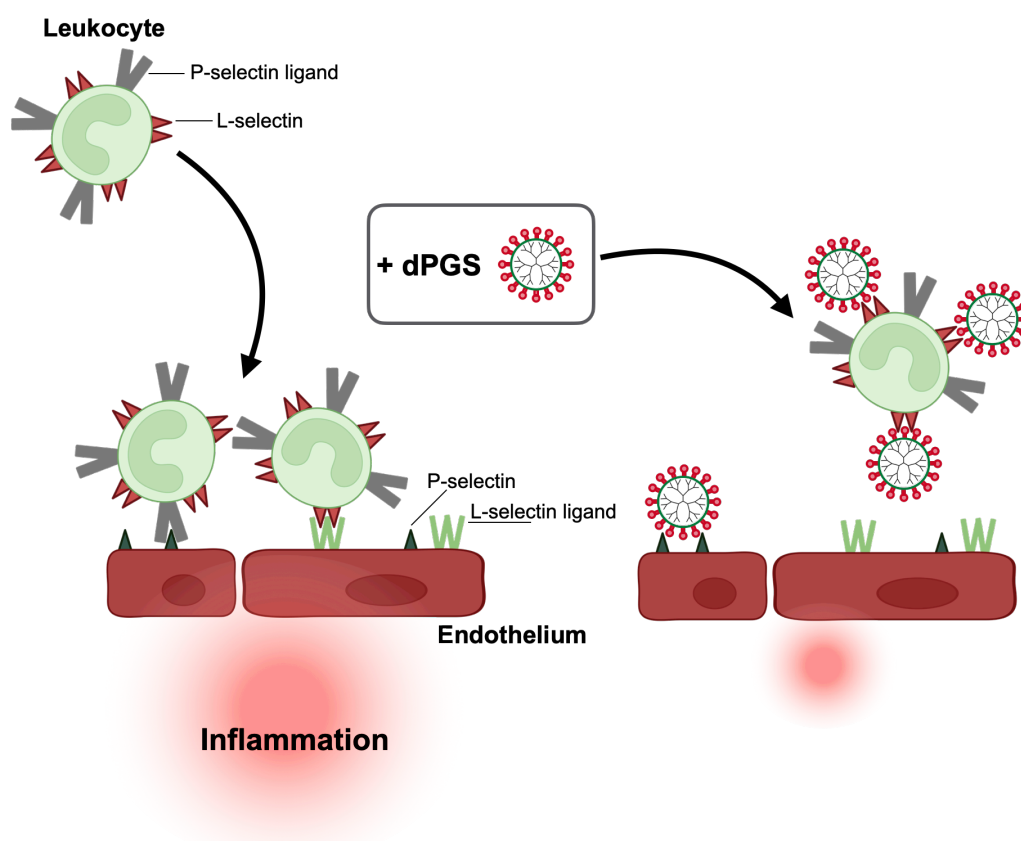
Figure 20. dPGS weakens the inflammatory response by reducing leukocyte extravasation. dPGS inhibits leukocyte extravasation by adhering to the P and L-selectins.

The motivation behind employing sulfates as active targeting groups was inspired by the discovery of their treatment against inflammatory diseases. An uncontrolled immune response, caused by chronic inflammation could lead to substantial flux of leukocytes that can further

damage healthy tissues. Hence, to prevent this event from occurring, anti-inflammatory therapy relies on targeting leukocyte trafficking. Dernedde *et al.* reported a dendritic polyglycerol sulfate (dPGS) system as macromolecular inhibitors that can bind multivalently and mimic occurring ligands on leukocytes (L-selectin) and endothelial cells (P-selectin) and offer possible treatment for inflammatory responses (Figure 20).[174] Later, Weinhart *et al.* explored the role of dimension in multivalent binding of dPGS to L-selectin with respect to size (by varying the molecular weight) and surface charge density (by varying the degree of sulfation). They measured the efficacy of L-selectin inhibition via SPR-based *in vitro* assay and cell-based flow chamber assay for dPGS ranging from 3 to 800 kDa, while fixing the charge density and then fixing the molecular weight while varying the charge density by varying the degree of sulfation.[175] The half maximal inhibitory concentration (IC_{50}) values, resulting from the SPR measurements, were lower for higher molecular weight dPGS and higher charge density, meaning higher affinity to L-selectin (Figure 21A).[175] The structure-affinity relationship observed in dPGS indicates that its substantial inhibitory capability is attributable not only to the strong electrostatic interactions with cationic surface potentials on L-selectin but also to the steric hindrance of the carbohydrate binding site caused by the large, flexible particles of dPGS.[175] Weinhart *et al.* also explored different polyanions based on dendritic polyglycerol to conclude that sulfate groups demonstrated outstanding performance, evidenced by the exceptionally low IC_{50} obtained from the L-selectin inhibition assays.[176] The anionic functional groups tested were carboxylates, phosphates, phosphonates, sulfonates, and bisphosphonates and sulfates with a degree of functionalization higher than 80% (Figure 21B).[176] The biodegradable derivates of hPG with caprolactones incorporated in the polymeric backbone were also sulfated with a variety of degree of functionalization and confirmed to have low IC_{50} for high molecular weight of the polymer and high degree of sulfation.[177]
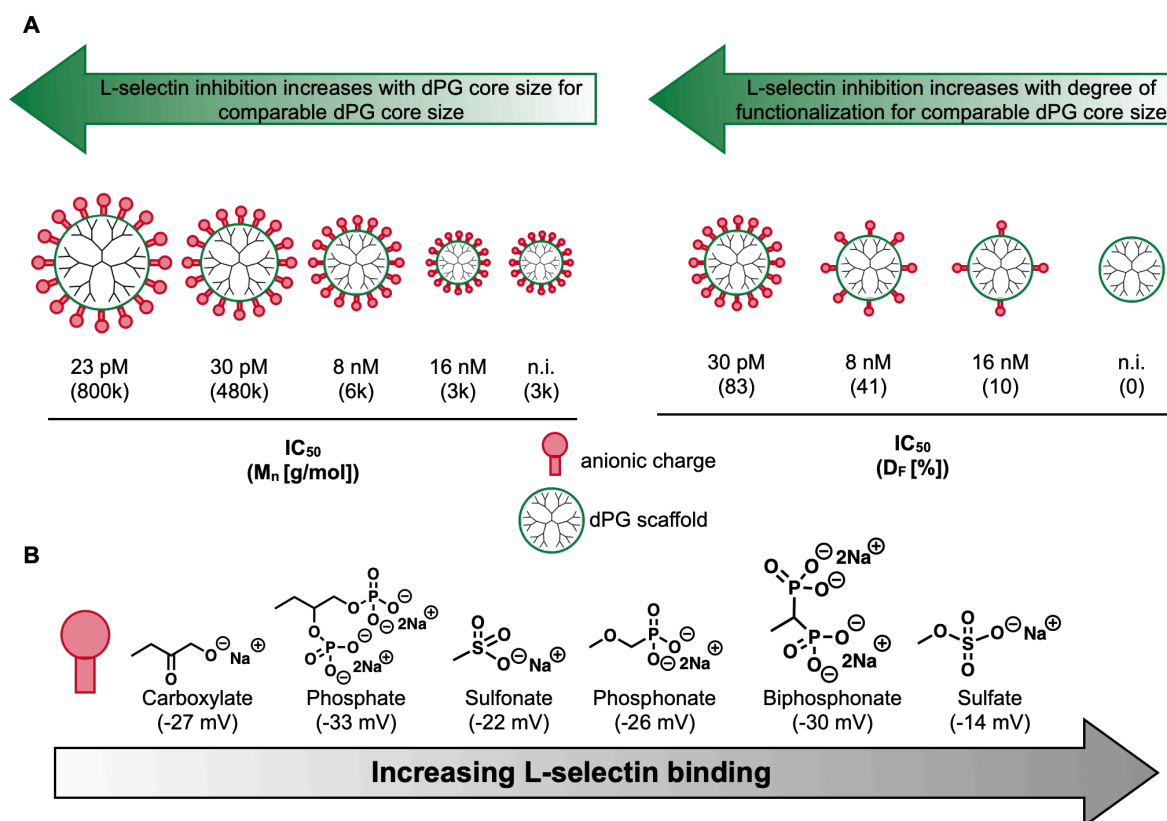
Figure 21. A) L-selectin inhibition of dPGS. Inhibition is enhanced for a bigger core size with similar degree of functionalization (left) and for a higher degree of functionalization for the same core size (right). B) dPG-based anions and their affinity towards L-selectin. The degree of functionalization was set to 81%, however the L-selectin biding could not be directly correlated to the surface charge represented by the ζ-potential measurements (shown in brackets).

The overexpression of cell-adhesion molecules (CAMs) for the mediation of leukocyte recruitment and extravasation, including selectins are known to contribute to cancer metastasis through co-option of inflammatory pathways.[178] Thus, scientists started exploring conjugates of natural structures with high anti-inflammatory activity such as heparin, a highly sulfated glycosaminoglycan for tumor targeting. Chung *et al.* reported an enhanced tumor targeting nanoparticles based on heparin coated with PLGA and proved its interaction with surface receptors of the cells.[179] This ultimately led to the employment of dPGS in drug delivery systems for site-specific tumor targeting. The sheddable dendritic polyglycerol sulfate redox-responsive micelles loaded with doxorubicin (DOX) reported by Zhong *et al.* demonstrated high abilities in tumor cell-targeting when tested *in vivo*.[180]

2 Scientific Goals

The three main challenges that researchers are tackling when addressing new drug delivery systems are (i) the solubilization of hydrophobic drugs to ameliorate their transport, (ii) the prevention of the accumulation of the material in the human body and (iii) the specific targeting and delivery of the API.
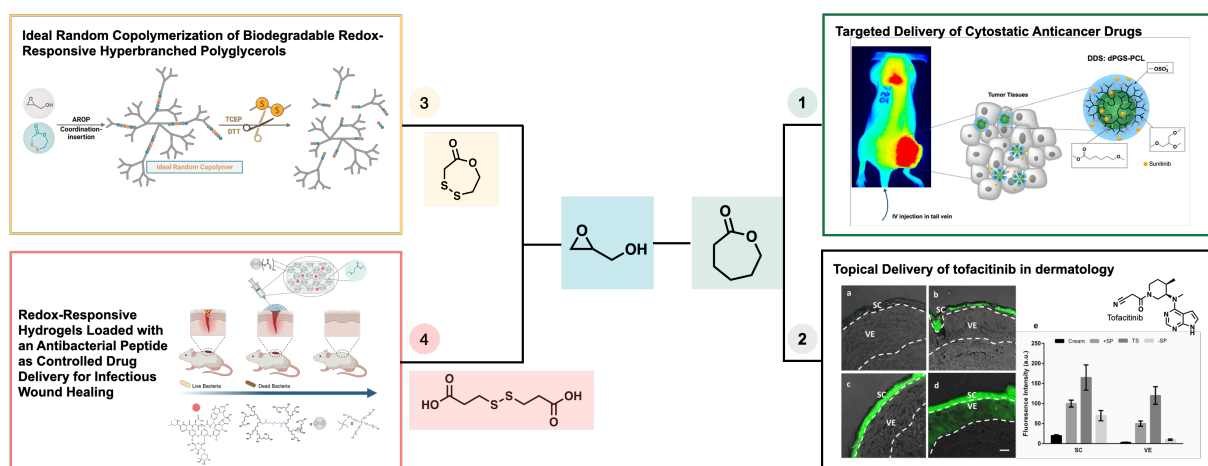
Figure 22. Schematic representation of the four projects covered in this thesis.

These challenges are addressed in this thesis by designing a system that is based on polyglycerol as a highly soluble and biocompatible polymer with a globular architecture. Glycidol, the monomer that forms polyglycerol, is randomly copolymerized with cyclic 7-membered ring lactones that contain moieties that are degradable under biological stimuli. Another comonomer that can be integrated in the polyglycerol backbone is a linear diacid containing a disulfide (Project 4). The advantage of integrating these biodegradable moieties addresses two points: (i) the avoidance of the accumulation of the polymeric material by ensuring that the system will breakdown in size and is eliminated from the body and (ii) through the degradation of the system the encapsulated cargo will be released. The targeting characteristic of the system is achieved by sulfating the hydroxyl end-groups of the biodegradable polyglycerol that has been previously studied intensively and shown to specifically act against inflammation. Another important scientific focus of this thesis, in addition to the parameters mentioned previously is to design a system that is relatively simple, following a straightforward synthesis that is reproducible and scalable. As well as, reducing the use of organic solvents during synthesis, purification as well as for the drug encapsulation. The loading of the drug in the DDS was a complete water-based protocol, where the API is physically encapsulated in the system instead of covalently bonded.

In the first two projects, glycidol was copolymerized with ε-caprolactone and then sulfated. The system was fully characterized in terms of molecular weight, size, zeta-potential, and TEM images before and after the encapsulation of API. For first project (Figure 22.1), sunitinib, an anti-cancer medication and a protein kinase inhibitor was encapsulated in the system. The performance of the system was tested through *in vitro* release studies, cytotoxicity, cellular uptake, and *in vivo* accumulation and effect on tumor reduction. The application of the second project was oriented towards inflammatory skin diseases (Figure 22.2). The encapsulated API was tofacitinib a JAK inhibitor. The objective was to improve the delivery and penetration of tofacitinib through the transport carrier and thus increasing its efficacy. The system's penetration was tested on *ex-vivo* human skin model, and for its effect on IL-6 and IL-8 release and STAT3 and STAT6 activation. Since the biodegradable sulfated polyglycerol with caprolactone incorporated in the backbone (dPGS-PCL) contains only an ester as a degradable moiety that can undergo degradation under an enzymatic stimulus, the aim was to develop another system that works on another stimulus that is more effective. GSH is a reducing agent that is overly express in tumor cells, so the third project aimed to use a 7-membered ring lactone that is an analogue to caprolactone but contains an additional disulfide bond within the ring (Figure 22.3). Since the comonomers quite similar, the project was dedicated to deducting the effects of the disulfide bond on the copolymerization especially regarding the end-structure of the copolymer formed. Through the synthesis of different polymers with different disulfide ratios following two copolymerization mechanisms, the project also focused on the effect of the disulfide ratio on the final characteristic of the polymer. At the end, the degradation of the copolymer was studied in addition to the biocompatibility by performing *in vitro* cytotoxicity and hemolysis assays. The fourth project integrated the disulfide bond into the system by using a diacid that contains a disulfide bond as a proton donor, hence an initiator for the polymerization (Figure 22.4). The resulting polymer was then integrated into a hydrogel that was then loaded with antibacterial peptide for a controlled drug delivery to infectious wound healing, the loaded hydrogel was tested through several antibacterial assays as well as *in vivo*. In conclusion, the thesis focused on the diversity of synthesizing biodegradable systems not only in the mechanism of synthesis, their formation in different architectures but also the diversity of their applications.

3 Publications

3.1 Biodegradable Dendritic Polyglycerol Sulfate for the Targeted Delivery of Cytostatic Anticancer Drugs

Mariam Cherri[‡], Magda Ferraro[‡], Ehsan Mohammadifar*, Elisa Quaas, Katharina Achazi, Kai Ludwig, Carsten Grötzinger, Michael Schirner, Rainer Haag*

ACS Biomaterials Science & Engineering **2021***, 7(6), 2569-2579.*

[‡] equal contribution
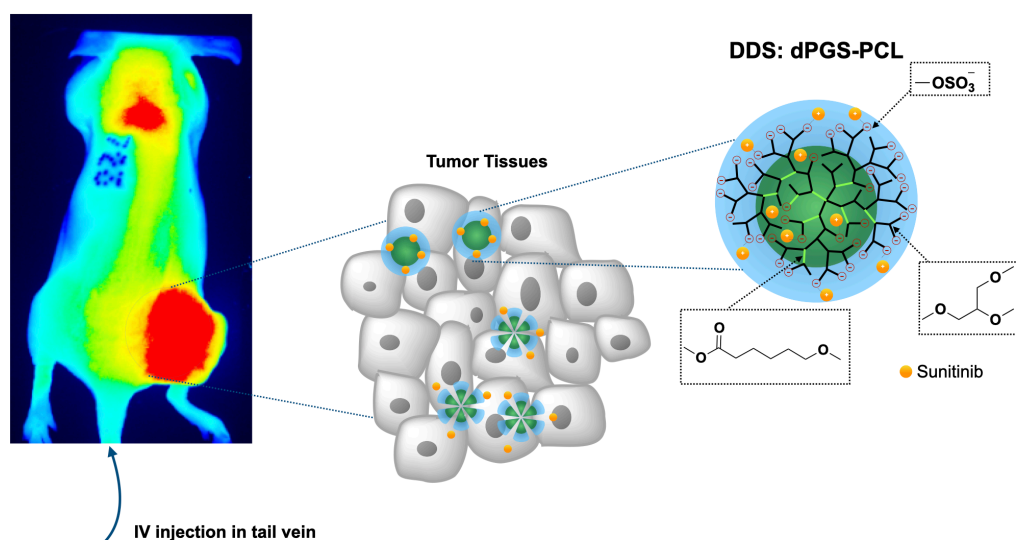
Figure 23. Reproduced from ref.[181]

Authors' Contribution

Mariam Cherri synthesized and characterized the sulfated copolymers, performed the encapsulation and release study of sunitinib, planned for the cellular uptake experiments and cell viability assays, interpreted the data, and co-wrote the first draft of the manuscript. Magda Ferraro supervised the project and co-wrote the first draft of the manuscript. Ehsan Mohammadifar developed the idea, supervised the project, and revised the first draft of the manuscript. Elisa Quaas performed the cell viability assays and the cellular uptake experiments. Katharina Achazi supervised and guided the biology part of the project. Kai Ludwig performed and interpreted the TEM images. Carsten Grötzinger performed and interpreted the *in vivo* bioaccumulation images. Michael Schirner provided planning and consulting for the *in vivo* experiments. Rainer Haag acquired funding, supervised, and guided the project.

3.2 Power of the Disulfide Bond: An Ideal Random Copolymerization of Biodegradable Redox-Responsive Hyperbranched Polyglycerols

Mariam Cherri*, J. Fernanda Romero, Luca Steiner, Mathias Dimde, Hanna Koeppe, Beate Paulus, Ehsan Mohammadifar, and Rainer Haag*
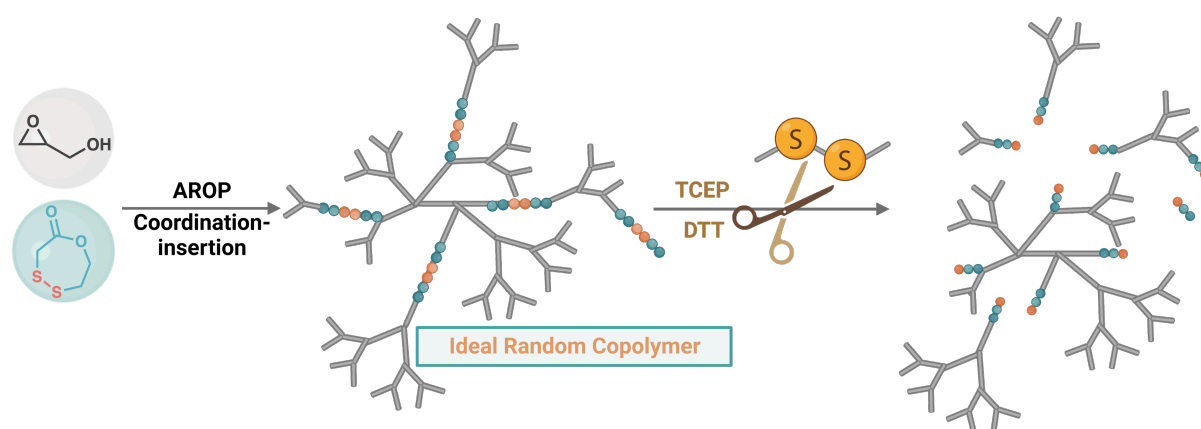
Figure 24. Reproduced with permission from ref. [182]

Authors' Contribution

Mariam Cherri developed the project idea, established the kinetics experiments for the copolymerization parameters calculations, synthesized and characterized the copolymers with different feed ratios and molecular weights according to both mechanisms AROP and coordination-insertion, performed the degradation studies and developed a set-up for the bioassays and wrote the manuscript. J. Fernanda Romero performed the experiments for the copolymerization parameters calculations, including data interpretation and revised the first draft of the manuscript. Luca Steiner developed, performed, and interpreted the theoretical calculations. Mathias Dimde recorded the TEM images and helped with data interpretation and the revision of the first draft of the manuscript. Hanna Koeppe performed the hemolysis assays. Beate Paulus provided guidance for the theoretical calculations. Ehsan Mohammadifar provided his guidance throughout the project and revised the first draft of the manuscript. Rainer Haag provided guidance, supervision, and guidance.

3.3 Topical Delivery of Tofacitinib in Dermatology: the Promise of a Novel Therapeutic Class Using Biodegradable Dendritic Polyglycerol Sulfates

Fatemeh Zabihi[‡], **Mariam Cherri**[‡], Xiao Guo, Fiorenza Rancan, Fabian Schumacher, Ehsan Mohammadifar, Burkhard Kleuser, Wolfgang Bäumer, Michael Schirner, Annika Vogt*, Rainer Haag*.

[‡] equal contribution
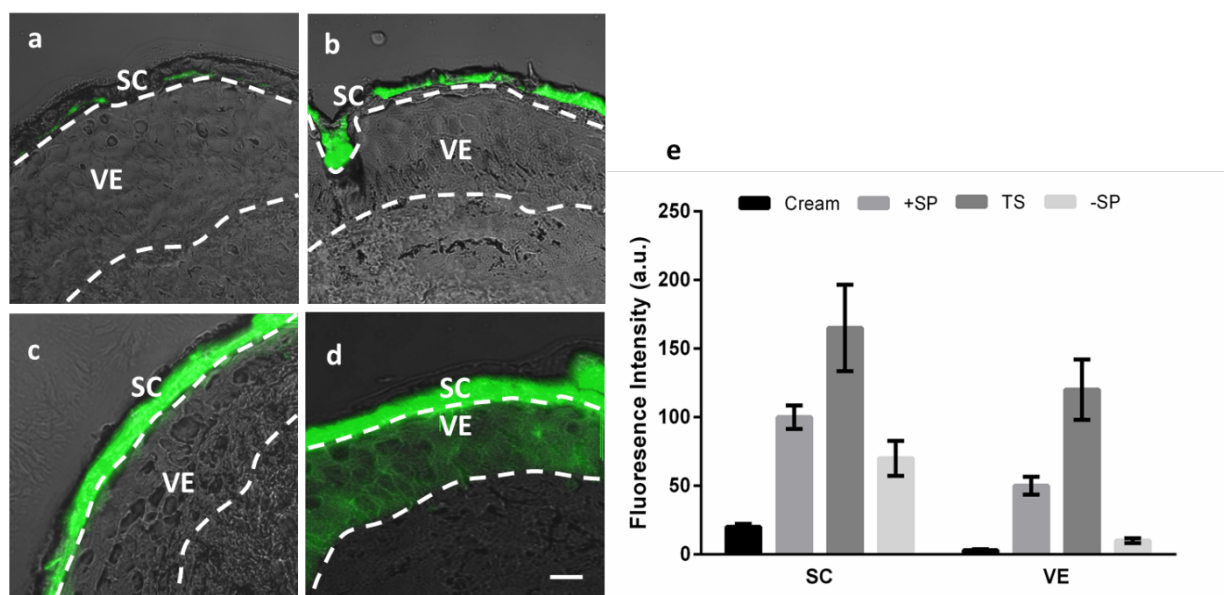
Figure 25. Reproduced with permission from ref. [183]

Authors' Contribution

Mariam Cherri synthesized and characterized the dPGS-PCL system loaded it with sunitinib and tofacitinib and purified it, performed the release studies and *in vitro* assays, and wrote, reviewed, and edited the manuscript. Fatemeh Zabihi performed the *ex vivo* skin studies in addition to writing, reviewing, and editing the manuscript. Xiao Guo and Fiorenza Rancan participated in the performance of the *ex vivo* skin studies. Fabian Schumacher was responsible for LC-MS/MS measurements to characterize the loading and release of tofacitinib from the carrier. Ehsan Mohammadifar supervised the synthesis. Burkhard Kleuser, Wolfgang Bäumer and Michael Schirner participated in the conceptualization of the project. Annika Vogt, and Rainer Haag conceptualized, supervised, and acquired funds for the project.

3.4 Redox-Responsive Hydrogels Loaded with an Antibacterial Peptide as Controlled Drug Delivery for Infectious Wound Healing

Mariam Cherri, Paraskevi Stergiou, Zainab Ahmadian, Tatyana L. Povolotsky, Boonya Thongrom, Xin Fan, Ehsan Mohammadifar*, Rainer Haag*

 (submitted)
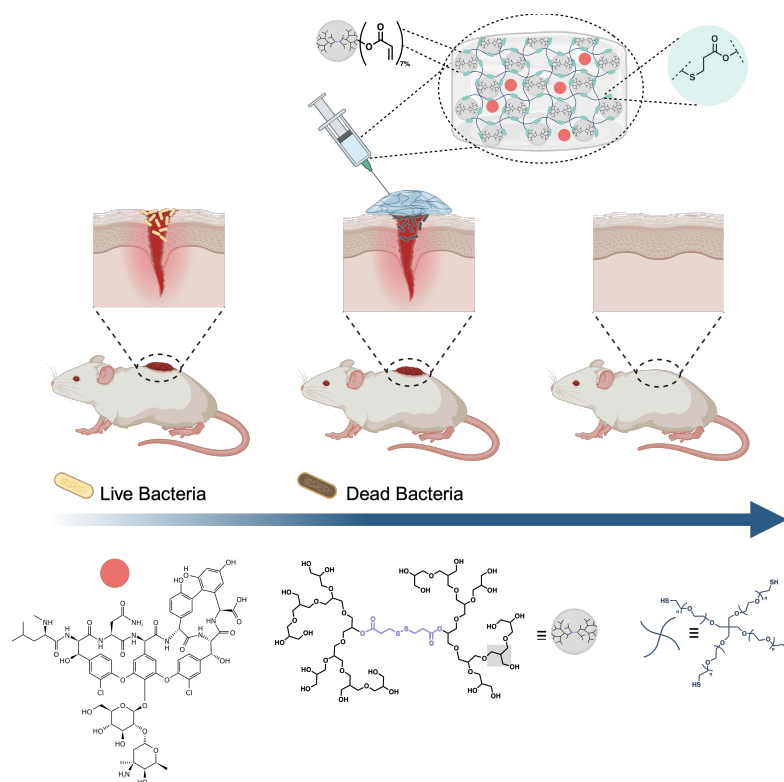
Figure 26. Graphical Abstract for Manuscript 3.4

Authors' Contribution

Mariam Cherri synthesized the redox-responsive hyperbranched polyglycerol building block of the hydrogel, and the hydrogel formation including the characterization of both. In addition to conceptualizing the degradation studies, encapsulation of both FITC-Albumin and vancomycin in addition to the release studies. Mariam Cherri conceptualized and performed the cytotoxicity assays for the hydrogels. Paraskevi Stergiou co-performed the synthesis and formation of the hydrogel, and characterization including rheology measurements, encapsulation, and release of APIs. Zainab Ahmadian conceptualized and performed the *in vivo* studies. Tatyana L. Povolotsky performed the antibacterial assays. Boonya Thongrom synthesized the 4-arm-PEG. Xin Fan recorded the SEM images. Ehsan Mohammadifar Conceptualized and supervised the project. Rainer Haag conceptualized, supervised, and acquired funds for the project.

Redox-Responsive Hydrogels Loaded with an Antibacterial Peptide as Controlled Drug Delivery for Healing Infectious Wounds

Mariam Cherri, Paraskevi S. Stergiou, Zainab Ahmadian, Tatyana L. Povolotsky, Boonya Thongrom, Xin Fan, Ehsan Mohammadifar*, Rainer Haag*

M. Cherri, P. S. Stergiou, B. Thongrom, X. Fan, T. L. Povolotsky, E. Mohammadifar, R. Haag
Institute of Chemistry and Biochemistry
Freie Universität Berlin
Takustr. 3, 14195 Berlin, Germany
Z, Ahmadian
Department of Pharmaceutics, School of Pharmacy
Lorestan University of Medical Sciences
Khorramabad, Iran

ehsan@zedat.fu-berlin.de
haag@chemie-berlin.de

Abstract: Infectious wounds occur when harmful microorganisms such as bacteria or viruses invade a wound site. Its problems associated include delayed healing, increased pain, swelling, and the potential for systemic infections. Therefore, developing new wound dressing materials with antibacterial effects is crucial for improving the healing process. Here we developed a redox-degradable hydrogel loaded with an antibacterial peptide (vancomycin) in a straightforward gram-scale synthesis. The hydrogel structure consists of a disulfide bond-containing hyperbranched polyglycerol (SS-hPG) which is cross-linked by 4-arm polyethylene glycol-thiol (4-arm PEG-SH). The polymerization mechanism and full characterization of SS-hPG are described as we report this synthesis for the first time. The controlled release of antibacterial peptide follows, as the hydrogel degrades in a reductive environment triggered by glutathione. We used rheology to ascertain the hydrogel's mechanical characteristics, such as stiffness, and self-healing, determining these properties for different ratios and concentrations of both blocks. Fluorescein isothiocyanate-albumin (FITC-albumin) and vancomycin were both

loaded into the gel, and the guest release kinetics were assessed for both slow and on-demand releases. Finally, our *in-vitro* and *in-vivo* experiments proved that the vancomycin-loaded hydrogel acts as an antibacterial barrier for wound dressing and accelerates the healing of infectious wounds in a mouse model.

1. Introduction

The most important function of the skin, as the first line of defense, is to protect the body against microbial invasions. However, as the outermost organ, it is always vulnerable to damage caused by wounds. Injured skin offers a suitable site for the accumulation and proliferation of bacteria, leading to infection and delaying wound healing.[1] The optimal process of wound healing can be divided into four phases, which occur interdependently and simultaneously: (i) vasoconstriction and coagulation, collectively leading to hemostasis, (ii) acute inflammation, (iii) cellular proliferation and (iv) wound remodeling.[2] In proliferation, new extra cellular matrix (ECM), collagen and fibronectin by fibroblasts, their differentiated counterparts, and the myofibroblasts are deposited.[2-3] Acute inflammatory response is a crucial stage in the course of wound healing, providing early protection against bacteria by first recruiting pathogen-destroying phagocytic neutrophils and later recruiting macrophages.[2-3] Since long-term inflammatory responses are correlated to chronic wounds, bacterial infection is one of the most serious complications affecting wound healing and tissue regeneration. The treatment of these infections usually consists of the continuous administration of oral or intravenous antibiotics over a period of weeks or months. This can lead to inefficient antibiotic delivery to the target site, which in in turn can cause, in severe cases, sepsis – an infection throughout the entire body.[4] Furthermore, applying antibiotics to the body as a whole, and not only the target area, also causes collateral damage by killing the natural microbiota of the host. This effect can lead to further weakening of the immune system, allowing pathogenic or antibiotic-resistant bacteria to dominate the colonization of the host.[5] These challenges highlight the need for topical delivery systems that can increase antibiotic effectiveness by releasing it locally to the targeted wound site, while reducing side effects by decreasing the dosage. To accelerate the healing process, especially for extensively damaged chronic wounds of the types caused by injury or specific diseases, wounds should be covered by an effective dressing material, with features such as high biocompatibility, ability to retrain moisture, and mechanical properties well-suited to injured tissue and antibacterial action.[6] Conventional wound dressings, such as gauze, must be changed frequently, and the risks of infection, secondary damage during removal, and their lack of biological properties for wound healing

hampers their usage.[7] Hydrogels have gained high interest for wound dressing and healing applications due to several outstanding properties, such as wound adhesion, moisture retention, skin like softness, resemblance to biological tissues, and biocompatibility, all of which provide favorable conditions for wound healing. Additionally, the three-dimensional porous structure of hydrogels provides a suitable scaffold for loading antibacterial drugs, which can then be released and delivered in a controlled process. The drug release is achieved through either diffusion or the passive degradation of hydrogel.[8] Eventually, such degradation enables the dressing material to be removed from the wound without secondary damage. Degradable hydrogels are typically prepared by introducing a stimuli-responsive moiety into the backbone of a gel macromonomer, allowing degradation in response to stimuli such as pH, temperature, enzyme, redox state, etc.[9] This stimuli-responsive hydrogel degradation serves in turn as a stimulus to release therapeutic agents in a controlled manner, or to ensure the hydrogel's ultimate removal in cases when it is used as a bandage for infected wounds. Among different approaches for "on-demand" degradable hydrogels, the redox-responsive approach has directed much interest toward polymer-based hydrogels, which are typically synthesized by introducing a disulfide bond in a polymer backbone. Disulfide bonds can be cleaved to two thiol groups in response to variation in environmental redox state. In particular, redox-responsive hydrogels show enhanced degradation in response to the overexpression of glutathione (GSH) or reactive oxygen species (ROS) in tumor tissues, wounds, or bacterial infection sites.[10] The redox imbalance that prevails in the infected wound environment can stimulate either therapeutic agent release or hydrogel degradation. Recently, multiple redox-responsive hydrogels have been reported for improving wound healing, with applications including the release of therapeutic agents, mainly proteins.[11] GSH is a tripeptide (γ-Glu-Cys-Gly), sulfhydryl-containing compound that is abundant in different types of organisms; in fact, it is the most dominant intracellular thiol-containing tripeptide.[12] It is a biochemical workhorse: it participates in the regulation of gene expression, cell proliferation and apoptosis, signal transduction, enzyme and protein functions, and oxidative stress in biological systems.[12c, 13] Szabó *et al.* showed clear differences between molecular patterns of wound fluids in acute and chronic wounds through redox profiling.[14] The study has shown that, similarly to radical scavenging activity, GSH levels were elevated in chronic wound fluids in comparison to acute wounds.[14] In another study, Shukla and Rasik showed that in the analysis of 7 day wound

tissue, higher levels of GSH were shown in athymic mice in comparison to the wound tissue of normal mice.[15]

In this work, we present a one-step straightforward synthesis of a disulfide bond-containing hyperbranched polyglycerol macromonomer (SS-hPG). The synthesis is catalyst-free and solvent-free, and we carried it out on a 30 g scale. The synthesized SS-hPG is employed as a building block of a redox-responsive hydrogel that is chemically crosslinked to 4-arm-PEG-SH via thiol-Michael addition click reaction. An antibacterial peptide, vancomycin, was loaded in the redox-responsive hydrogel to be released either gradually or on demand. Crucially, the viscoelastic properties, mechanical strength, and degradation of SS-hPG, and the release time of the loaded antibiotic, can be tuned by varying the concentration of the polymeric components in the hydrogel.

2. Results & Discussion

2.1. Synthesis of redox-responsive hyperbranched polyglycerol
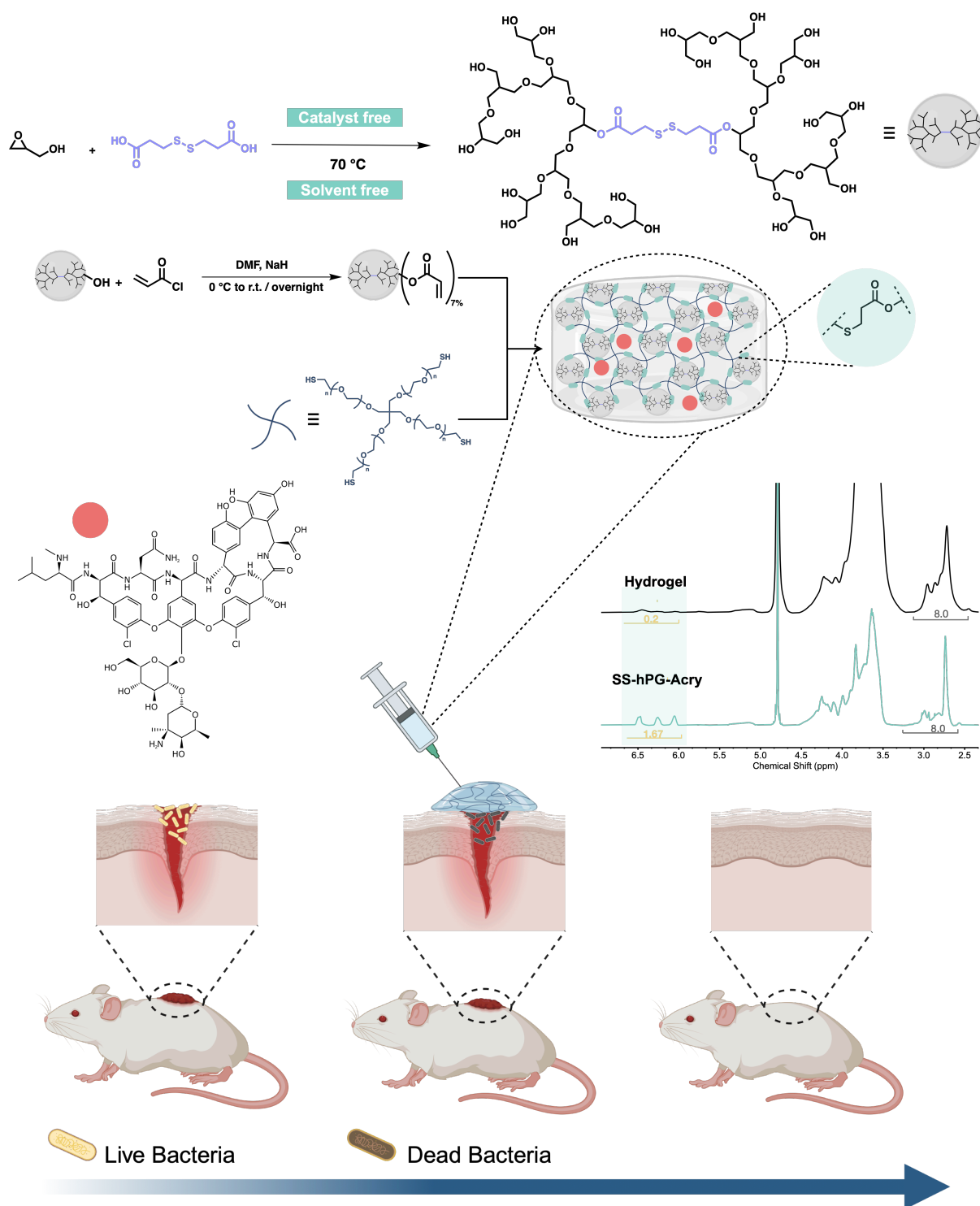
Figure 27. Overall scheme representing the synthesis of the hPG building block in addition to its acrylation and the hydrogel formulation. ^{1}H NMR verifies the formation of the hydrogel through the disappearance of the acrylate correspondent peaks, confirming the thiol-ene click reaction. The hydrogels were then loaded with vancomycin and applied over wounds in mice, destroying the existing bacteria and facilitating wound healing.

As one of the hydrogel components, the redox-responsive hyperbranched polyglycerol was achieved on a 30 g scale through the cationic polymerization of glycidol using 3,3'-dithiodipropanoic acid (DTDPA) as a monomer activator in a solvent-free reaction under mild conditions. (Figure S1A). DTDPA, with its two carboxylic acids (pK$_a$ 3.9), can activate the epoxide ring of glycidol toward cationic polymerization. Since DTDPA has two carboxylic acid groups on each end, the polyglycerol backbone could propagate telechelically, ending up with one molecule of DTDPA in the center of the hyperbranched polyglycerol backbone. The suggested mechanism was an activated-monomer (AM) cationic ring opening polymerization (Scheme S1), starting with proton transfer from the DTDPA's carboxylic acid groups to the epoxide ring, resulting in an activated glycidol. The deprotonated carboxylates of DTDPA could further open the activated epoxide rings, resulting in its incorporation in the polymer backbone. The reaction mechanism of carboxylic acid-containing molecules and glycidol has been fully investigated in our group's previously reported work, in which we copolymerized citric acid and glycidol.[16] We should mention that the hydroxyl group of glycidol could also initiate the ring opening, as hydroxyl groups are more reactive in nucleophilic attack than carboxylate,[17] but due to the high concentration of DTDPA and the high reactivity of protonated glycidol, carboxylate groups can also initiate the polymerization.

To study the effect of DTDPA on the polymer structure, experiments with different molar ratios of glycidol to DTDPA [Gly]:[DTDPA]; 5, 10 and 20 were carried out at 70 °C. The respective products of these experiments are called hPG$_5$-DTDPA, hPG$_{10}$-DTDPA, and hPG$_{20}$-DTDPA. The polymers were fully characterized using various spectroscopic and analytical methods to verify the incorporation of DTDPA in the polymeric backbone, quantify the disulfide content, and identify the degree of branching of the hyperbranched polyglycerol. The proton signals at 2.6-3.0 ppm are assigned to the methylene groups adjacent to the disulfide and ester-carbonyl in ^{1}H NMR and can be used as a first proof of the integration of DTDPA in the polymer structure. The decrease in the intensity of the ester-carbonyl stretches when decreasing the amount of initiator in the feed enforces the participation of DTDPA in the polymerization (Figure S1B). In FTIR, the absorbance of the ester-carbonyl stretch was present at 1729.6 cm^{-1} (Figure S1C). By comparison, the value for the carboxylic acid-carbonyl stretch of DTDPA was 1630.2 cm^{-1} (Figure S2). Figure S1D also shows the inverse-gated ^{13}C NMR spectrum of the resulting polymer. We identified the different structural units and calculated

their relative abundance as well as the degree of branching of AB_2 type monomers (Table S1), as reported by Hölter and Frey.[18]

The molecular weight of the resulting polymers is also reported in Table 1, as calculated from ^{1}H NMR (Equation S1). For chain growth polymerizations, including cationic polymerization, the degree of polymerization can be related to the kinetic chain length, which is the result of the number of consumed monomers per initiated chain.[19] Therefore, increasing the initiator concentration will lead to a decrease in the degree of polymerization, and hence a decrease of the average molecular weight of the polymer. hPG$_5$-DTDPA, with its 5:1 ratio of monomer to initiator, has a lower molecular weight than hPG$_{20}$-DTDPA with its 20:1 ratio. On the other hand, the degree of branching is inversely proportional to the ratio of DTDPA present in the feed. This may be related to the availability of many glycidol monomers that can be activated in the presence of a larger amount of DTDPA – and therefore the increased possibility of reaction between the secondary hydroxyl groups and other monomers.

We observed from the inverse gated ^{13}C NMR spectrum (Figure S1D) that the relative abundance of the $L_{1,4}$ structural units was high compared to the obtained $L_{1,4}$ structural units when glycidol was polymerized in an anionic fashion. The excessive presence of $L_{1,4}$ structural units also indicates that the mechanism of polymerization was through the activated monomer (AM) mechanism, where the glycidol monomers were first activated by carboxylic acid groups before undergoing the ring opening polymerization. We also demonstrated that DTDPA was incorporated in the dendritic polyglycerol core through two-dimensional heteronuclear multi-bond connectivity (HMBC) NMR (Figure S1E). The correlation between the proton signals of polyglycerol backbone at 3.5 and 4.2 ppm and the ester-carbonyl signal at 180 ppm was an indication for the existence of DTDPA in the polymeric core. To prove that the DTDPA has a major role in the polymerization of glycidol, we performed a control reaction under the same reaction conditions (catalyst free, solvent free and at 70 °C), but without DTDPA. After performing dialysis with a membrane of a molecular weight cutoff (MWCO) of 1 kDa, the reaction yield was negligible (less than 5%). Hence, we could conclude that DTDPA was essential in initiating the reaction.

We aimed to prove that the hyperbranched polyglycerol with DTDPA can undergo degradation under reductive conditions before incorporating it as a building block in a hydrogel. We wanted to present a proof of concept that the disulfide bond can be reduced in the presence of a reducing agent, while also identifying the resulting degradation products. hPG$_{10}$-DTDPA, referred to as SS-hPG throughout the remainder of this manuscript, was incubated in an aqueous solution containing 10 mM of 3,3′,3″-phosphanetriyltripropanoic acid (TCEP) as reducing

agent to cleave the disulfide bonds. After 3 days, ^{1}H NMR was used to identify the resulting degradation products (Figure S3). In the ^{1}H NMR of degradation products, the peak at 3.0 ppm, assigned to the methylene protons adjacent to the disulfide bond, disappeared, while a new peak appeared at 2.9 ppm, which is assigned to the methylene protons adjacent to thiol groups. Hence, our degradation products are a polyglycerol chain with a free thiol group, a polyglycerol chain completely detached from DTDPA due to the ester cleavage, and 3-mercaptopropanoic acid resulting from the cleavage of both ester and disulfide groups.

2.2. Formation and characterization of the hydrogel

To achieve a cross-linkable SS-hPG, 7% of the hydroxyl groups were converted into acrylate groups by esterification with acryloyl chloride to obtain SS-hPG-Acry. The hydrogel was subsequently formed by mixing the PBS solution of SS-hPG-Acry and 4-arm-PEG-SH with a determined concentration after overnight incubation at room temperature. The hydrogels were prepared at different weight percent concentrations to investigate the effect of gel concentration on the stiffness and mechanical properties of the hydrogels. The hydrogels were prepared by chemical cross-linking of the thiol groups of the 4-arm-PEG-SH and the acrylates of the SS-hPG-Acry via a thiol-Michael addition click reaction (Figure S7A). After gelation, the ^{1}H NMR spectrum showed 90% reduction in the peaks associated with the protons of the alkene group of the acrylate in the region between 6.0 and 6.6 ppm (Figure S7B) after 1 hour. When observing the corresponding FTIR spectra of the compounds, an alkene band appeared after acrylation at 800 cm^{-1} and disappeared in result of gelation. The thiol stretching absorbance band at 2700 cm^{-1} disappeared as well in the hydrogel spectra, indicating the thiol-ene click reaction.
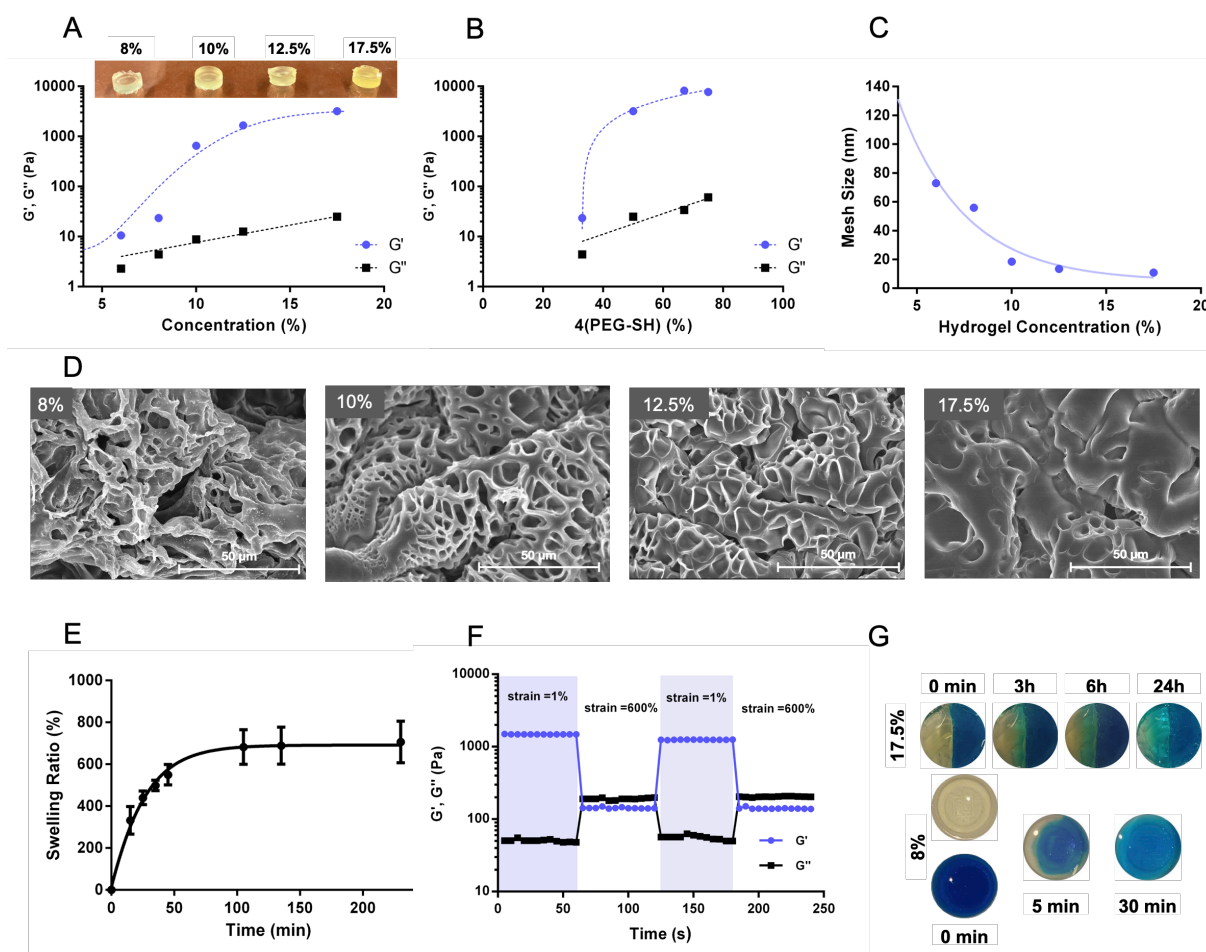
Figure 2. (A) Elastic and viscous modulus values (G′ and G′′) of different concentrations of reducible hPG block and 4-arm-PEG-SH crosslinker for a 1:1 ratio. (B) G′ and G′′of hydrogels for different reducible hPG block and 4-arm-PEG-SH crosslinker ratios at a concentration of 17.5%. (C) Mesh size of hydrogels with different components' concentrations at 1:1 ratio according to the Canal-Peppas equation. (D) SEM images of freeze-dried hydrogels with different concentrations of the building components. (E) Swelling ratio of 17.5% hydrogel. (E) G′ and G′′of 17.5% hydrogel measured in cycles of 1% and 600% strain. (F) Photos taken at different time points of 17.5% and 8% hydrogel, one half without dye and second half with blue dye, combined together to prove the self-healing properties of the hydrogel.

Redox-responsive hydrogels were prepared by mixing SS-hPG-Acry and 4-arm-PEG-SH in a 1:1 molar ratio at varying weight concentrations (%W/V) of (6%, 8%, 10%, 12.5% and 17.5%). The rheological properties of the hydrogels were compared through the elastic and viscous modulus values G′ and G′′, respectively. G′ and G′′provide insights into how materials respond to deformation under oscillatory shear. G' indicates the solid-like behavior (elasticity), while G" indicates the liquid-like behavior (viscosity). G′ and G′′ are calculated from the frequency sweep test, where the shear strain is fixed at 1% and the G′ and G′′ values are set

according to the linear region when varying the frequency. The gel with lower concentrations of polymeric content exhibited lower G′ and G′′and behaved as a soft gel. At increased concentrations a noticeable increase in G′ and G′′was observed, along with increased gel stiffness (Figure 2A). The mesh size of the hydrogels was calculated according to the Canal-Peppas equation, with G′ as the varying parameter. Figure 2C, showing the results of the calculations, expresses a trend of decreasing mesh size with increased polymeric content concentration; in other words, the mesh size was inversely proportional to G′. Recorded SEM images of freeze-dried hydrogels showed smaller hydrogel mesh size for hydrogels with higher concentrations of SS-hPG-Acry and 4-arm-PEG-SH (Figure 3D). The elastic and viscous moduli were also tested when fixing the concentration at 17.5% and varying the SS-hPG-Acry:4-arm-PEG-SH ratio. Gels did not form for a 3:1 ratio. The values of G′ and G′′increased drastically for a ratio of 1:1 and almost plateaued when further increasing the 4-arm-PEG-SH to SS-hPG ratio (Figure 2B). Moreover, the 17.5% gel was able to swell from its dried state, showing an almost eightfold weight increase over two hours (Figure 2D). The gels exhibited self-healing properties due to the dynamic nature of the disulfide bonds. To investigate these self-healing properties, extreme strain (600%) and mild strain (1%) were applied to the 17.5% hydrogel in alternating cycles (Figure 2E). Under 600% strain the gel was totally deformed: G′ dropped around 10 folds and became even lower than G′′. G′, as a representative of the crosslinked network density, get lower because the network collapses, losing the storage energy which is normally stored via the crosslinked network while G′′ get higher due to the applied energy that dissipates due to the lower network density which collapses when applying high shear strain force. However, when strain was reduced back to 1%, the gel showed instant recovery, with G′ and G′′returning to their original values. Thus, the hydrogels were able to conserve their viscoelastic properties and mechanical strength after their rupture if they remain partly intact. The self-healing property can also be tested visually by staining one hydrogel with a blue dye and leaving the other one uncolored. Both hydrogels were cut in half and brought in contact, then observed at different time points (Figure 2F). The test was performed on both 8% and 17.5% hydrogels, confirming that the gels were able to merge again, and that the 8% gel was able to heal faster.

2.3. Degradation and release properties of the hydrogel

The hydrogel degradation was tested by incubating different hydrogels, each corresponding to a point in time, in 1 mL PBS pH=7.4 (control) and in the presence of a reducing agent (10 mM GSH or 10 mM dithiothreitol, DTT). For each time point, 0.5 mL of the media was withdrawn and lyophilized to calculate the weight loss of the hydrogel upon

degradation, and the storage and loss moduli of the hydrogel were measured by applying the time sweep test (Figure 3A). The hydrogel was completely deformed when incubated in a reducing environment: the values of G´ and G´´decreased tremendously. The degradation in DTT was twice as fast as the degradation in GSH, and the hydrogel was able to conserve its mechanical properties in the control medium (Figure 3B and 3C). The degradation was also proven by measuring the weight loss of the hydrogel over time. When the disulfide bonds were reduced, the hydrogel gradually lost the crosslinked network configuration, which allowed for the degraded segments to become soluble in the reducing media. Once the solution was lyophilized, the weight of those segments was calculated and the degradation profile of the hydrogels versus time was plotted (Figure 3D). The SEM images of freeze-dried hydrogels (10% and 17.5% concentrations) recorded before and after incubation with 10 mM DTT show a deformation in the hydrogel network where the pore's configuration was disrupted; hence, we were able to visualize the consequential degradation of the hydrogel's network (Figure 3E).
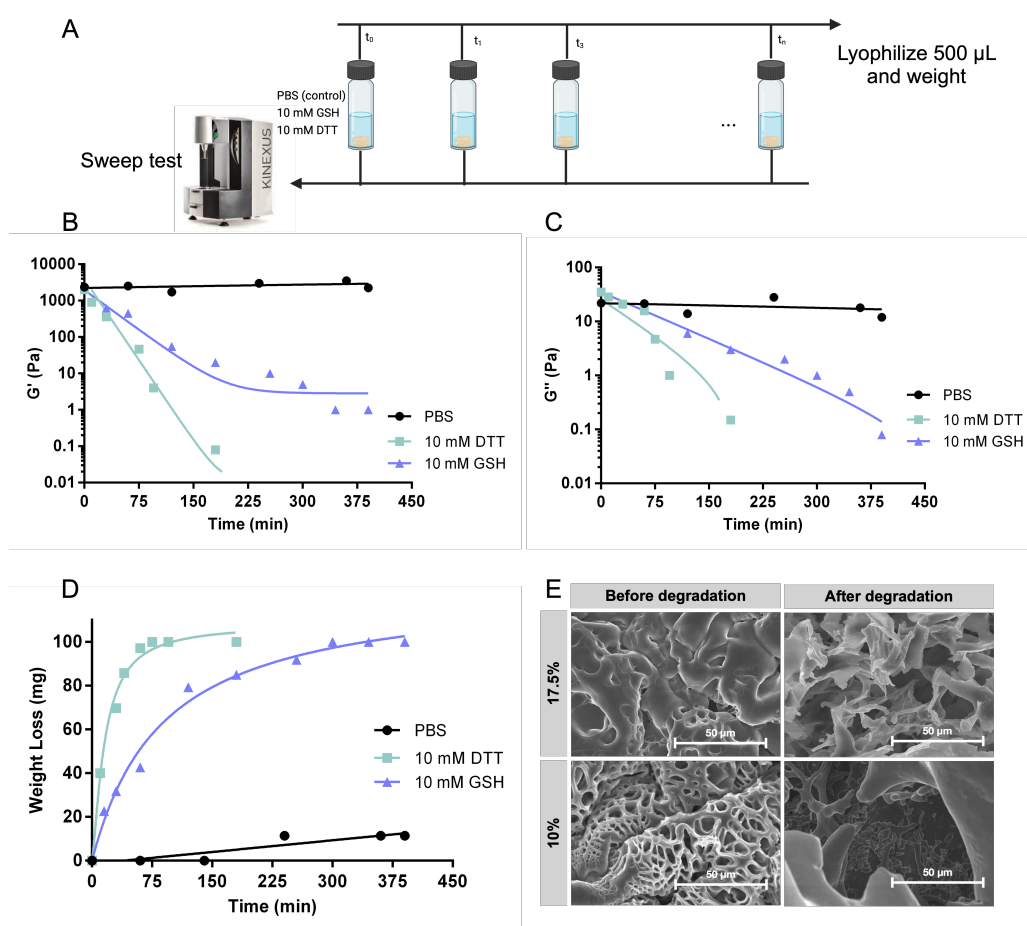
Figure 3. (A) Scheme representing the degradation experiment. Several 17.5% hydrogels were incubated in 1 mL of media (PBS, 10 mM GSH and 10 mM DTT). At each time point, G´ and G´´were measured, and 500 µL of the solution media was lyophilized and weighed to identify the loss in the hydrogel weight. (B), (C) and (D) Degradation of the 17.5% hydrogels identified

by recording G′, G′′and the hydrogel weight loss respectively, at different time points, in GSH or DTT media. (F) SEM images of freeze-dried 10% and 17.5% hydrogels recorded before and after incubation with 10 mM DTT for 24 h.

Following the degradation of the hydrogels in a reductive environment, a model protein, albumin−fluorescein isothiocyanate conjugate (FITC-BSA) was encapsulated in the hydrogel's network to evaluate the triggered protein release, either spontaneously or on-demand, by adding high concentrations of the reducing agent at a certain time point. The encapsulation of FITC-BSA was performed during the formation of the hydrogel by adding a solution of 2 % wt. FITC-BSA during the mixing of the hydrogel's components, as shown in Figure 4A. As for the release profiles, the hydrogel could successfully release the FITC-BSA in a reductive environment with the presence of either 10 mM GSH or DTT in a controlled fashion. The hydrogel barely leached any FTIC-BSA in PBS (<20%), which indicates that the release was due to degradation of the hydrogel backbone, not physical diffusion (Figure 4B). In another experiment, the hydrogels were only incubated in PBS solution, and after 3 h, a high concentration of GSH or DTT was added to the media to observe the sudden release of FTIC-BSA from the hydrogels. This proved that the release from the hydrogel can also occur on demand (Figure 4C). In Figure 4D, we took photos under UV illumination (λ= 665 nm) of FTIC-BSA-loaded hydrogels in PBS and 10 mM DTT solutions over the course of 4 hours. The hydrogel incubated in PBS remained intact. However, the hydrogel in the reducing environment completely dissolved and the entire media became fluorescent, indicating the release of the FITC-albumin from the hydrogel after complete network degradation.
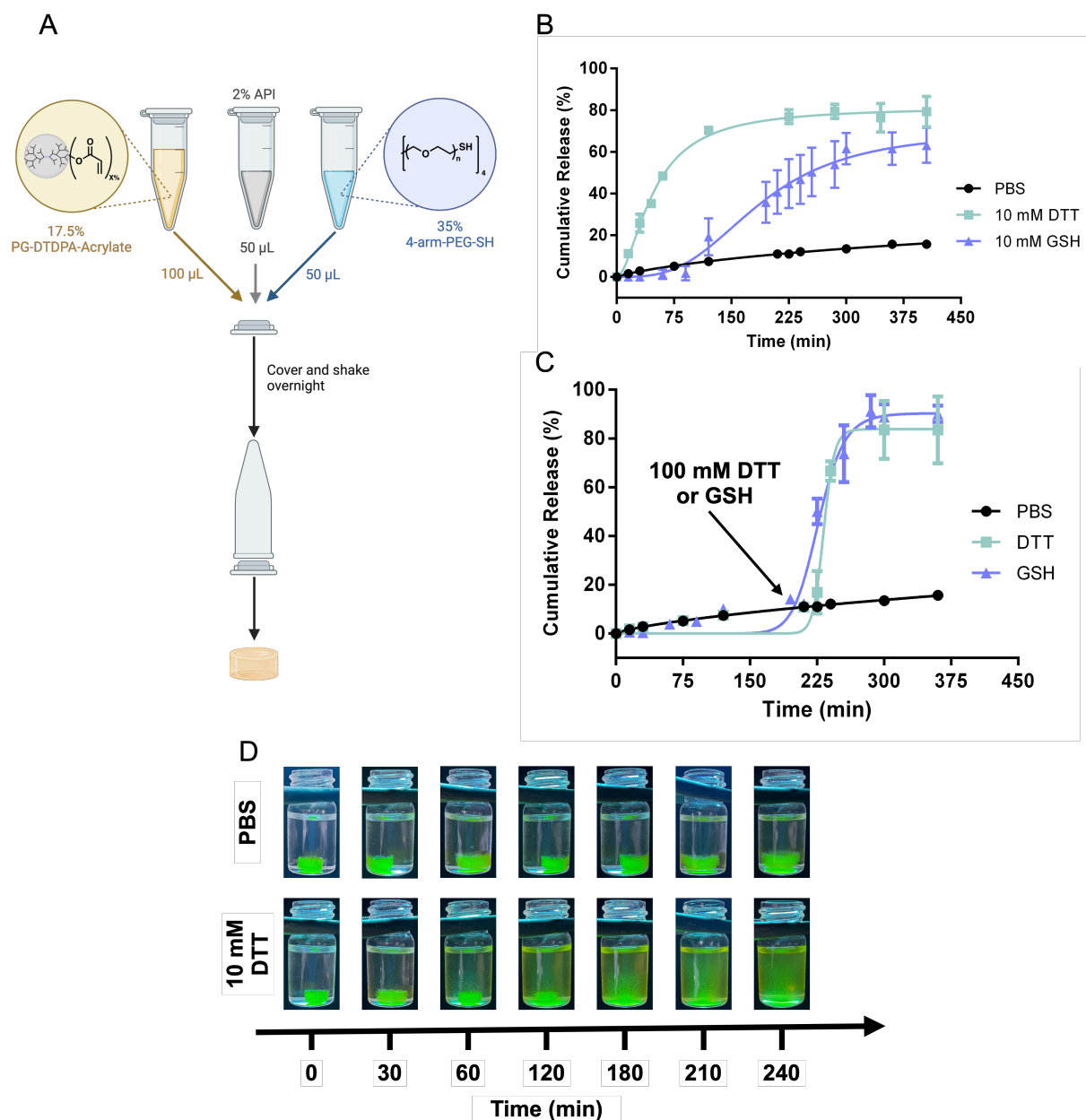
Figure 4. (A) Scheme representing the encapsulation of active pharmaceutical ingredient (FITC-BSA or vancomycin) in the hydrogel. (B) and (C) slow and on-demand release profiles, respectively, of FITC-BSA-loaded 17.5% hydrogel incubated in PBS, 10 mM GSH and DTT for on-demand release. The hydrogel was incubated in PBS and a high concentration of GSH or DTT was added after 3 h. (D) photos of FITC-BSA-loaded 17.5% hydrogel incubated in PBS and 10 mM DTT, captured at different time points.

2.4. Cell viability and *in-vitro* antibacterial activity

The biocompatibility of the hydrogels with different concentrations (17.5%, 12.5% and 8%) was tested on L929 mouse fibroblast cells using PrestoBlue™ cell viability assay. The experiment was set up to mimic a real-life skin model by inserting a Transwell™ cell culture insert on top of the cell media to act as a porous barrier between the cells and the hydrogel

(Figure 5A). In addition, a solution of 5 mM GSH was added to the hydrogels to trigger degradation and to allow investigation of the degradation products' cytotoxicity. Figure 5B shows a live/dead assay result in the form of a microscopic fluorescent image recorded for the cells incubated with 17.5% hydrogel after 24 h. Incubated cells were stained with a mixture of calcein-AM and propidium iodide dyes, which differentiated their live or dead state through green and red fluorescence, respectively. The remarkably dominant green color showed that an great majority of the cells remained alive. As for the PrestoBlue™ assay tested on the variable concentrations and degradation products of the hydrogels, cells showed excellent viability after 24 h as well as 96 h, which demonstrated the high biocompatibility of the systems.
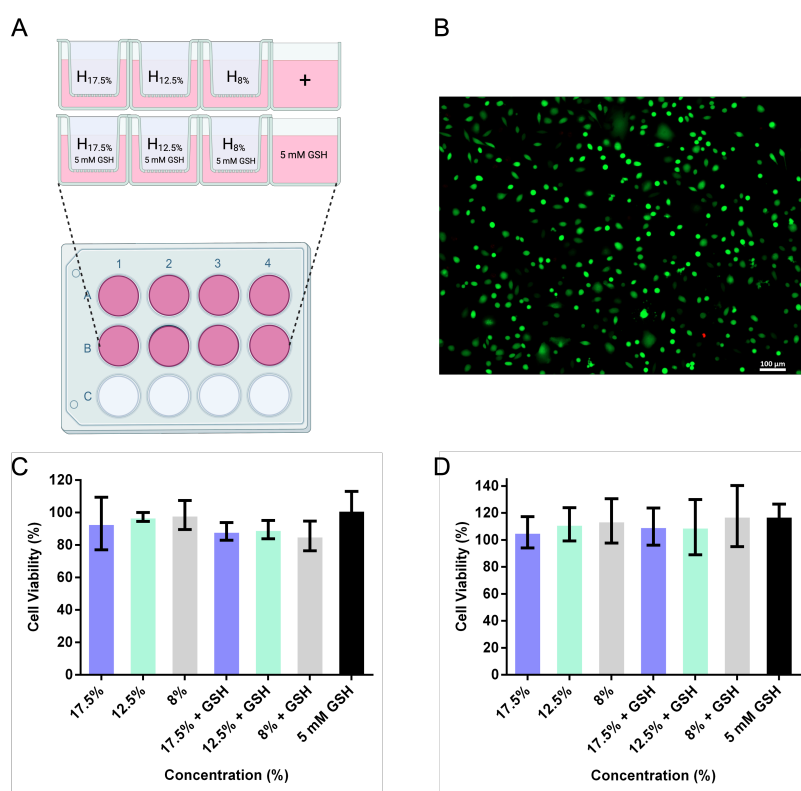
Figure 5. (A) Scheme of the cytotoxicity assay setup, where a Transwell™ insert containing different hydrogel concentrations was inserted on top of the plate's well, with and without the addition of 5 mM GSH. (B) Fluorescence microscopy images of the live/dead cell viability assay upon treatment with the 17.5% hydrogel after 24 h. (C) and (D) Cell viability assays of cells treated with different hydrogels, with and without the addition of GSH, after 24 h and 96 h respectively.

We envision these hydrogels serving as a delivery platform to ensure the controlled topical transport of active pharmaceutical ingredients. We therefore encapsulated vancomycin in the hydrogel network during hydrogel preparation. Vancomycin is a glycopeptide antibiotic medication used to treat bacterial infections. It is applied intravenously as a treatment for

complicated skin infections, bloodstream infections, endocarditis, and bone and joint infections. To treat infected skin tissues, vancomycin is administrated intravenously in high doses to achieve effective results.[20] The high doses often lead to challenges such as kidney failure, local pain, thrombophlebitis, and even anaphylaxis or erythema; all the while potentially contributing to resistance development.[21] Therefore, delivering vancomycin topically can be an alternative option to overcome those challenges. The release profiles of vancomycin-loaded hydrogels were plotted for the different reductive media and the control medium and were observed to show a controlled trend (Figure 6A). The spontaneous release for different gel concentrations (i.e. different mesh sizes) was also tested and found negligible between a concentration of 8% and 17.5%. (Figure 6B).

Next, we evaluated the hydrogels' antibacterial efficacy by exposing their surfaces to bacterial suspension. 100 µL of gels at different concentrations (8%, 12.5% and 17.5%), without and with loaded vancomycin, were prepared in the wells of a 96-well plate and then challenged with bacteria (5 µL K-12 *E. coli* culture, 100 µL LB, starting OD600 was 0.01). Hydrogels loaded with vancomycin showed an effective antibacterial activity against *E. coli* after 6 h. Hydrogels acting as a topical cover over an infected wound should also prevent the penetration of further bacteria and act as a block to any bacterial propagation. Hence, a hydrogel-coated Transwell™ model with a pore size of 3 µm (large enough for *E. coli* to pass through) was placed on top of the wells of a 24-well plate, and the bacterial solution was then placed on top of the hydrogels. We tested hydrogels with concentrations of 8 and 17.5%, both empty and loaded with vancomycin. We then grew CFUs from the media from the bottom of the well and calculated CFUs/mL. We observed that bacterial penetration was blocked regardless of the component's concentration or the presence of vancomycin (Figure 6D). Finally, the long-lasting effect of the hydrogel loaded with vancomycin was tested, compared to vancomycin and *E-coli* as controls. The optical density at 600 nm was measured every 15 min for 20 h (Figure 6E). The vancomycin-loaded hydrogels showed a long-lasting antibacterial activity, and the hydrogel with the lowest concentration was the most effective. The empty hydrogels showed bacterial growth even above the *E. coli* control, with the lowest-concentration hydrogel having the highest bacterial growth.
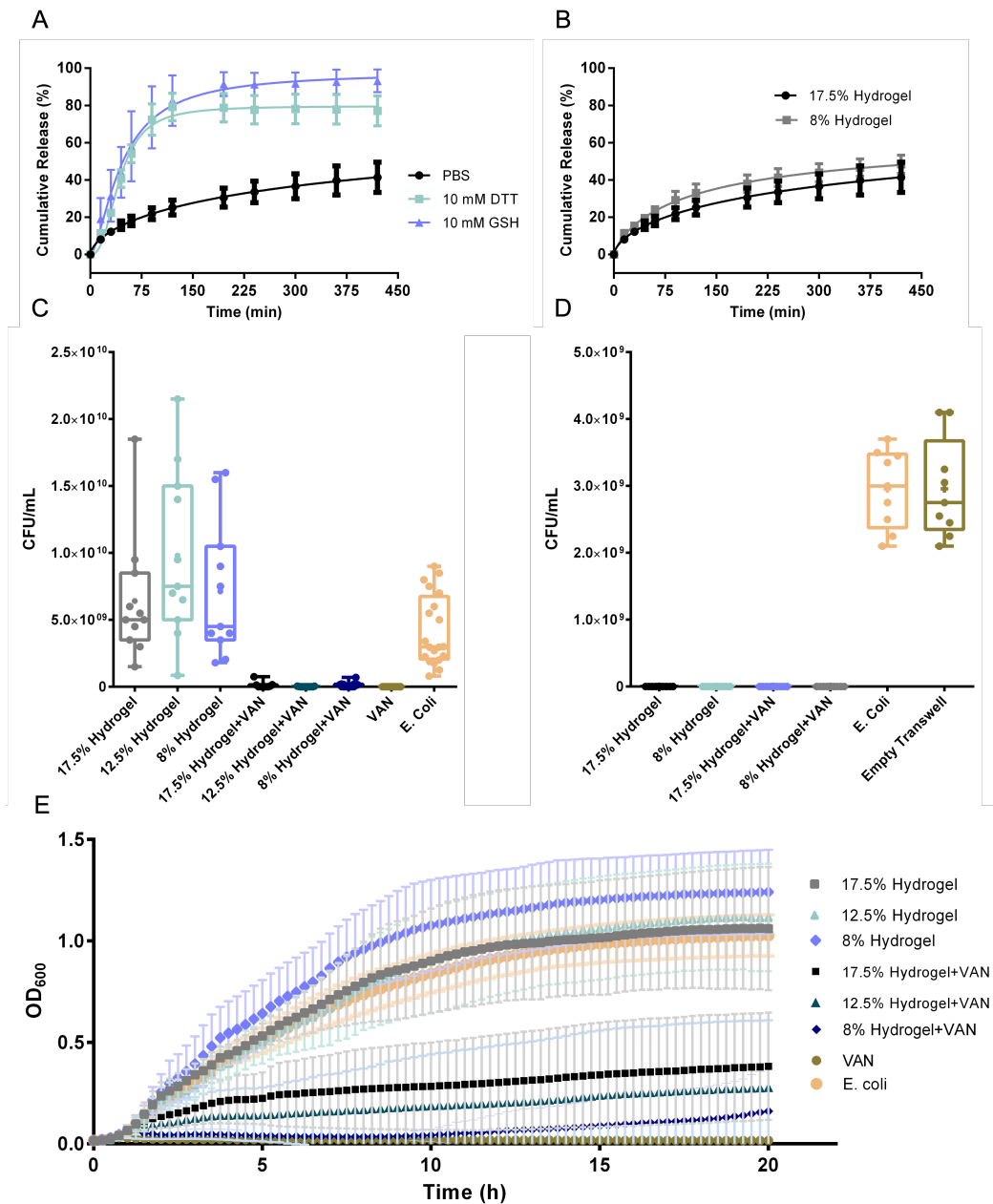
Figure 6. (A) and (B) Release profiles of vancomycin (VAN)-loaded hydrogels in different media for the same 17.5% concentration and in PBS for the 17.5% and 8% hydrogels in PBS only. (C) Antibacterial assays, , measurement of CFU after 20hr incubation with bacteria. (D) Bacterial blockage. (E)) Bacterial growth curve showing long-lasting antibacterial activity.

2.5. *In vivo* wound healing and toxicity studies
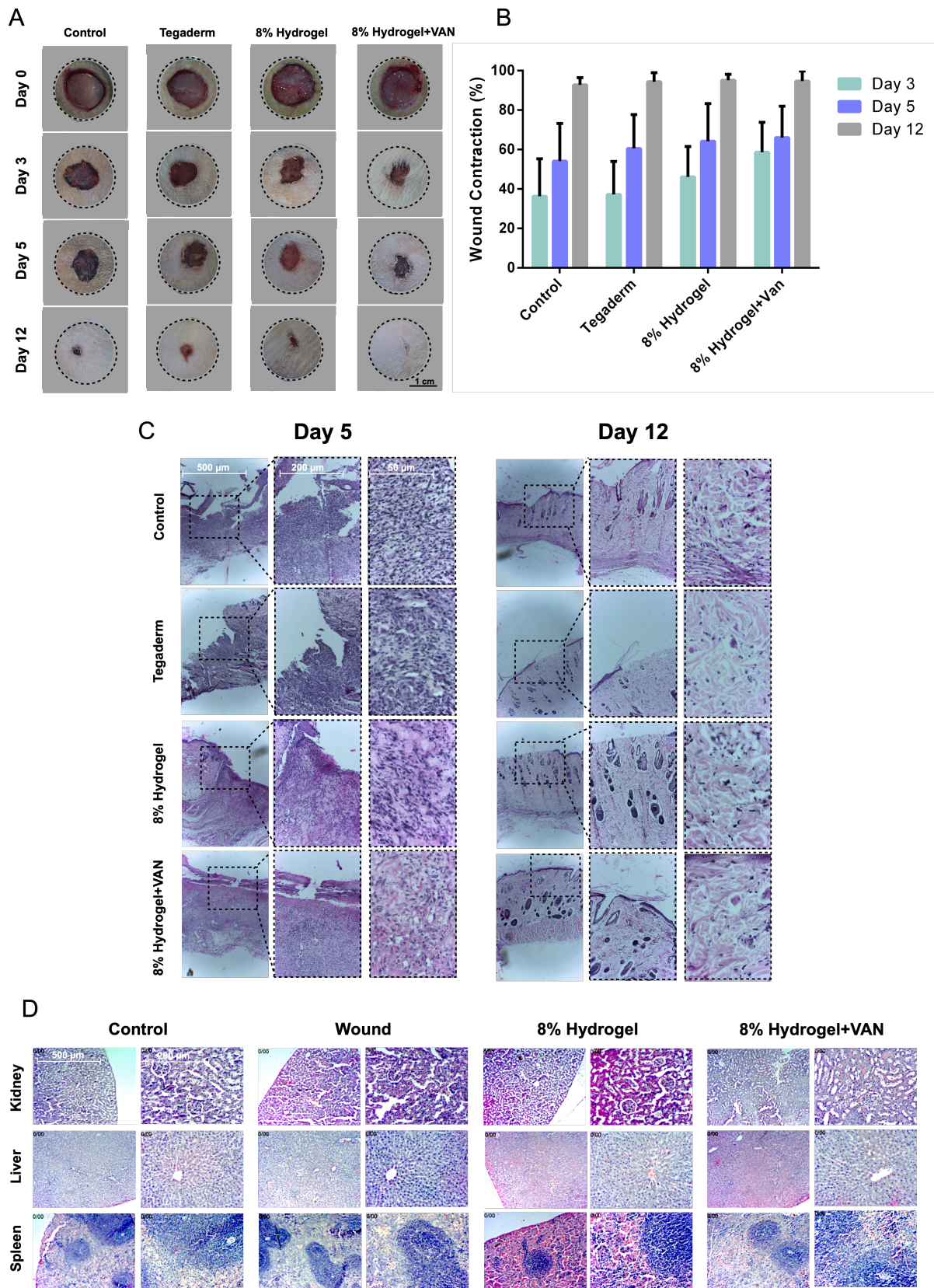
Figure 7. *In-vivo* wound healing model: (A) Photographs of wound cuts for control, Tegaderm, 8% hydrogel and 8% hydrogel+VAN groups at day 0, 3, 5 and 12. (B) Wound concentration in

percentage determined by ImageJ for the groups after 3, 5 and 12 days. (C) hematoxylin-eosin staining (H&E) of rat's wound tissues at day 5 and 12 for the same test groups.

As shown in the photographs of the wounds (Figure 7A) and the percentage of wound contraction as determined by ImageJ software (Figure 7B), the Tegaderm and wound groups displayed slow healing during the 12-day period. In fact, the results demonstrate that the healing progress speed was much higher in the 8% hydrogel and 8% hydrogel+VAN groups: 3 days after surgery, the percentage of wound contraction is $46.12\pm15\%$ for 8% hydrogel and 58.65 ± 15.1 for 8% hydrogel+VAN, respectively. By contrast, these values were $37.2\pm16.2\%$ and $36.3\pm18\%$ for the Tegaderm and control groups, respectively. Moreover, Figure 7C demonstrates the results of hematoxylin-eosin staining (H&E) staining of rats' wound tissues at day 5 and day 12 post-surgery. The results at day 5 displayed many inflammatory cells and disorganized micro-architectures in control groups compared to other groups. At day 12, the collagen fibers in 8% hydrogel and 8% hydrogel+VAN groups were more organized. In 8% hydrogel+VAN groups, a new layer of epidermis is observable. The histopathology results of H&E staining of the rat's main organs, including kidney, liver, and spleen (Figure 7D), did not show histopathological alterations such as dead tissue or alterations in the structure of cells. In addition, there was no signs of inflammation in 8% hydrogel, 8% hydrogel+VAN and Tegaderm groups compared to control group.

Figure S8 demonstrates the results of blood hematological and biochemical factors. As shown in the graphs, biochemical factors, including total protein (TP), albumin (ALB), calcium (Ca), blood urea nitrogen (BUN), creatinine (CREA) are not significantly different in 8% Hydrogel and 8% Hydrogel+VAN. Moreover, white blood cells (WBCs), red blood cells (RBCs), hemoglobin (HGB), hematocrit (HCT) and platelets (PLT), mean corpuscular volume (MCV), mean corpuscular hemoglobin (MCH), and mean corpuscular hemoglobin concentration (MCHC) are not significantly different among different groups.

3. Conclusion

In this work, an antibacterial hydrogel was prepared on a multigram scale using a straightforward process. The hydrogel was loaded with an antibacterial peptide for topical delivery to infectious wound sites and to prevent bacterial contamination. Due to the incorporated disulfide bonds, the hydrogel backbone can be degraded in the reductive environment of infectious wounds, releasing its cargo of the antibacterial peptide; the hydrogel will eventually be removed after degradation, without causing any secondary damage to the wound. The *in-vitro* results show that the hydrogel and its degradation products are non-toxic

to cells, and the hydrogel loaded with vancomycin acts as a barrier against bacteria, with a significant antibacterial effect against *E. coli*. The hydrogels loaded with vancomycin exhibited improved healing of infected wounds in an *in-vivo* dermatological mouse model. The high biocompatibility, degradability and antibacterial properties of this disulfide-based hydrogel qualify it as a promising wound dressing for topical drug delivery to infected wounds.

4. Experimental Section

Materials: glycidol (96.0%) from Sigma-Aldrich (distilled) and 3,3'-dithiodipropionic Acid (>99.0%) from Tokyo Chemical Industry (TCI) were used for the polymer synthesis. Acryloyl chloride (96.0% stabilized with phenothiazine) purchased from ABCR and Sodium hydride (60.0% dispersion in mineral oil in soluble bags), from ACROS Organics were used for the acrylation. Albumin-fluorescein isothiocyanate conjugate and vancomycin hydrochloride purchased from Sigma-Aldrich were encapsulated in the hydrogels. For the release studies, Glutathione (GSH, 98.0%) and DL-1,4-Dithiotreitol (DTT, 98.0%) from Thermo Scientific were the reducing agents employed. The PBS solution was prepared with 1x PBS tablets for 1000 mL from ChemSolute, Th. Geyer. Methanol (MeOH, $\geq$99.9%) and anhydrous dimethyl ether (DMF) were purchased from Acros Organics. Cellulose ester dialysis membrane (MWCO = 1.0 kDa) was purchased from Carl Roth GmbH + Co.

Instrumentation: ^{1}H NMR and ^{13}C NMR spectra were recorded either on a Bruker AVANCE III 500 (Bruker Corporation), or a Jeol ECP 600 (JEOL GmbH). Chemical shifts are reported in δ (ppm) and referenced to the respective solvent. Deuterated water (D$_2$O) was used for the characterization of the final polymeric products. Infrared spectroscopy measurements of the compounds were conducted using a JASCO FT/IR-6700 FT-IR Spectrometer. For the encapsulation and release experiments, UV/vis measurements were conducted on an Agilent Cary 8454 UV/visible spectrophotometer, using semi-micro reusable cuvettes. The rheological trends of the hydrogels were evaluated by using a Malvern Kinexus rheometer. A plate upper geometry (8 mm diameter) and a cone upper geometry (1:20 mm diameter) were used as test geometries depending on the viscosity of the hydrogels. Time and frequency sweep tests were conducted before the measurements and fixed at 1 Hz and 1% strain. A closed system was used to avoid evaporation of water from the hydrogels during measurements. The surface morphologies of lyophilized hydrogel samples were analyzed using a Scanning Electron Microscope (SEM), with an SU8030 Hitachi instrument, operating at an accelerating voltage of 15 kV.

Synthesis of reducible hyperbranched polyglycerol (hPG-DTDPA): to a 100-mL 3-neck Schlenk flask equipped with a mechanical stirrer 4.62 g (0.022 mol) 3,3'-dithiodipropanoic acid

(DTDPA) was added, dried under high vacuum for 1 hour and flushed with Argon. 5, 10 or 20 equivalent amounts of glycidol was then added and the reaction was left to stir at 100 rpm at 70 °C for 3 days. Afterwards, the reaction was quenched with water/methanol (1:1 v/v) and dialyzed against the same solution for the first day, changing the medium 3 times per day and eventually against only water for 2 days using a membrane with a MWCO of 1 kDa. The purified product was concentrated under reduced pressure and lyophilized to obtain the final product.

For the Acrylation, 2.54 g of SS-hPG was dried in a 50-mL Schlenk flask under high vacuum at 40 °C overnight. Next day, the polymer was flushed with Argon and left to cool off before dissolving it in 10 mL of anhydrous DMF. 205 mg (0.15 eq / OH groups) Sodium hydride was then added to the flask at 0 °C. The reaction was left to stir for an hour to enable the deprotonation of the hydroxyl groups. Subsequently, 0.46 g (0.15 eq / OH groups) of acryloyl chloride was added dropwise and the reaction was left to stir at room temperature overnight. Afterwards, the reaction was dialyzed against water for 2 days using a 1 kDa MWCO membrane. The final product was concentrated and lyophilized and then redissolved in phosphate buffered saline solution (PBS) for a 100 mg /100 µL concentration stock solution and stored at -4 °C. The degree of acrylation was calculated according to the ^{1}H NMR spectrum and is found to be 6.5% (Equation S2).

Synthesis of 4-arm-PEG-thiol: 4-arm-PEG-thiol was synthesized in accordance to what is previously published in literature.[22] 4-arm-PEG was functionalized with thiol group by using thiourea. First a mesyl group was introduced then the thiolation and hydrolysis were carried out at 80°C. After purification, a pale yellowish precipitate was obtained in a high yield. The final product was characterized by ^{1}H NMR and the functionalized thiol groups were quantified by Ellman's assay, which showed approximately 3.7 groups per molecule (Page S4-S6).

Hydrogel chemical crosslinking: hydrogels were prepared for different building block and crosslinker concentrations (8%, 10%, 12.5% and 17.5%) and ratios (3:1, 2:1, 1:1, 1:2 and 3:1) to define their viscoelastic properties through rheology measurements. The hydrogel is formed via the thiol-ene click reaction between the acrylate groups of the hPG and the thiol groups of the PEG in PBS solution at a pH of 7.4. The general procedure consisted of preparing two solutions of SS-hPG-Acry and 4-arm-PEG-thiol in PBS solution. 100 µL of 4-arm-PEG-thiol was first added to a 2-mL Eppendorf cap, followed by 100 µL SS-hPG-Acry solution and mixed with the help of an Eppendorf pipette. The cap was then sealed with the inversed Eppendorf and the hydrogels were left to shake at 100 rpm overnight.

Hydrogel swelling: freshly prepared hydrogel samples (200 mg) were freeze-dried and immersed in deionized water (5 mL) at room temperature. At periodic time intervals, the weight of the hydrogels was recorded after removing the surface water. The swelling percentage was calculated as the percentage of weight increase of the swollen state at an interval t (W_t-W_0) with respect to the initial weight of the dry hydrogel (W_0) (Equation 1). Swelling experiments were repeated for three different samples (n=3) and plotted as Mean±SD.

$$\%swelling = \frac{W_t - W_0}{W_0} \times 100 \tag{1}$$

Hydrogel self-healing test: the 8% and 17.5% (w/v) hydrogels (with and without a blue food dye) were prepared in the Eppendorf cap as mentioned previously. After their formation, the gels were cut in half using a blade. One of each halves were then pressed into each other in the same orientation as the cut. The combined hydrogels were observed at t=0, 3, 6 and 24 h to visualize the self-healing properties.

For rheological assessment of self-healing, the 17.5% hydrogel subjected to high (600%) and low (1%) strains in cycles for a total of 3 cycles. G′ and G′′were recorded and plotted with respect to time to assess the conservation of hydrogel properties throughout the cycles.

Hydrogel mesh size calculation: the mesh size of the hydrogels with different concentrations was calculated using the Canal-Peppas equation based on the elastic modulus of the gel[23] according to Equation 2.

$$\xi = \left(\frac{RT}{G'N_A}\right)^{\frac{1}{3}} \tag{2}$$

Where R is the gas constant in J·mol^{-1}K^{-1}, T is the temperature in K, G′ is the elastic modulus N·m^{-2}, and N_A is Avogadro's constant.

Hydrogel redox-responsive degradation: rheological experiments were carried out to demonstrate the disassociation of the gel matrix in the presence of a reducing agent. 17.5% hydrogels were incubated in 1 mL of PBS, 10 mM GSH, and 10 mM DTT media for different time points. At each time point the degradation of the gel was investigated using time sweep tests on a rheometer recording G′ and G′′. Simultaneously, 0.5 mL of each media at a certain time point was removed and lyophilized and the degradation was assessed based on the weight loss of the initial hydrogel. For visual assessment of degradation, two fluorescein isothiocyanate-labeled bovine serum albumin (FITC-BSA) loaded hydrogels were incubated in

PBS and 10 mM DTT solutions respectively. Photographs of vials were taken under UV illumination (365 nm) to indicate the gel degradation.

Active pharmaceutical ingredient loading and release studies: FITC-BSA and vancomycin were used as a model protein and antimicrobial glycopeptide as active pharmaceutical ingredient (API) respectively. The APIs were encapsulated into hydrogels during gelation. In short, a concentration of 1 mg/50 µL of API, 17.5 mg/50 µL of 4-arm-PEG-thiol and 17.5/100 µL of hPG-DTDPA were prepared in PBS solution. In an Eppendorf's cap the 4-arm-PEG, API and hPG-DTDPA were added sequentially. The gel was mixed, sealed, and left to shake overnight. After gelation, hydrogels were placed into 5 mL of PBS, 10 mM GSH and 10 mM DTT containing vials. At different time point, 2 mL samples were taken out and the amount of API released in the supernatant was determined using a UV−vis spectrophotometer at 495 nm and 280 nm for FITC-BSA and vancomycin respectively. For the on-demand release study, hydrogels were treated with 100 mM GSH and 100 mM DTT after 3 h of passive release. The release experiment was repeated 3 times for each set of hydrogels.

In vitro cytotoxicity assays: Cytotoxicity of the hydrogels with different concentrations with and without addition of GSH was investigated via a PrestoBlue™ viability assay on L929 mouse fibroblast cells. Cells (69,000 cells/well) were seeded on a 12-well plate with 2 mL of the culture medium and incubated at 37 °C overnight to grow and adhere. Transwell™ with a pore size of 0.45 µm were inserted on top of the plate's well. 200 mg hydrogels (17.5%, 12.5% and 8%) with and without the addition of 5 mM GSH were placed on inside the Transwell™. The hydrogels were incubated in the cells for 24 and 96 h. After the incubation time, 100 µL was taken of each well in three replicates and treated with 10% of PrestoBlue™ solution for 3 h, and the absorbance values at 570 nm were measured using a microplate reader. Non-treated cells were used as a positive control, and cells treated with 5 mM GSH were used as a control for the degradation experiment.

Live/Dead cell viability assay: the L929 mouse fibroblast cells adhered on the previous 12-well plate were rinsed twice with PBS and the cells were stained according to the protocol of the live/dead assay kit (Sigma, 04511-1KT-F). The cells were stained with PBS solution containing 10 µL of calcein-AM and then with 5 µL of propidium iodide (PI) for 30 min at 37 °C. After removing the solution and washing with PBS, the cells were imaged using a fluorescence microscope (Zeiss Observer A1 equipped with AxioCam MRc5) and AxioVision

software. The live and dead cells exhibited green and red fluorescence respectively due to calcein-AM and PI.

|*In vitro antibacterial activity and growth curves:* In this study the K-12 *E. coli* DH5α was streaked out on LB agar from frozen stock. Liquid culture was created from a single colony isolated from the LB plates and allowed to grow for 6 hours at 37°C in 5 mL of LB media. 100 µL of LB media was added on top of 100 µL of solidified hydrogel of varying concentrations with the presence or absence of vancomycin in a 96-well plate (round bottom, Sarstedt), followed by 5 µL of bacterial culture. The lid of the 96-well plate was coated in anti-fog solution (0.05% TritonX-100, 20% Ethanol in water[24] and allowed to completely dry under the clean bench hood. The closed with lid 96-well plate was placed in the Agilent BioTek Epoch 2 Microplate Spectrophotometer and allowed to grow for 20 hours at 37°C with continuous shaking (double orbital) measuring at OD_{600} in 15 min intervals.

Colony forming units (CFUs) were then preformed after the 20-hour growth curve using the resultant culture as described in Maan *et al.*[25] Briefly, the culture was transferred to a 96-well plate and a serial dilution from 10^0 to 10^{-7} was performed in DPBS. 20 µL of varying dilutions were spotted onto LB agar plates and allowed to dry completely in clean bench hood. Plates were incubated overnight at 37°C and CFUs were then counted.

Bacterial-blockage activity: hydrogels of concentrations 17.5% and 8% with the presence and absence of vancomycin were formed in parafilm wrapped Transwell™ (pore size 3 µm) and hardened overnight. Parafilm was carefully removed from Transwell™ in clean bench hood and Transwell™ were placed in 24-well plate that contained 100 µL of L B media (The Transwell™ was partially bathing in the 100µL of the LB). 100 µL of LB media was then added to the top of each Transwell™ followed by 5 µL of *E. coli* culture (prepared in the same way as described above). Plates were covered and incubated overnight at 37 °C in static conditions. The following day, Transwells™ were carefully removed and culture from 100 µL of LB was transferred to a 96-well plate and CFUs were performed as described above.

In vivo wound healing and toxicity studies: In all *in vivo* studies, the rats were kept in their houses for one week to acclimate them to the new conditions. During the studies, the cycle of 12 hours of light and 12 hours of darkness was maintained in the house, as well as the ambient temperature of 21-23 ºC and relative humidity of 50-60%. All principles of working with laboratory rats and methods were in accordance with the ethical standards and instructions of the Committee for Working with Laboratory Animals of Lorestan University of Medical Sciences (Ethical code: IR.LUMS.REC.1402.213). *S. aureus*-infected full thickness skin was employed to investigate the wound healing potential of hydrogels in a rat model. For this

purpose, rats (male Sprague-Dawley rats, 180-220 g) were randomly divided into 4 groups (*n* =6) including wound alone without any treatment (Wound), the commercially-available dressing as a positive control (Tegaderm), Hydrogel (Gel) and drug loaded hydrogel (Gel-D). Before the wound creation, the rats were anesthetized with a mixture of ketamine and xylazine. Then, two wounds were created on the back side of animals with a diameter of 10 mm after shaving them. Afterward, 20 µl of a 0.5 MaFarland *S. aureus* suspensions was employed for each wound to infect it. After 15 min, the related treatments were employed in each group. The wounds in each group were monitored and photographed at days 0, 3, 5, and 12. The images were analyzed by ImageJ software. on the 5 and 12th day, the wound and the surrounding repaired tissue were harvested and fixed in 4% paraformaldehyde. After dehydration with respectively: alcohol 70 %, 80%, 90%, absolute 1 and absolute 2, the samples were embedded in paraffin, section with 5-7 µm thickness were obtained by a microtome, finally, the samples were stained by H&E to investigate the wound repair and inflammation.

To investigate the animal toxicity of hydrogel, in addition to measuring the toxic effect of hydrogel and drug-containing hydrogel on important organs such as kidney, liver and spleen, the function of these organs is also evaluated. For this purpose, at day 12, 2 ml of blood was taken to check hematological parameters including White blood cells (WBCs), Red blood cells (RBCs), hemoglobin (HGB), Hematocrit (HCT) and Platelets (PLT), Mean corpuscular volume (MCV), mean corpuscular hemoglobin (MCH), mean corpuscular hemoglobin concentration (MCHC), and biochemical factors including total protein (TP), albumin (ALB), calcium (Ca), phosphorus (ph), blood urea nitrogen (BUN), creatinine (CREA). Moreover, to evaluate the morphological changes in main organ of animals including kidney, liver and spleen, the tissue of these organ was harvested and first fixed in 4% paraformaldehyde, dehydrated, embedded in melted paraffin, cut into thin slices with a microtome, and stained with H&E and was observed under an optical microscope.

Statistical analysis: the experiments were performed with at least three biological repeats with three technical repeats within each biological repeat. Error bars represent ±SD. Statistical analysis was executed using the GraphPad Prism software (GraphPad Software, Inc., San Diego, CA).

Supporting Information

Supporting Information is available from the author.

References

[1]   a) P. Im, H. Shin, J. Kim, *Biomacromolecules* **2024**, 25, 1153; b) B. Huang, D. Hu, A. Dong, J. Tian, W. Zhang, *Biomacromolecules* **2022**, 23, 4766.

[2]   a) C. Dunnill, T. Patton, J. Brennan, J. Barrett, M. Dryden, J. Cooke, D. Leaper, N. T. Georgopoulos, *International Wound Journal* **2017**, 14, 89; b) P. Teller, T. K. White, *Surg Clin North Am* **2009**, 89, 599; c) S. Enoch, D. J. Leaper, *Surgery (Oxford)* **2008**, 26, 31.

[3]   S. Werner, T. Krieg, H. Smola, *J Invest Dermatol* **2007**, 127, 998.

[4]   a) D. E. Reichman, J. A. Greenberg, *Rev Obstet Gynecol* **2009**, 2, 212; b) L. Hall-Stoodley, J. W. Costerton, P. Stoodley, *Nat Rev Microbiol* **2004**, 2, 95.

[5]   T. L. Povolotsky, A. Keren-Paz, I. Kolodkin-Gal, *Trends Genet* **2021**, 37, 4.

[6]   Y. Liang, J. He, B. Guo, *ACS Nano* **2021**, 15, 12687.

[7]   a) M. L. Patton, R. F. Mullins, D. Smith, R. Korentager, *Journal of Burn Care & Research* **2013**, 34, 674; b) E. A. Kamoun, E.-R. S. Kenawy, X. Chen, *Journal of Advanced Research* **2017**, 8, 217.

[8]   a) Z. Lu, J. Cui, F. Liu, C. Liang, S. Feng, Y. Sun, W. Gao, Y. Guo, B. Zhang, W. Huang, *Advanced Healthcare Materials* n/a, 2303499; b) M. Li, Y. Zhang, L. Lian, K. Liu, M. Lu, Y. Chen, L. Zhang, X. Zhang, P. Wan, *Advanced Functional Materials* **2022**, 32, 2208141.

[9]   a) E. Fleige, M. A. Quadir, R. Haag, *Advanced Drug Delivery Reviews* **2012**, 64, 866; b) P. T. Wong, S. K. Choi, *Chem Rev* **2015**, 115, 3388.

[10]   a) W. Cheng, Y. Liu, in *Biopolymer-Based Composites*, DOI: https://doi.org/10.1016/B978-0-08-101914-6.00002-8 (Eds: S. Jana, S. Maiti, S. Jana), Woodhead Publishing **2017**, p. 31; b) Y.-J. Jo, M. Gulfam, S.-H. Jo, Y.-S. Gal, C.-W. Oh, S.-H. Park, K. T. Lim, *Carbohydrate Polymers* **2022**, 286, 119303.

[11]   a) R. Kilic Boz, D. Aydin, S. Kocak, B. Golba, R. Sanyal, A. Sanyal, *Bioconjugate Chemistry* **2022**, 33, 839; b) I. Altinbasak, R. Sanyal, A. Sanyal, *RSC Advances* **2016**, 6, 74757; c) I. Altinbasak, S. Kocak, R. Sanyal, A. Sanyal, *Biomacromolecules* **2022**, 23, 3525.

[12]   a) A. Meister, M. E. Anderson, *Annu Rev Biochem* **1983**, 52, 711; b) O. W. Griffith, *Free Radic Biol Med* **1999**, 27, 922; c) H. Sies, *Free Radic Biol Med* **1999**, 27, 916.

[13]   a) A. Meister, *Cancer Res* **1994**, 54, 1969s; b) I. Rahman, W. MacNee, *Free Radic Biol Med* **2000**, 28, 1405.

[14]   E. Bodnár, E. Bakondi, K. Kovács, C. Hegedűs, P. Lakatos, A. Robaszkiewicz, Z. Regdon, L. Virág, É. Szabó, *Oxid Med Cell Longev* **2018**, 2018, 5286785.

[15]   A. M. Rasik, A. Shukla, *Int J Exp Pathol* **2000**, 81, 257.

[16]   E. Mohammadifar, A. Bodaghi, A. Dadkhahtehrani, A. Nemati Kharat, M. Adeli, R. Haag, *ACS Macro Letters* **2017**, 6, 35.

[17]   S. Penczek, J. Pretula, *ACS Macro Letters* **2021**, 10, 1377.

[18]   D. Hölter, A. Burgath, H. Frey, *Acta Polymerica* **1997**, 48, 30.

[19]   in *Studies in Surface Science and Catalysis*, Vol. 131 (Eds: V. Dragutan, R. Streck), Elsevier **2000**, p. 967.

[20]   S. Patel, C. V. Preuss, F. Bernice, in *StatPearls*, StatPearls Publishing
Copyright © 2023, StatPearls Publishing LLC., Treasure Island (FL) ineligible companies. Disclosure: Charles Preuss declares no relevant financial relationships with ineligible companies. Disclosure: Fidelia Bernice declares no relevant financial relationships with ineligible companies. **2023**.

[21]   A. Shariati, M. Dadashi, M. T. Moghadam, A. van Belkum, S. Yaslianifard, D. Darban-Sarokhalil, *Sci Rep* **2020**, 10, 12689.

[22]   B. Thongrom, M. Dimde, U. Schedler, R. Haag, *Macromolecular Chemistry and Physics* **2023**, 224, 2200271.

[23]   T. Canal, N. A. Peppas, *Journal of Biomedical Materials Research* **1989**, 23, 1183.

[24]   J. D. Brewster, *Journal of Microbiological Methods* **2003**, 53, 77.

[25]   H. Maan, T. L. Povolotsky, Z. Porat, M. Itkin, S. Malitsky, I. Kolodkin-Gal, *Computational and Structural Biotechnology Journal* **2022**, 20, 15.

Supporting Information

Redox-Responsive Hydrogels Loaded with an Antibacterial Peptide as Controlled Drug Delivery for Infectious Wound Healing

Mariam Cherri, Paraskevi S. Stergiou, Zainab Ahmadian, Tatyana L. Povolotsky, Boonya Thongrom, Xin Fan, Ehsan Mohammadifar*, Rainer Haag*
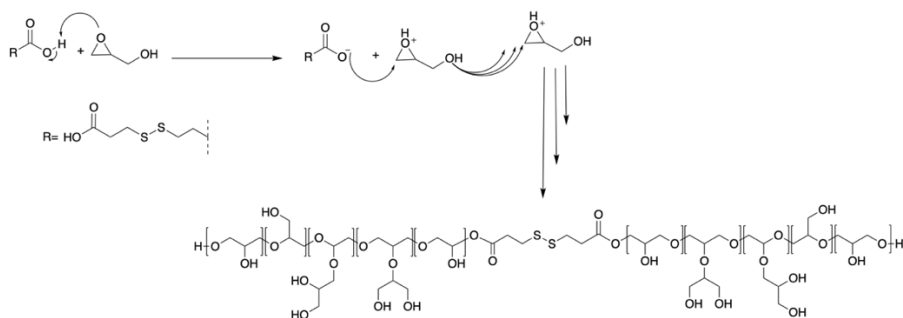
Scheme S1. Suggested reaction mechanism of the activated monomer (AM) cationic ring opening polymerization of glycidol with DTDPA acting as an initiator.

Synthesis and characterization of hPG-DTDPA
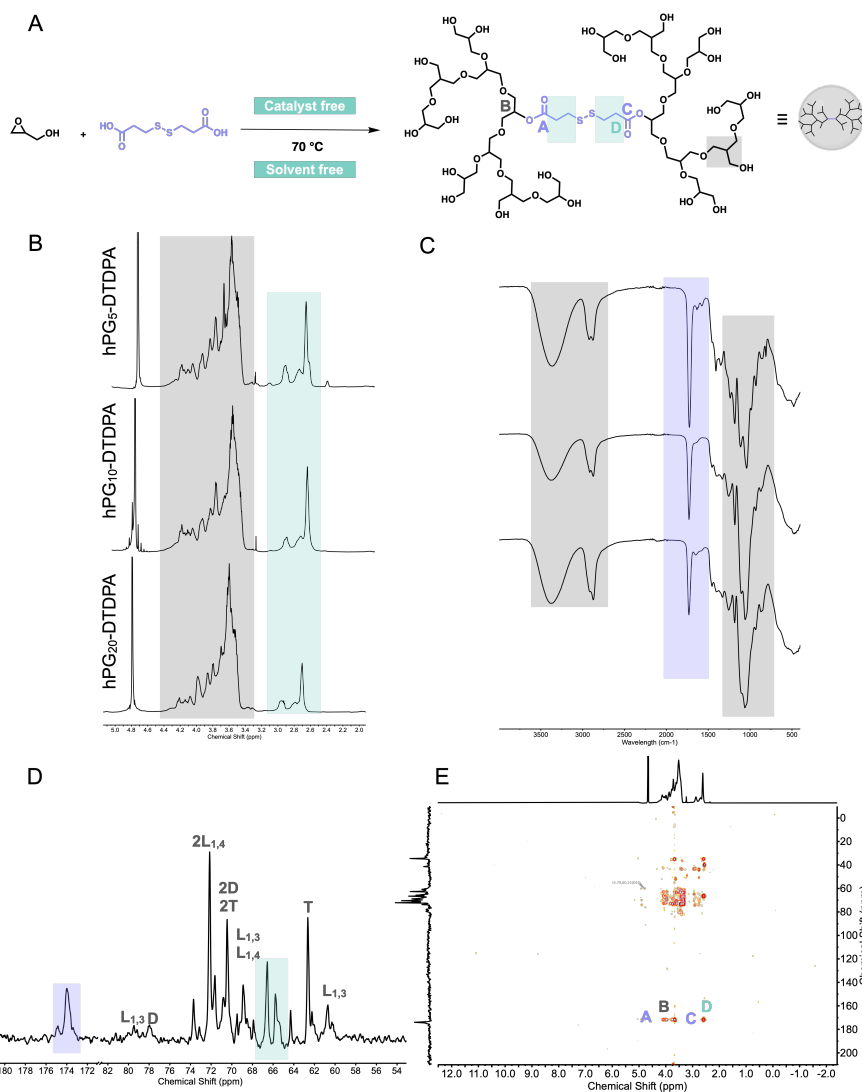
Figure S28. (A) Synthesis's scheme of the solvent-free, catalyst-free activated monomer cationic ring opening polymerization of glycidol using DTDPA, (B) and (C) ^{1}H NMR and FTIR spectra of hPG-DTDPA for different molar ratios [Gly]:[DTDPA] respectively, and (D) and

(E) inverse-gated ^{13}C NMR and HMBC spectra of hPG$_{10}$-DTDPA in D$_2$O in 500 or 600 Hz magnetic field.

Table S5. Characterization of reducible hPGs synthesized by different feed molar ratios of [Gly]:[DTDPA]

	hPG$_5$-DTDPA	hPG$_{10}$-DTDPA	hPG$_{20}$-DTDPA
Molar ratio of [Gly]:[DTDPA]	5:1	10:1	20:1
Degree of branching[a]	0.33	0.35	0.18
Terminal units[a] (%)	27	43	61
Dendritic units[a] (%)	14	12	4
Linear 1,3 units[a] (%)	11	7	6
Linear 1,4 units[a] (%)	47	43	61
M$_n$[b] (g/mol)	1600	2000	2400
Disulfide content[b] (%)	12.5	10.0	4.76
Disulfide content[c] (%)	14.16	11.08	4.76
Yield (%)	30	62	71

[a]Inverse-gated ^{13}C NMR in D$_2$O, [b]^{1}H NMR in D$_2$O and [c]elemental analysis.
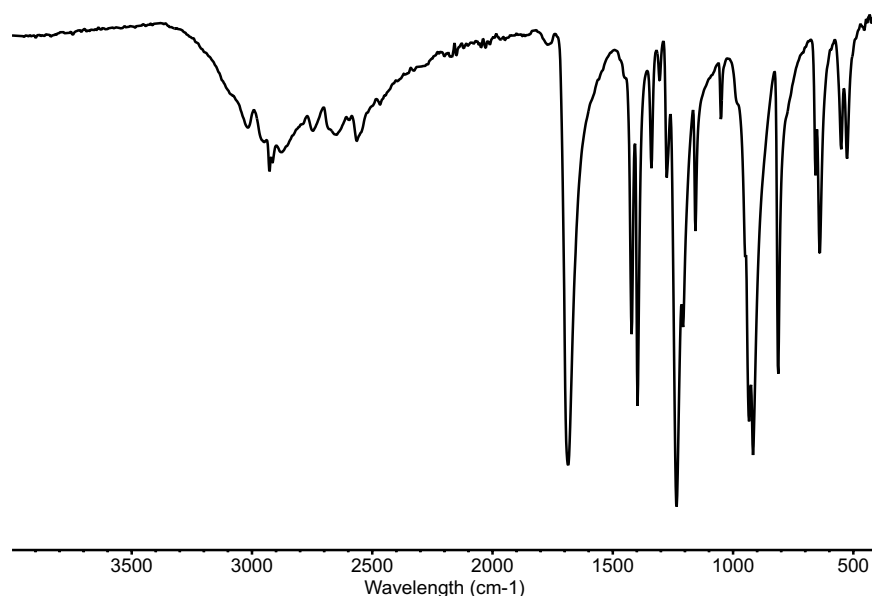
Figure S2. FTIR spectra of DTDPA showing the carbonyl stretch of the carboxylic acid at 1630 cm^{-1}.

^{1}H NMR molecular weight calculation

The molecular weight of the polymer is calculated by fixing the protons corresponding to DTDPA to 8.00, since there is only one molecule of DTDPA incorporated in the polymer. The

protons belonging to the polyglycidol backbone (3.4 – 4.4 ppm) were divided by 5 (number of protons in a repeating unit of glycidol) to calculate the number of glycidol repeating unit. The number of glycidol repeating units was then multiplied by the molecular weight of one repeating unit (74.08 g/mol) and added to the molecular weight of DTDPA (395.35 g/mol) to have the total molecular weight of the polymer (Equation S1).

$$M_n \ (g/mol) = \frac{\int 3.4 - 4.4 \ ppm}{5} \times M_{gly} + M_{DTDPA} \qquad \text{S1}$$

Degradation of SS-hPG with TCEP
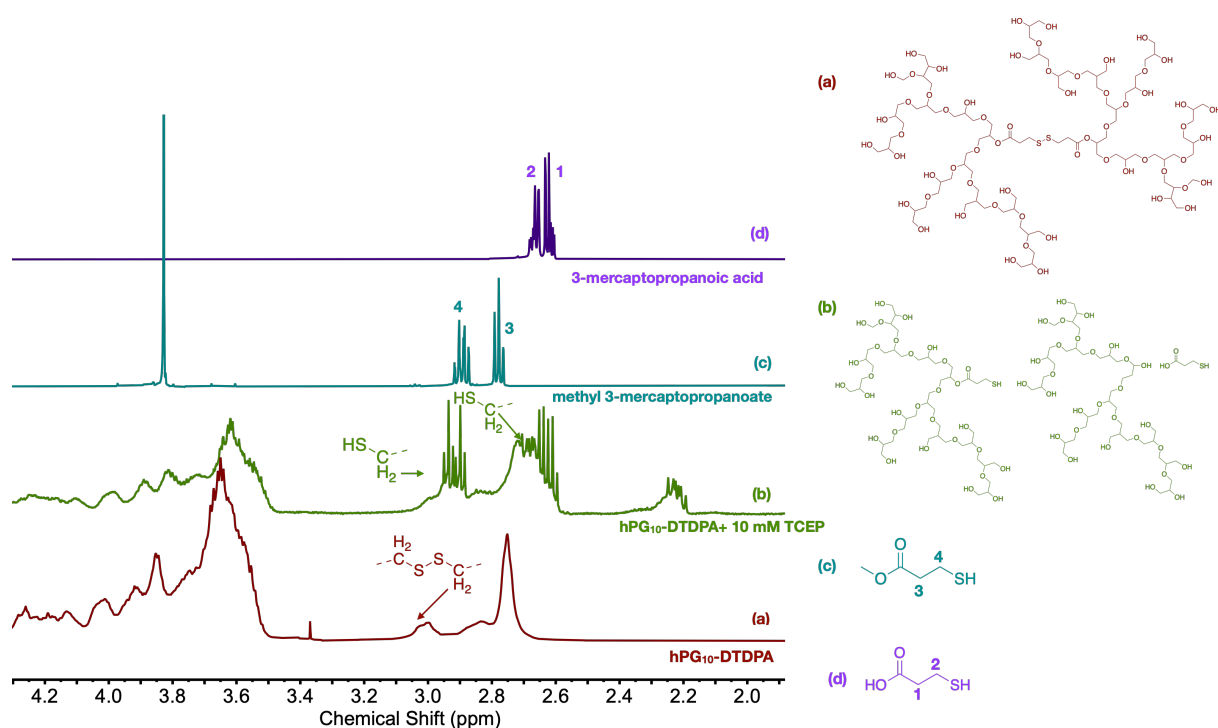
Figure S3. ^{1}H NMR in D$_2$O and structure corresponding to hPG$_{10}$-DTDPA (a), hPG$_{10}$-DTDPA + 10 mM TCEP (b), methyl 3-mercaptopropanoate (c) and 3-mercaptopropanoic acid (d). The objective was to identify the degradation products of hPG$_{10}$-DTDPA after its incubation with 10 mM TCEP.

To identify the correspondent of this peak, methyl 3-mercaptopropanoate and 3-mercaptopropionic acid ^{1}H NMR were recorded in D$_2$O. The reason is the presence of a methylene group adjacent to a thiol in both molecules and a methylene group adjacent to an ester and to a carboxylic acid in methyl 3-mercaptopropanoate and 3-mercaptopropionic respectively. Observing the spectra, the peaks of the protons of the methylene group adjacent to the thiol in both molecules overlap with the peaks in the degradation spectra. In addition, the

143

peaks of the protons of the methylene groups adjacent to an ester and carboxylic acid overlap as well. An acidic medium will partially hydrolyze the ester bonds, and knowing that TCEP will make the medium acidic, we except it to also hydrolyze the ester bonds partially in addition to cleaving the disulfide bond. Having the peaks overlap between the degradation spectra and the methyl 3-mercaptopropaoate and the 3-mercaptopropanoic acid spectra, can indicate that the presence of thiols, esters, and carboxylic acids in the degradation products.

Degree of acrylation calculation (dAcrylate %)

The degree of acrylation was calculated by fixing the integral of the protons corresponding to the glycidol (3.4-4.4 ppm) to 5.0 (number of protons in one glycidol repeating unit) to obtain the integral of the protons between 6.0 and 6.6. these protons belong to the alkene of the acrylate. This integral was then divided by 3 (number of protons in one alkene unit).

$$dAcrylate\ (\%) = \frac{\int 6.0 - 6.6\ ppm}{3} \times 100 \qquad \text{S2}$$

4-arm-PEG-thiol *synthesis & characterization*
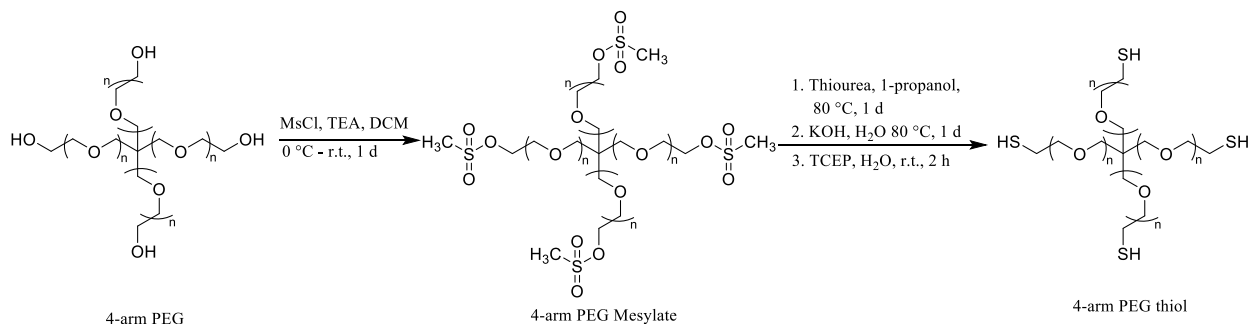
Scheme S2. Synthesis scheme of 4-arm-PEG-thiol.

Materials and Methods: Chemicals and solvents were purchased from Merck KGaA, Darmstadt, Germany and used directly without any purification unless stated otherwise. Diethyl ether (100%) was purchased from VWR chemicals. Potassium hydroxide (99.5%), and dichloromethane (DCM, 99%) were purchased from Fischer Scientific. 4-arm PEG 10 kDa was purchased from JenKem Technology USA Inc. Tris(2-carboxyethyl) phosphine hydrochloride (TCEP) was purchased from TCI Deutschland GmbH. All NMR spectra (1H and 13C) were recorded at 300 K by a Jeol Eclipse 500 MHz (Tokyo, Japan) or a Bruker AVANCE III 700 MHz spectrometer (Billerica, MA, USA). Chemical shifts δ were reported in ppm and the deuterated solvent peak was used as a standard. The determination of thiol group was performed

by an Agilent Cary 8454 UV/visible spectrophotometer using disposable semi-micro-UV cuvette.

Synthesis of 4-arm PEG mesylate: 10 kDa dried 4-arm PEG OH (Figure S1, 7 g, 0.7 mmol, 1 eq.) was dissolved in anhydrous dichloromethane (DCM, 50 mL) and TEA (0.97 mL, 7 mmol, 10 eq.) was added to the reaction flask. The mixture was cooled in an ice bath and methane sulfonyl chloride (0.43 mL, 5.6 mmol, 8 eq.) was added dropwise. The reaction was left to stir for 24 h. Afterwards, the crude product was washed three time with brine, dried with Na_2SO_4, and concentrated under high vacuum. The crude mixture was precipitated in cooled diethyl ether, collected, and dried overnight under high vacuum. The precipitate product was obtained as a white powder with an 85% isolated yield (Figure S2).
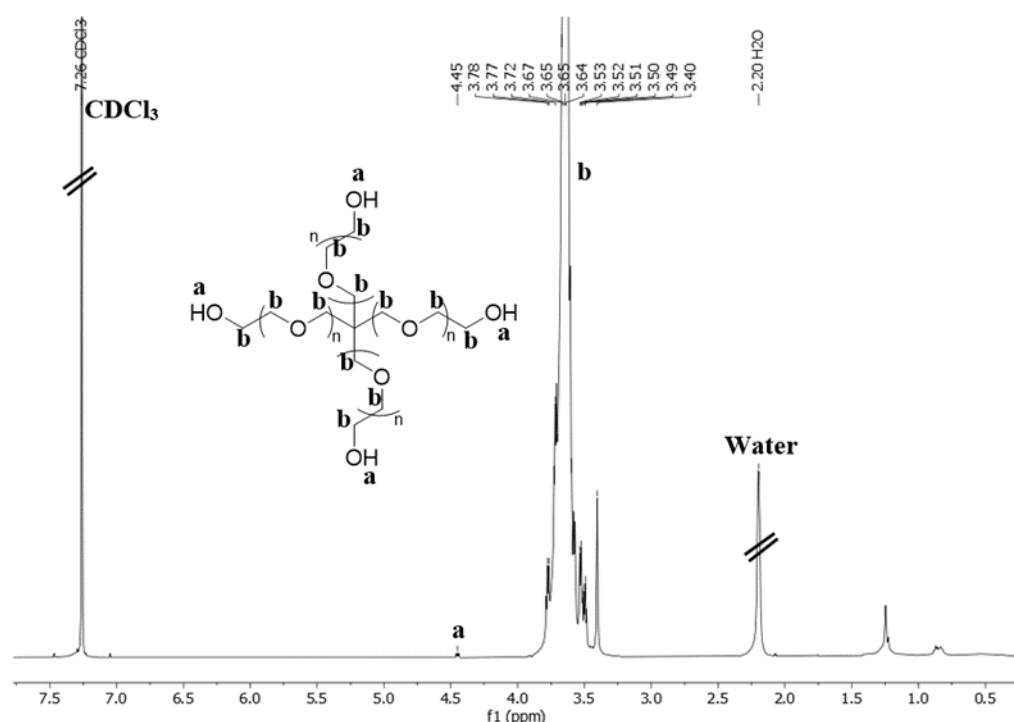
Figure S4. ^{1}H NMR of 4-arm PEG in $CDCl_3$.
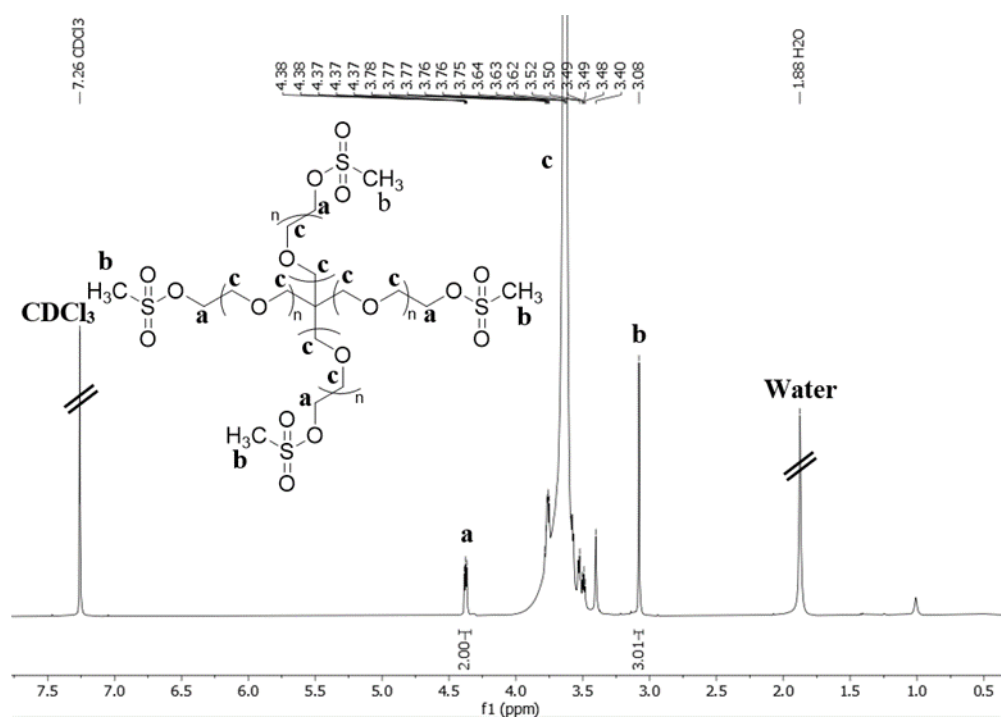
Figure S5. ^{1}H NMR of 4-arm PEG mesylate in CDCl$_3$.

Synthesis of 4-arm PEG thiol: 4-arm PEG mesylate (4.33 g, 0.43 mmol, 1 eq.) and thiourea (0.66 g, 8.7 mmol, 20 eq.) were added to the reaction flask containing 1-propanol (10 mL). The reaction stirred for 24 h at 80 °C to obtain the 4-arm PEG isothiouronium intermediate. After removing 1-propanol, KOH (0.024 g, 0.43 mmol, 4 eq.) and water (40 mL) were added to the reaction flask and the solution was heated again to 80 °C for 24 h. TCEP (0.5 g, 1.7 mmol, 4 eq.) was added to the crude mixture that was stirred for 2 h. The product was purified by first saturating the crude mixture with NaCl, second extracting the product with DCM three times, and drying it with Na$_2$SO$_4$, third concentrating the DCM layer, and finally precipitating it in cooled diethyl ether. Dried 4-arm PEG thiol was obtained as a pale yellowish powder with a 90% isolated yield (Figure 3). Free thiol content was also characterized by Ellman's assay following the protocol of Thermofischer Scientific. The number of thiol groups was quantified using the standard calibration curve of cysteine which contains 1 thiol group. The result shows that the number of thiol group on 4-arm PEG thiol is approximately 3.7 groups).
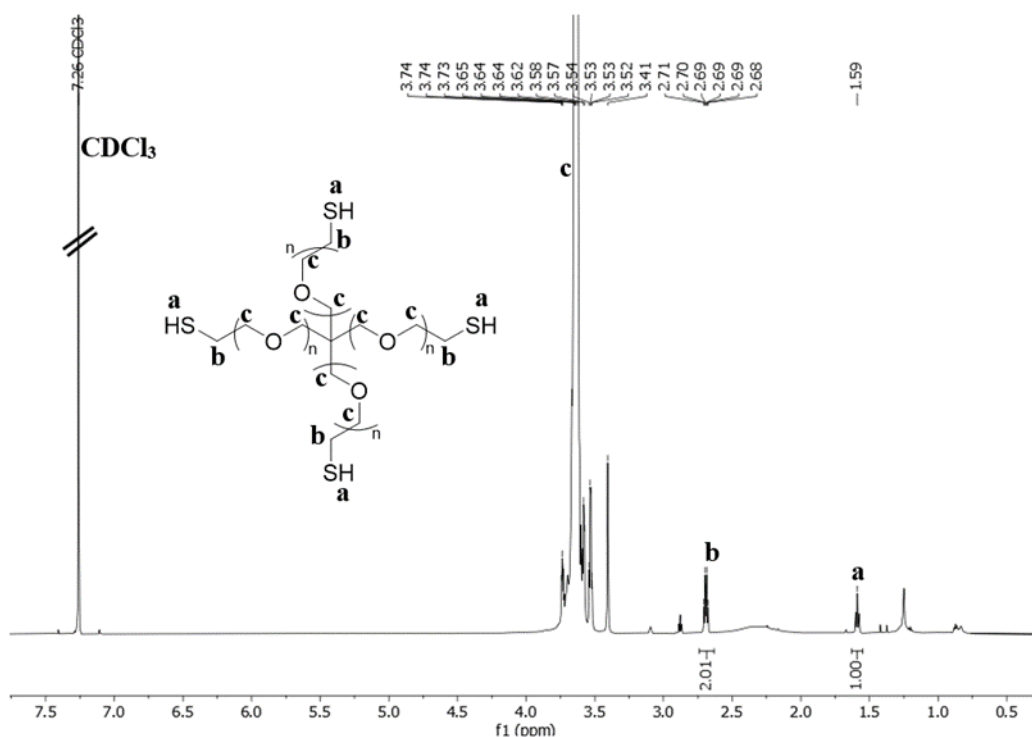
Figure S6. ^{1}H NMR of 4-arm PEG thiol in CDCl$_3$.

Formation of the hydrogel
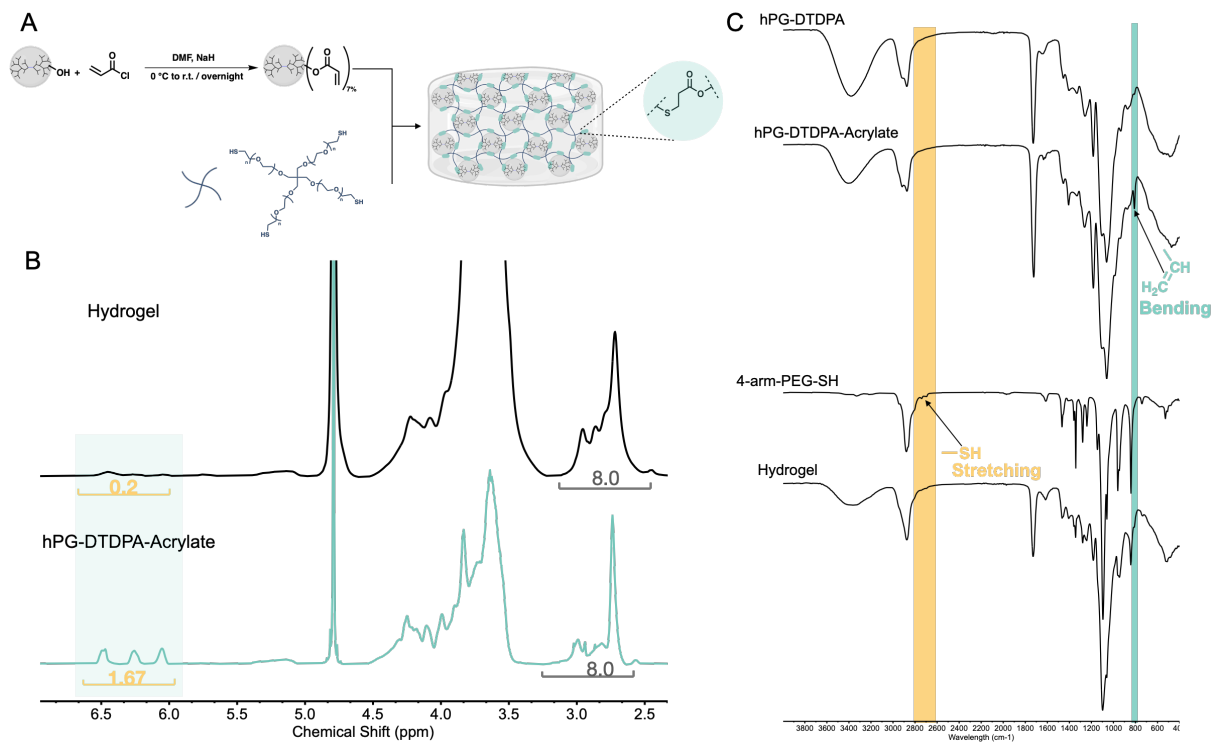
Figure S7. (A) Hydrogel's synthesis scheme by first preforming acrylation of 7% of the hydroxyl groups of hPG$_{10}$-DTDPA and crosslinking it with 4-arm-PEG-SH via a thiol-ene click

reaction in PBS solution, (B) ^{1}H NMR of hPG$_{10}$-DTDPA-Acrylate and the formed hydrogel in deuterated PBS buffer, the disappearance of peaks corresponding to the alkene's protons prove the occurrence of the click reaction in deuterated PBS buffer and (C) FTIR spectra of hPG$_{10}$-DTDPA, hPG$_{10}$-DTDPA-acrylate, 4-arm-PEG-SH and the formed hydrogel, the peaks corresponding the alkene bending and thiol stretching disappears in the formed hydrogel, proving the reaction.
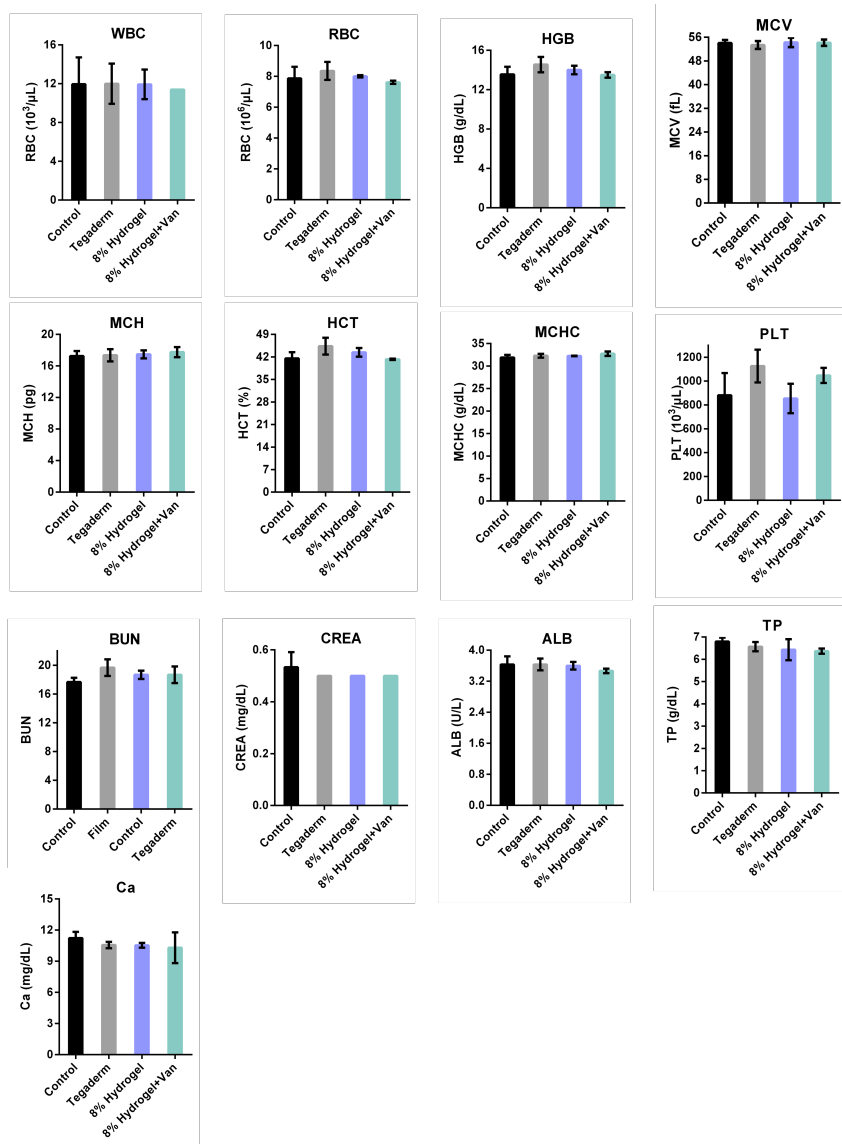
Figure S8. Blood hematological and biochemical factors for the control, Tegaderm, 8% Hydrogel and 8% Hydrogel+Van groups

4 Conclusion & Summary

This work aims to develop novel systems for the transport of active pharmaceutical ingredient (API) especially small molecules to specific target in biological entities by tackling the main three challenges that this domain faces. The challenges of solubilizing hydrophobic drugs, the elimination of drugs from the blood stream and specific targeting to a defined site. The system is based on biodegradable polyglycerol copolymers by integrating biodegradable moieties into the polyglycerol backbone via the copolymerization of the glycidol monomer with 7-membered lactone rings containing an ester functional group or an ester and disulfide bond functional group, and a linear diacid that contains a disulfide bond. In the first two projects where the comonomer chosen was caprolactone, two host molecules were encapsulated in the DDS, sunitinib for cancer therapy and tofacitinib for skin inflammation therapy. The structure of the project can be divided into the following packages: (i) bulk straightforward-synthesis of the copolymer, (ii) chemical and physical characterization, (iii) encapsulation and release of the chosen API (iv) *in vitro* biological assays, and (v) *in vivo* or *ex vivo* tests. In both cases the system was proven to increase the solubilization of the guest drug significantly and improve its performance in comparison to the drug alone. The introduction of the sulfate end groups into the system led to its accumulation into the specific site *in vivo*.

In the first project, the copolymers were synthesized on a large scale (20 g) through a simple two-step process. *In vivo* fluorescence imaging revealed significant accumulation of the DDS in tumor environments. Sunitinib, an anticancer drug, was loaded into the DDS, and its toxicity was assessed both *in vitro* and *in vivo*. Results showed similar toxicities between the drug encapsulated in dPGS-PCL and the free drug in A431 and HT-29 cells, with comparable cellular uptake. In the second project, the chosen API was tofacitinib. Inflammatory skin disorders, such as psoriasis and alopecia areata, stem from dysregulation in the innate immune system, triggering the Janus kinase-signal transducer and activator of transcription (JAK-STAT) inflammatory pathway by cytokines like interleukin 6 (IL-6). JAK inhibitors, notably tofacitinib, disrupt this pathway by binding to JAK enzymes. However, topical applications of these inhibitors show limited efficacy, particularly for alopecia areata. This study introduces a novel carrier, sulfated dendritic polyglycerol with caprolactone segments (dPGS-PCL), to improve tofacitinib delivery. Testing on ex-vivo human skin models demonstrates enhanced skin penetration of tofacitinib when loaded into dPGS-PCL compared to free tofacitinib. Anti-inflammatory efficacy was evaluated through IL-6 and IL-8 release, and STAT3 and STAT5 activation assays in inflamed skin models, indicating reduced activation of inflammatory markers with increased tofacitinib penetration.

The second system and third project, glycidol was copolymerized with the comonomer containing an ester and a disulfide bond, were investigated thoroughly in terms of structure and physical characteristics. The purpose was to understand the effect of the disulfide bond, whether on the initial stages like synthesis or later stages like the chemical and physical characteristics of the copolymer. Its copolymerization with glycidol was compared to the copolymerization of caprolactone with glycidol under the same conditions via two different copolymerization mechanisms. Interestingly, the structure obtained when using the comonomer containing the disulfide bond was unique: an ideal random copolymer. This was not the case when the comonomer used was caprolactone. Moreover, three different copolymers of the same molecular weight with different disulfide ratios were tested for degradation and behavior in aqueous solution. The project also focused on the biocompatibility of the copolymer for future employment in biological entities.

Third system and fourth project, glycidol was copolymerized with a diacid that contains a disulfide bond in a simple manner, without another catalyst or solvent. The diacid acted as the proton donor to initiate the polymerization and was integrated in the polyglycerol backbone. Redox-degradable hydrogels loaded with an antibacterial peptide (vancomycin) were formed using the reducible polyglycerol as a building block, cross-linked by 4-arm polyethylene glycol-thiol (4-arm PEG-SH). The hydrogel degrades under reductive conditions triggered by glutathione, leading to the controlled release of the antibacterial peptide. Rheological analysis was conducted to assess the mechanical properties, including stiffness, softness, and self-healing capability, for various ratios and concentrations of both components. Hydrogel degradation was confirmed through rheological measurements and weight loss analysis. FITC-albumin and vancomycin were successfully loaded into the hydrogel, and the release kinetics were evaluated for both sustained and on-demand release profiles. Furthermore, *in vitro*, and *in vivo* experiments demonstrated that the vancomycin-loaded hydrogel acts as an effective antibacterial barrier for wound dressing and accelerates the healing of infectious wounds in a mouse model.

In conclusion, the design of straightforward, scalable, and solvent free drug delivery systems is crucial for an adequate translation of the system from research to application stage. However, the knowledge around the system should be complete and the performance should be maximized. Moving forward from the first system into the second, and third the expectation of the improvement of the system is suggested by introducing a second degradable moiety that will in retrospect enhance the drug release. Therefore, the future steps should focus on the encapsulation of a guest molecule and its release and testing the disulfide containing system *in*

vivo, to be able to compare the performance to the caprolactone containing system, keeping in mind that challenges might also arise along the way due to the sensitive nature of the disulfide bond.

5 Zusammenfassung

Ziel dieser Arbeit ist die Entwicklung neuartiger Systeme für den Transport von Wirkstoff, insbesondere von kleinen Molekülen, zu spezifischen Zielen in biologischen Einheiten, indem die drei wichtigsten Herausforderungen in diesem Bereich angegangen werden. Die Herausforderungen sind die Solubilisierung hydrophober Arzneimittel, die Beseitigung von Arzneimitteln aus dem Blutkreislauf und die spezifische Ausrichtung auf eine bestimmte Stelle. Das System basiert auf biologisch abbaubaren Polyglycerin-Copolymeren, in die biologisch abbaubaren Komponenten durch Copolymerisation des Glycidol-Monomers mit 7-gliedrigen Lactonringen, die eine funktionelle Estergruppe oder eine funktionelle Ester- und Disulfidbindungsgruppe enthalten, und einer linearen Disäure, die eine Disulfidbindung enthält, in das Polyglycerin-Grundgerüst integriert werden. In den ersten beiden Projekten, bei denen als Comonomer Caprolacton gewählt wurde, wurden zwei Wirtsmoleküle in die DDS eingekapselt, Sunitinib für die Krebstherapie und Tofacitinib für die Therapie von Hautentzündungen. Die Struktur des Projekts kann in folgende Pakete unterteilt werden: (i) einfache Synthese des Copolymers, (ii) chemische und physikalische Charakterisierung, (iii) Verkapselung und Freisetzung des ausgewählten Wirkstoffs, (iv) biologische In-vitro-Tests und (v) In-vivo- oder Ex-vivo-Tests. In beiden Fällen wurde nachgewiesen, dass das System die Solubilisierung des Gastarzneimittels signifikant erhöht und seine Leistung im Vergleich zum Arzneimittel allein verbessert. Die Einführung der Sulfat-Endgruppen in das System führte zu seiner Anreicherung an der spezifischen Stelle *in vivo*.

Im ersten Projekt wurden die Copolymere in großem Maßstab (20 g) in einem einfachen zweistufigen Verfahren synthetisiert. *in vivo*-Fluoreszenzaufnahmen zeigten eine signifikante Anreicherung der DDS in der Tumorumgebung. Sunitinib, ein Krebsmedikament, wurde in die DDS eingebracht, und seine Toxizität wurde sowohl *in vitro* als auch *in vivo* untersucht. Die Ergebnisse zeigten eine ähnliche Toxizität des in dPGS-PCL eingekapselten Wirkstoffs und des freien Wirkstoffs in A431- und HT-29-Zellen bei vergleichbarer zellulärer Aufnahme. Im zweiten Projekt wurde der Wirkstoff Tofacitinib ausgewählt. Entzündliche Hauterkrankungen wie Psoriasis und Alopecia areata sind auf eine Fehlregulierung des angeborenen Immunsystems zurückzuführen, die durch Zytokine wie Interleukin 6 (IL-6) den Janus-Kinase-Signalüberträger und Aktivator der Transkription (JAK-STAT) Entzündungsweg auslöst. JAK-Inhibitoren, insbesondere Tofacitinib, unterbrechen diesen Signalweg durch Bindung an die JAK-Enzyme. Die topische Anwendung dieser Inhibitoren ist jedoch nur begrenzt wirksam, insbesondere bei Alopecia areata. In dieser Studie wird ein neuartiger Träger, sulfatiertes dendritisches Polyglycerin mit Caprolacton-Segmenten (dPGS-PCL), vorgestellt, um die

Abgabe von Tofacitinib zu verbessern. Tests an menschlichen *ex-vivo*-Hautmodellen zeigen eine verbesserte Hautpenetration von Tofacitinib, wenn es in dPGS-PCL geladen ist, im Vergleich zu freiem Tofacitinib. Die entzündungshemmende Wirksamkeit wurde anhand der Freisetzung von IL-6 und IL-8 sowie der STAT3- und STAT5-Aktivierung in entzündeten Hautmodellen bewertet, was auf eine geringere Aktivierung von Entzündungsmarkern bei erhöhter Tofacitinib-Penetration hindeutet.

Im zweiten System und dritten Projekt wurde Glycidol mit einem Comonomer, dass einen Ester und eine Disulfidbindung enthält, copolymerisiert und gründlich auf seine Struktur und physikalischen Eigenschaften hin untersucht. Ziel war es, die Auswirkungen der Disulfidbindung zu verstehen, sei es auf die Anfangsphasen wie die Synthese oder auf spätere Phasen wie die chemischen und physikalischen Eigenschaften des Copolymers. Die Copolymerisation mit Glycidol wurde mit der Copolymerisation von Caprolacton mit Glycidol unter den gleichen Bedingungen über zwei verschiedene Copolymerisationsmechanismen verglichen. Interessanterweise war die Struktur, die bei Verwendung des Comonomers mit der Disulfidbindung erhalten wurde, einzigartig: ein ideales statistisches Copolymer. Dies war nicht der Fall, wenn das verwendete Comonomer Caprolacton war. Darüber hinaus wurden drei verschiedene Copolymere desselben Molekulargewichts mit unterschiedlichen Disulfidverhältnissen auf ihre Abbaubarkeit und ihr Verhalten in wässriger Lösung getestet. Das Projekt konzentrierte sich auch auf die Biokompatibilität des Copolymers für den zukünftigen Einsatz in biologischen Einheiten.

Im dritten System und vierten Projekt wurde Glycidol mit einer Disäure, die eine Disulfidbindung enthält, auf einfache Weise ohne einen weiteren Katalysator oder ein Lösungsmittel copolymerisiert. Die Disäure diente als Protonendonator zur Initiierung der Polymerisation und ist in das Polyglycerin-Grundgerüst integriert. Unter Verwendung des reduzierbaren Polyglycerins als Baustein wurden mit einem antibakteriellen Peptid (Vancomycin) beladene, redox-abbaubare Hydrogele gebildet, die durch 4-armiges Polyethylenglykol-Thiol (4-armiges PEG-SH) vernetzt sind. Das Hydrogel wird unter reduktiven Bedingungen, ausgelöst durch Glutathion, abgebaut, was zu einer kontrollierten Freisetzung des antibakteriellen Peptids führt. Es wurden rheologische Analysen durchgeführt, um die mechanischen Eigenschaften, einschließlich Steifheit, Weichheit und Selbstheilungsfähigkeit, für verschiedene Verhältnisse und Konzentrationen der beiden Komponenten zu bewerten. Der Abbau des Hydrogels wurde durch rheologische Messungen und Gewichtsverlustanalysen bestätigt. FITC-Albumin und Vancomycin wurden erfolgreich in das Hydrogel geladen, und die Freisetzungskinetik wurde sowohl für anhaltende als auch für

bedarfsgesteuerte Freisetzungsprofile bewertet. Darüber hinaus zeigten *in vitro*- und *in vivo*-Experimente, dass das mit Vancomycin beladene Hydrogel als wirksame antibakterielle Barriere für Wundverbände fungiert und die Heilung von infektiösen Wunden in einem Mausmodell beschleunigt.

Zusammenfassend lässt sich sagen, dass die Entwicklung einfacher, skalierbarer und lösungsmittelfreier Systeme für die Verabreichung von Arzneimitteln von entscheidender Bedeutung für eine angemessene Umsetzung des Systems von der Forschung in die Anwendung ist. Allerdings sollte das Wissen um das System vollständig sein und die Leistung sollte maximiert werden. Wenn man vom ersten System zum zweiten und dritten übergeht, wird eine Verbesserung des Systems durch die Einführung einer zweiten abbaubaren Komponente vorgeschlagen, die im Nachhinein die Freisetzung des Medikaments verbessern wird. Daher sollten sich künftige Schritte auf die Verkapselung eines Gastmoleküls und dessen Freisetzung konzentrieren und das disulfidhaltige System *in vivo* testen, um die Leistung mit der des caprolactonhaltigen Systems vergleichen zu können, wobei zu berücksichtigen ist, dass aufgrund der empfindlichen Natur der Disulfidbindung auf dem Weg dorthin auch Herausforderungen auftreten können.

6   References

1.   Ehrlich, P. Beitrage zur Theorie und Praxis der histologischen Farbung. Beitrage zur Theorie und Praxis der histologischen Farbung, Leipzig, 1878.

2.   Ehrlich, P., Theorie und Praxis der Chemotherapie. *Folia Serologica* **1911,** *7*, 697-714.

3.   Bäumler, E.; Ehrlich, P., *Forscher für das Leben*. 3rd ed.; Minerva, Frankfurt am Main, 1997.

4.   Ehrlich, P., Die Wertbemessung des Diphterieheilserums und deren theoretische Grundlagen. *Klinisches Jahrbuch* **1897,** *6*, 299–326.

5.   Ehrlich, P.; Morgenroth, J., Ueber Haemolysine: dritte Mittheilung. *Berliner klinische Wochenschrift* **1900,** *37*, 453–458.

6.   Ehrlich, P., Chemotherapeutische Trypanosomen-Studien. *Berliner klinische Wochenschrift* **1907,** *44*, 233–236.

7.   Ehrlich, P., Die Behandlung der Syphilis mit dem Ehrlichschen Präparat 606. *Deutsche medizinische Wochenschrift* **1910**, 1893-1896.

8.   Strebhardt, K.; Ullrich, A., Paul Ehrlich's magic bullet concept: 100 years of progress. *Nat. Rev. Cancer* **2008,** *8* (6), 473-480.

9.   Ehrlich, P., *The Collected Papers of Paul Ehrlich*. F. Himmelweit ed.; Pergamon Press: 1960.

10.   Friche, E.; Jensen, P. B.; Sehested, M.; Demant, E. J.; Nissen, N. N., The solvents cremophor EL and Tween 80 modulate daunorubicin resistance in the multidrug resistant Ehrlich ascites tumor. *Cancer Commun.* **1990,** *2* (9), 297-303.

11.   Weiszhár, Z.; Czúcz, J.; Révész, C.; Rosivall, L.; Szebeni, J.; Rozsnyay, Z., Complement activation by polyethoxylated pharmaceutical surfactants: Cremophor-EL, Tween-80 and Tween-20. *Eur. J. Pharm. Sci.* **2012,** *45* (4), 492-8.

12.   Cardiac glycosides. In *Meyler's Side Effects of Drugs (Sixteenth Edition)*, Aronson, J. K., Ed. Elsevier: Oxford, 2016; pp 117-157.

13.   Gelderblom, H.; Verweij, J.; Nooter, K.; Sparreboom, A., Cremophor EL: the drawbacks and advantages of vehicle selection for drug formulation. *Eur. J. Cancer* **2001,** *37* (13), 1590-8.

14.   Coors, E. A.; Seybold, H.; Merk, H. F.; Mahler, V., Polysorbate 80 in medical products and nonimmunologic anaphylactoid reactions. *Ann. Allergy, Asthma, Immunol.* **2005,** *95* (6), 593-599.

15.   Kerwin, B. A., Polysorbates 20 and 80 used in the formulation of protein biotherapeutics: structure and degradation pathways. *J. Pharm. Sci.* **2008,** *97* (8), 2924-35.

16.   Chou, D. K.; Krishnamurthy, R.; Randolph, T. W.; Carpenter, J. F.; Manning, M. C., Effects of Tween 20® and Tween 80® on the Stability of Albutropin During Agitation. *J. Pharm.l Sci.* **2005,** *94* (6), 1368-1381.

17.   Min, Y.; Akbulut, M.; Kristiansen, K.; Golan, Y.; Israelachvili, J., The role of interparticle and external forces in nanoparticle assembly. *Nat. Mater.* **2008,** *7* (7), 527-538.

18.   Dagastine, R. R.; Manica, R.; Carnie, S. L.; Chan, D. Y.; Stevens, G. W.; Grieser, F., Dynamic forces between two deformable oil droplets in water. *Science* **2006,** *313* (5784), 210-3.

19.   Kim, H. Y.; Sofo, J. O.; Velegol, D.; Cole, M. W.; Lucas, A. A., Van der Waals dispersion forces between dielectric nanoclusters. *Langmuir* **2007,** *23* (4), 1735-40.

20.   Nel, A. E.; Mädler, L.; Velegol, D.; Xia, T.; Hoek, E. M. V.; Somasundaran, P.; Klaessig, F.; Castranova, V.; Thompson, M., Understanding biophysicochemical interactions at the nano–bio interface. *Nat. Mater.* **2009,** *8* (7), 543-557.

21.   Evans, D. F.; Wennerström, H., The colloidal domain: where physics, chemistry, biology, and technology meet. **1999**.

22.   Hunter, R. J.; White, L. R.; Chan, D. Y., Foundations of colloid science. *(No Title)* **1987**.

23.   Israelachvili, J. N., Surface forces. In *The Handbook of Surface Imaging and Visualization*, CRC Press: 2022; pp 793-816.

24.   Derjaguin, B. V., Theory of the stability of strongly charged lyophobic sol and of the adhesion of strongly charged particles in solutions of electrolytes. *Acta phys. chim. URSS* **1941,** *14*, 633.

25.   Overbeek, J. T. G.; Verwey, E., *Theory of the stability of lyophobic colloids: the interaction of sol particles having an electric double layer*. 1948.

26.   Baca, H. K.; Ashley, C.; Carnes, E.; Lopez, D.; Flemming, J.; Dunphy, D.; Singh, S.; Chen, Z.; Liu, N.; Fan, H.; López, G. P.; Brozik, S. M.; Werner-Washburne, M.; Brinker, C. J., Cell-Directed Assembly of Lipid-Silica Nanostructures Providing Extended Cell Viability. *Science* **2006,** *313* (5785), 337-341.

27.   Baca, H. K.; Carnes, E.; Singh, S.; Ashley, C.; Lopez, D.; Brinker, C. J., Cell-directed assembly of bio/nano interfaces-a new scheme for cell immobilization. *Acc. Chem. Res.* **2007,** *40* (9), 836-45.

28. Dobrovolskaia, M. A.; McNeil, S. E., Immunological properties of engineered nanomaterials. *Nat. Nanotechnol.* **2007,** *2* (8), 469-478.

29. Swanson, J. A., Shaping cups into phagosomes and macropinosomes. *Nat. Rev. Mol. Cell Biol.* **2008,** *9* (8), 639-49.

30. Chen, H.; Langer, R.; Edwards, D. A., A Film Tension Theory of Phagocytosis. *J. Colloid Interface Sci.* **1997,** *190* (1), 118-33.

31. McNeil, S. E., Nanoparticle therapeutics: a personal perspective. *Wiley Interdiscip Rev Nanomed. Nanobiotechnol.* **2009,** *1* (3), 264-71.

32. Goodman, C. M.; McCusker, C. D.; Yilmaz, T.; Rotello, V. M., Toxicity of Gold Nanoparticles Functionalized with Cationic and Anionic Side Chains. *Bioconjugate Chem.* **2004,** *15* (4), 897-900.

33. Xia, T.; Kovochich, M.; Liong, M.; Zink, J. I.; Nel, A. E., Cationic polystyrene nanosphere toxicity depends on cell-specific endocytic and mitochondrial injury pathways. *ACS Nano* **2008,** *2* (1), 85-96.

34. Grayson, S. M.; Godbey, W. T., The role of macromolecular architecture in passively targeted polymeric carriers for drug and gene delivery. *J. Drug Target.* **2008,** *16* (5), 329-56.

35. Fang, J.; Islam, W.; Maeda, H., Exploiting the dynamics of the EPR effect and strategies to improve the therapeutic effects of nanomedicines by using EPR effect enhancers. *Adv. Drug Delivery Rev.* **2020,** *157*, 142-160.

36. Matsumura, Y.; Maeda, H., A new concept for macromolecular therapeutics in cancer chemotherapy: mechanism of tumoritropic accumulation of proteins and the antitumor agent smancs. *Cancer Res.* **1986,** *46* (12 Pt 1), 6387-92.

37. Seymour, L. W.; Duncan, R.; Strohalm, J.; Kopecek, J., Effect of molecular weight (Mw) of N-(2-hydroxypropyl)methacrylamide copolymers on body distribution and rate of excretion after subcutaneous, intraperitoneal, and intravenous administration to rats. *J. Biomed. Mater. Res.* **1987,** *21* (11), 1341-58.

38. Choi, H. S.; Liu, W.; Misra, P.; Tanaka, E.; Zimmer, J. P.; Itty Ipe, B.; Bawendi, M. G.; Frangioni, J. V., Renal clearance of quantum dots. *Nat. Biotechnol.* **2007,** *25* (10), 1165-70.

39. Longmire, M.; Choyke, P. L.; Kobayashi, H., Clearance properties of nano-sized particles and molecules as imaging agents: considerations and caveats. *Nanomedicine (Lond)* **2008,** *3* (5), 703-17.

40.   Vicent, M. J.; Duncan, R., Polymer conjugates: nanosized medicines for treating cancer. *Trends Biotechnol.* **2006,** *24* (1), 39-47.

41.   Danhier, F.; Feron, O.; Préat, V., To exploit the tumor microenvironment: Passive and active tumor targeting of nanocarriers for anti-cancer drug delivery. *J. Controlled Release* **2010,** *148* (2), 135-46.

42.   Kavand, A.; Anton, N.; Vandamme, T.; Serra, C. A.; Chan-Seng, D., Synthesis and functionalization of hyperbranched polymers for targeted drug delivery. *J. Controlled Release* **2020,** *321*, 285-311.

43.   Golombek, S. K.; May, J.-N.; Theek, B.; Appold, L.; Drude, N.; Kiessling, F.; Lammers, T., Tumor targeting via EPR: Strategies to enhance patient responses. *Adv. Drug Delivery Rev.* **2018,** *130*, 17-38.

44.   Sindhwani, S.; Syed, A. M.; Ngai, J.; Kingston, B. R.; Maiorino, L.; Rothschild, J.; MacMillan, P.; Zhang, Y.; Rajesh, N. U.; Hoang, T.; Wu, J. L. Y.; Wilhelm, S.; Zilman, A.; Gadde, S.; Sulaiman, A.; Ouyang, B.; Lin, Z.; Wang, L.; Egeblad, M.; Chan, W. C. W., The entry of nanoparticles into solid tumours. *Nat. Mater.* **2020,** *19* (5), 566-575.

45.   Farkhani, S. M.; Valizadeh, A.; Karami, H.; Mohammadi, S.; Sohrabi, N.; Badrzadeh, F., Cell penetrating peptides: efficient vectors for delivery of nanoparticles, nanocarriers, therapeutic and diagnostic molecules. *Peptides* **2014,** *57*, 78-94.

46.   Ruoslahti, E., Tumor penetrating peptides for improved drug delivery. *Adv. Drug Delivery Rev.* **2017,** *110-111*, 3-12.

47.   Zhang, X. X.; Eden, H. S.; Chen, X., Peptides in cancer nanomedicine: drug carriers, targeting ligands and protease substrates. *J. Controlled Release* **2012,** *159* (1), 2-13.

48.   Liu, J.; Wei, T.; Zhao, J.; Huang, Y.; Deng, H.; Kumar, A.; Wang, C.; Liang, Z.; Ma, X.; Liang, X. J., Multifunctional aptamer-based nanoparticles for targeted drug delivery to circumvent cancer resistance. *Biomaterials* **2016,** *91*, 44-56.

49.   Chen, K.; Liu, B.; Yu, B.; Zhong, W.; Lu, Y.; Zhang, J.; Liao, J.; Liu, J.; Pu, Y.; Qiu, L.; Zhang, L.; Liu, H.; Tan, W., Advances in the development of aptamer drug conjugates for targeted drug delivery. *Wiley Interdiscip. Rev. Nanomed. Nanobiotechnol.* **2017,** *9* (3).

50.   Ray, P.; White, R. R., Aptamers for Targeted Drug Delivery. *Pharmaceuticals (Basel)* **2010,** *3* (6), 1761-1778.

51.   Zhao, X.; Li, H.; Lee, R. J., Targeted drug delivery via folate receptors. *Expert Opin. Drug Delivery* **2008,** *5* (3), 309-19.

52. Marchetti, C.; Palaia, I.; Giorgini, M.; De Medici, C.; Iadarola, R.; Vertechy, L.; Domenici, L.; Di Donato, V.; Tomao, F.; Muzii, L.; Benedetti Panici, P., Targeted drug delivery via folate receptors in recurrent ovarian cancer: a review. *Onco. Targets Ther.* **2014,** *7*, 1223-36.

53. Fleige, E.; Quadir, M. A.; Haag, R., Stimuli-responsive polymeric nanocarriers for the controlled transport of active compounds: Concepts and applications. *Adv. Drug Delivery Rev.* **2012,** *64* (9), 866-884.

54. Wong, P. T.; Choi, S. K., Mechanisms of drug release in nanotherapeutic delivery systems. *Chem. Rev.* **2015,** *115* (9), 3388-432.

55. Colson, Y. L.; Grinstaff, M. W., Biologically responsive polymeric nanoparticles for drug delivery. *Adv. Mater.* **2012,** *24* (28), 3878-86.

56. Fleige, E.; Quadir, M. A.; Haag, R., Stimuli-responsive polymeric nanocarriers for the controlled transport of active compounds: concepts and applications. *Ad.v Drug Delivery Rev.* **2012,** *64* (9), 866-84.

57. Karimi, M.; Eslami, M.; Sahandi-Zangabad, P.; Mirab, F.; Farajisafiloo, N.; Shafaei, Z.; Ghosh, D.; Bozorgomid, M.; Dashkhaneh, F.; Hamblin, M. R., pH-Sensitive stimulus-responsive nanocarriers for targeted delivery of therapeutic agents. *Wiley Interdiscip Rev Nanomed. Nanobiotechnol.* **2016,** *8* (5), 696-716.

58. Kratz, F.; Müller, I. A.; Ryppa, C.; Warnecke, A., Prodrug strategies in anticancer chemotherapy. *ChemMedChem* **2008,** *3* (1), 20-53.

59. Filomeni, G.; Rotilio, G.; Ciriolo, M. R., Cell signalling and the glutathione redox system. *Biochem. Pharmacol.* **2002,** *64* (5), 1057-1064.

60. Niu, B.; Liao, K.; Zhou, Y.; Wen, T.; Quan, G.; Pan, X.; Wu, C., Application of glutathione depletion in cancer therapy: Enhanced ROS-based therapy, ferroptosis, and chemotherapy. *Biomaterials* **2021,** *277*, 121110.

61. Bansal, A.; Simon, M. C., Glutathione metabolism in cancer progression and treatment resistance. *J. Cell Biol.* **2018,** *217* (7), 2291-2298.

62. Quinn, J. F.; Whittaker, M. R.; Davis, T. P., Glutathione responsive polymers and their application in drug delivery systems. *Polym. Chem.* **2017,** *8* (1), 97-126.

63. Bajza, Á.; Kocsis, D.; Berezvai, O.; Laki, A. J.; Lukács, B.; Imre, T.; Iván, K.; Szabó, P.; Erdő, F., Verification of p-glycoprotein function at the dermal barrier in diffusion cells and dynamic "skin-on-a-chip" microfluidic device. *Pharmaceutics* **2020,** *12* (9), 804.

64. Nicol, N. H., Anatomy and physiology of the skin. *Dermatol. Nurs.* **2005,** *17* (1), 62.

65. Supe, S.; Takudage, P., Methods for evaluating penetration of drug into the skin: A review. *Skin Ress and Technol.* **2021,** *27* (3), 299-308.

66. Czekalla, C.; Schönborn, K. H.; Lademann, J.; Meinke, M. C., Noninvasive Determination of Epidermal and Stratum Corneum Thickness in vivo Using Two-Photon Microscopy and Optical Coherence Tomography: Impact of Body Area, Age, and Gender. *Skin Pharmacol. Physiol.* **2019,** *32* (3), 142-150.

67. Mojumdar, E. H.; Madsen, L. B.; Hansson, H.; Taavoniku, I.; Kristensen, K.; Persson, C.; Morén, A. K.; Mokso, R.; Schmidtchen, A.; Ruzgas, T.; Engblom, J., Probing Skin Barrier Recovery on Molecular Level Following Acute Wounds: An In Vivo/Ex Vivo Study on Pigs. *Biomedicines* **2021,** *9* (4).

68. Kitaoka, M.; Wakabayashi, R.; Kamiya, N.; Goto, M., Solid-in-oil nanodispersions for transdermal drug delivery systems. *Biotechnol. J.* **2016,** *11* (11), 1375-1385.

69. Schoellhammer, C. M.; Blankschtein, D.; Langer, R., Skin permeabilization for transdermal drug delivery: recent advances and future prospects. *Expert Opin. Drug Delivery* **2014,** *11* (3), 393-407.

70. Herman, A.; Herman, A. P., Essential oils and their constituents as skin penetration enhancer for transdermal drug delivery: a review. *J. Pharm. Pharmacol.* **2015,** *67* (4), 473-85.

71. Phatale, V.; Vaiphei, K. K.; Jha, S.; Patil, D.; Agrawal, M.; Alexander, A., Overcoming skin barriers through advanced transdermal drug delivery approaches. *J. Controlled Release* **2022,** *351*, 361-380.

72. Yewale, C.; Tandel, H.; Patel, A.; Misra, A., Chapter 5 - Polymers in Transdermal Drug Delivery. In *Applications of Polymers in Drug Delivery (Second Edition)*, Misra, A.; Shahiwala, A., Eds. Elsevier: 2021; pp 131-158.

73. Alexander, A.; Dwivedi, S.; Ajazuddin; Giri, T. K.; Saraf, S.; Saraf, S.; Tripathi, D. K., Approaches for breaking the barriers of drug permeation through transdermal drug delivery. *J. Controlled Release* **2012,** *164* (1), 26-40.

74. Magnusson, B. M.; Walters, K. A.; Roberts, M. S., Veterinary drug delivery: potential for skin penetration enhancement. *Advanced Drug Delivery Reviews* **2001,** *50* (3), 205-227.

75. Langer, R.; Peppas, N. A., Advances in biomaterials, drug delivery, and bionanotechnology. *AIChE J.* **2003,** *49* (12), 2990-3006.

76. Martinho, N.; Damg®¶, C.; Reis, C. P., Recent Advances in Drug Delivery Systems. *J. Biomater. and Nanobiotechnol.* **2011,** *Vol.02No.05*, 17.

77. Sung, Y. K.; Kim, S. W., Recent advances in polymeric drug delivery systems. *Biomater. Res.* **2020,** *24*, 12.

78. Liechty, W. B.; Kryscio, D. R.; Slaughter, B. V.; Peppas, N. A., Polymers for drug delivery systems. *Annu. Rev. Chem. Biomol. Eng.* **2010,** *1*, 149-73.

79. Jatzkewitz, H., [Incorporation of physiologically-active substances into a colloidal blood plasma substitute. I. Incorporation of mescaline peptide into polyvinylpyrrolidone]. *Hoppe Seylers Z. Physiol. Chem.* **1954,** *297* (3-6), 149-56.

80. Jansen, J. F.; de Brabander-van den Berg, E. M.; Meijer, E. W., Encapsulation of guest molecules into a dendritic box. *Science* **1994,** *266* (5188), 1226-9.

81. Jansen, J. F. G. A.; Meijer, E. W.; de Brabander-van den Berg, E. M. M., The Dendritic Box: Shape-Selective Liberation of Encapsulated Guests. *J. Am. Chem. Soc.* **1995,** *117* (15), 4417-4418.

82. Ringsdorf, H., Structure and properties of pharmacologically active polymers. *J. Polym. Sci., Part C: Polym. Symp.* **1975,** *51* (1), 135-153.

83. Tomalia, D. A.; Baker, H.; Dewald, J.; Hall, M.; Kallos, G.; Martin, S.; Roeck, J.; Ryder, J.; Smith, P., A New Class of Polymers: Starburst-Dendritic Macromolecules. *Polym. J.* **1985,** *17* (1), 117-132.

84. Frey, H.; Haag, R., Dendritic polyglycerol: a new versatile biocompatible material. *Rev. Mol. Biotechnol.* **2002,** *90* (3), 257-267.

85. Jain, N. K.; Gupta, U., Application of dendrimer–drug complexation in the enhancement of drug solubility and bioavailability. *Expert Opin. Drug Metab. Toxicol.* **2008,** *4* (8), 1035-1052.

86. Wooley, K. L.; Fréchet, J. M. J.; Hawker, C. J., Influence of shape on the reactivity and properties of dendritic, hyperbranched and linear aromatic polyesters. *Polymer* **1994,** *35* (21), 4489-4495.

87. Astruc, D.; Boisselier, E.; Ornelas, C., Dendrimers Designed for Functions: From Physical, Photophysical, and Supramolecular Properties to Applications in Sensing, Catalysis, Molecular Electronics, Photonics, and Nanomedicine. *Chem. Rev.* **2010,** *110* (4), 1857-1959.

88. Starpharma www.starpharma.com. (accessed July 2021).

89. McCarthy, T. D.; Karellas, P.; Henderson, S. A.; Giannis, M.; O'Keefe, D. F.; Heery, G.; Paull, J. R.; Matthews, B. R.; Holan, G., Dendrimers as drugs: discovery and preclinical and clinical development of dendrimer-based microbicides for HIV and STI prevention. *Mol. Pharm.* **2005,** *2* (4), 312-8.

90. Gong, E.; Matthews, B.; McCarthy, T.; Chu, J.; Holan, G.; Raff, J.; Sacks, S., Evaluation of dendrimer SPL7013, a lead microbicide candidate against herpes simplex viruses. *Antiviral Res.* **2005,** *68* (3), 139-46.

91. Tyssen, D.; Henderson, S. A.; Johnson, A.; Sterjovski, J.; Moore, K.; La, J.; Zanin, M.; Sonza, S.; Karellas, P.; Giannis, M. P.; Krippner, G.; Wesselingh, S.; McCarthy, T.; Gorry, P. R.; Ramsland, P. A.; Cone, R.; Paull, J. R.; Lewis, G. R.; Tachedjian, G., Structure activity relationship of dendrimer microbicides with dual action antiviral activity. *PLoS One* **2010,** *5* (8), e12309.

92. Price, C. F.; Tyssen, D.; Sonza, S.; Davie, A.; Evans, S.; Lewis, G. R.; Xia, S.; Spelman, T.; Hodsman, P.; Moench, T. R.; Humberstone, A.; Paull, J. R.; Tachedjian, G., SPL7013 Gel (VivaGel®) retains potent HIV-1 and HSV-2 inhibitory activity following vaginal administration in humans. *PLoS One* **2011,** *6* (9), e24095.

93. Dezzutti, C. S.; James, V. N.; Ramos, A.; Sullivan, S. T.; Siddig, A.; Bush, T. J.; Grohskopf, L. A.; Paxton, L.; Subbarao, S.; Hart, C. E., In vitro comparison of topical microbicides for prevention of human immunodeficiency virus type 1 transmission. *Antimicrob. Agents Chemother.* **2004,** *48* (10), 3834-44.

94. Patterson, C. M.; Balachander, S. B.; Grant, I.; Pop-Damkov, P.; Kelly, B.; McCoull, W.; Parker, J.; Giannis, M.; Hill, K. J.; Gibbons, F. D.; Hennessy, E. J.; Kemmitt, P.; Harmer, A. R.; Gales, S.; Purbrick, S.; Redmond, S.; Skinner, M.; Graham, L.; Secrist, J. P.; Schuller, A. G.; Wen, S.; Adam, A.; Reimer, C.; Cidado, J.; Wild, M.; Gangl, E.; Fawell, S. E.; Saeh, J.; Davies, B. R.; Owen, D. J.; Ashford, M. B., Design and optimisation of dendrimer-conjugated Bcl-2/xL inhibitor, AZD0466, with improved therapeutic index for cancer therapy. *Commun. Biol.* **2021,** *4* (1), 112.

95. Letchford, K.; Burt, H., A review of the formation and classification of amphiphilic block copolymer nanoparticulate structures: micelles, nanospheres, nanocapsules and polymersomes. *Eur. J Pharm. Biopharm.* **2007,** *65* (3), 259-69.

96. Xu, J.; Luo, S.; Shi, W.; Liu, S., Two-Stage Collapse of Unimolecular Micelles with Double Thermoresponsive Coronas. *Langmuir* **2006,** *22* (3), 989-997.

97. Gong, J.; Chen, M.; Zheng, Y.; Wang, S.; Wang, Y., Polymeric micelles drug delivery system in oncology. *J. Controlled Release* **2012,** *159* (3), 312-23.

98. Zeng, F.; Zimmerman, S. C., Dendrimers in Supramolecular Chemistry: From Molecular Recognition to Self-Assembly. *Chem. Rev.* **1997,** *97* (5), 1681-1712.

99.   Hawker, C. J.; Frechet, J. M. J., Preparation of polymers with controlled molecular architecture. A new convergent approach to dendritic macromolecules. *Journal of the American Chemical Society* **1990,** *112* (21), 7638-7647.

100.   Hawker, C. J.; Wooley, K. L.; Fréchet, J. M. J., Unimolecular micelles and globular amphiphiles: dendritic macromolecules as novel recyclable solubilization agents. *J. Am. Chem. Soc., Perkin Transactions 1* **1993,** (12), 1287-1297.

101.   Wallimann, P.; Seiler, P.; Diederich, F., Dendrophanes: Novel Steroid-Recognizing Dendritic Receptors. Preliminary Communication. *Helv. Chim. Acta* **1996,** *79* (3), 779-788.

102.   Smith, D. K.; Zingg, A.; Diederich, F., Dendroclefts: Optically Active Dendritic Receptors for the Selective Recognition and Chiroptical Sensing of Monosaccharide Guests. *Helv. Chim. Acta* **1999,** *82* (8), 1225-1241.

103.   Beezer, A. E.; King, A. S. H.; Martin, I. K.; Mitchel, J. C.; Twyman, L. J.; Wain, C. F., Dendrimers as potential drug carriers; encapsulation of acidic hydrophobes within water soluble PAMAM derivatives. *Tetrahedron* **2003,** *59* (22), 3873-3880.

104.   Macromol. Chem. Phys. 15/2007. *Macromol. Chem. Phys.* **2007,** *208* (15), 1607-1611.

105.   Voit, B. I.; Lederer, A., Hyperbranched and Highly Branched Polymer Architectures—Synthetic Strategies and Major Characterization Aspects. *Chem. Rev.* **2009,** *109* (11), 5924-5973.

106.   Zheng, Y.; Li, S.; Weng, Z.; Gao, C., Hyperbranched polymers: advances from synthesis to applications. *Chem. Soc. Rev.* **2015,** *44* (12), 4091-4130.

107.   Carlmark, A.; Hawker, C.; Hult, A.; Malkoch, M., New methodologies in the construction of dendritic materials. *Chemical Society Reviews* **2009,** *38* (2), 352-362.

108.   Abbina, S.; Vappala, S.; Kumar, P.; Siren, E. M. J.; La, C. C.; Abbasi, U.; Brooks, D. E.; Kizhakkedathu, J. N., Hyperbranched polyglycerols: recent advances in synthesis, biocompatibility and biomedical applications. *J. Mater. Chem. B* **2017,** *5* (47), 9249-9277.

109.   Svenson, S., The dendrimer paradox – high medical expectations but poor clinical translation. *Chem. Soc. Rev.* **2015,** *44* (12), 4131-4144.

110.   Hult, A.; Johansson, M.; Malmström, E., Hyperbranched Polymers. In *Branched Polymers II*, Roovers, J., Ed. Springer Berlin Heidelberg: Berlin, Heidelberg, 1999; pp 1-34.

111. Flory, P. J., Molecular Size Distribution in Three Dimensional Polymers. VI. Branched Polymers Containing A—R—Bf-1 Type Units. *J. Am. Chem. Soc.* **1952,** *74* (11), 2718-2723.

112. Bochenek, M.; Oleszko-Torbus, N.; Wałach, W.; Lipowska-Kur, D.; Dworak, A.; Utrata-Wesołek, A., Polyglycidol of Linear or Branched Architecture Immobilized on a Solid Support for Biomedical Applications. *Polym. Rev.* **2020,** *60* (4), 717-767.

113. Thomas, A.; Müller, S. S.; Frey, H., Beyond Poly(ethylene glycol): Linear Polyglycerol as a Multifunctional Polyether for Biomedical and Pharmaceutical Applications. *Biomacromolecules* **2014,** *15* (6), 1935-1954.

114. Wilms, D.; Stiriba, S.-E.; Frey, H., Hyperbranched Polyglycerols: From the Controlled Synthesis of Biocompatible Polyether Polyols to Multipurpose Applications. *Acc. Chem. Res.* **2010,** *43* (1), 129-141.

115. Herzberger, J.; Niederer, K.; Pohlit, H.; Seiwert, J.; Worm, M.; Wurm, F. R.; Frey, H., Polymerization of ethylene oxide, propylene oxide, and other alkylene oxides: synthesis, novel polymer architectures, and bioconjugation. *Chem. Rev.* **2016,** *116* (4), 2170-2243.

116. Tully, M.; Hauptstein, N.; Licha, K.; Meinel, L.; Lühmann, T.; Haag, R., Linear Polyglycerol for N-terminal-selective Modification of Interleukin-4. *J. Pharm. Sci.* **2022,** *111* (6), 1642-1651.

117. Tully, M.; Wedepohl, S.; Kutifa, D.; Weise, C.; Licha, K.; Schirner, M.; Haag, R., Prolonged activity of exenatide: Detailed comparison of Site-specific linear polyglycerol- and poly(ethylene glycol)-conjugates. *Eur. J. Pharm. Biopharm.* **2021,** *164*, 105-113.

118. Tully, M.; Dimde, M.; Weise, C.; Pouyan, P.; Licha, K.; Schirner, M.; Haag, R., Polyglycerol for Half-Life Extension of Proteins—Alternative to PEGylation? *Biomacromolecules* **2021,** *22* (4), 1406-1416.

119. Pouyan, P.; Nie, C.; Bhatia, S.; Wedepohl, S.; Achazi, K.; Osterrieder, N.; Haag, R., Inhibition of Herpes Simplex Virus Type 1 Attachment and Infection by Sulfated Polyglycerols with Different Architectures. *Biomacromolecules* **2021,** *22* (4), 1545-1554.

120. Nie, C.; Pouyan, P.; Lauster, D.; Trimpert, J.; Kerkhoff, Y.; Szekeres, G. P.; Wallert, M.; Block, S.; Sahoo, A. K.; Dernedde, J.; Pagel, K.; Kaufer, B. B.; Netz, R. R.; Ballauff, M.; Haag, R., Polysulfates Block SARS-CoV-2 Uptake through Electrostatic Interactions**. *Angewandte Chemie International Edition* **2021,** *60* (29), 15870-15878.

121. Gheybi, H.; Sattari, S.; Bodaghi, A.; Soleimani, K.; Dadkhah, A.; Adeli, M., 5 - Polyglycerols. In *Engineering of Biomaterials for Drug Delivery Systems*, Parambath, A., Ed. Woodhead Publishing: 2018; pp 103-171.

122. Knop, K.; Hoogenboom, R.; Fischer, D.; Schubert, U. S., Poly(ethylene glycol) in Drug Delivery: Pros and Cons as Well as Potential Alternatives. *Angew. Chem., Int. Ed.* **2010,** *49* (36), 6288-6308.

123. Wurm, F.; Dingels, C.; Frey, H.; Klok, H.-A., Squaric Acid Mediated Synthesis and Biological Activity of a Library of Linear and Hyperbranched Poly(Glycerol)–Protein Conjugates. *Biomacromolecules* **2012,** *13* (4), 1161-1171.

124. Fitton, A. O.; Hill, J.; Jane, D. E.; Millar, R., Synthesis of Simple Oxetanes Carrying Reactive 2-Substituents. *Synthesis* **1987,** *1987* (12), 1140-1142.

125. Taton, D.; Le Borgne, A.; Sepulchre, M.; Spassky, N., Synthesis of chiral and racemic functional polymers from glycidol and thioglycidol. *Macromol. Chem. Phys.* **1994,** *195* (1), 139-148.

126. Gervais, M.; Brocas, A.-L.; Cendejas, G.; Deffieux, A.; Carlotti, S., Synthesis of Linear High Molar Mass Glycidol-Based Polymers by Monomer-Activated Anionic Polymerization. *Macromolecules* **2010,** *43* (4), 1778-1784.

127. Walach, W.; Kowalczuk, A.; Trzebicka, B.; Dworak, A., Synthesis of High-Molar Mass Arborescent-Branched Polyglycidol via Sequential Grafting. *Macromol. Rapid Commun.* **2001,** *22* (15), 1272-1277.

128. Dworak, A.; Panchev, I.; Trzebicka, B.; Walach, W., Hydrophilic and amphiphilic copolymers of 2,3-epoxypropanol-1. *Macromol. Symp.* **2000,** *153* (1), 233-242.

129. Hans, M.; Keul, H.; Moeller, M., Chain transfer reactions limit the molecular weight of polyglycidol prepared via alkali metal based initiating systems. *Polymer* **2009,** *50* (5), 1103-1108.

130. Hans, M.; Gasteier, P.; Keul, H.; Moeller, M., Ring-Opening Polymerization of ε-Caprolactone by Means of Mono- and Multifunctional Initiators: Comparison of Chemical and Enzymatic Catalysis. *Macromolecules* **2006,** *39* (9), 3184-3193.

131. Erberich, M.; Keul, H.; Möller, M., Polyglycidols with Two Orthogonal Protective Groups: Preparation, Selective Deprotection, and Functionalization. *Macromolecules* **2007,** *40* (9), 3070-3079.

132. Thomas, A.; Niederer, K.; Wurm, F.; Frey, H., Combining oxyanionic polymerization and click-chemistry: a general strategy for the synthesis of polyether polyol macromonomers. *Polym. Chem.* **2014,** *5* (3), 899-909.

133. Gunkel, G.; Weinhart, M.; Becherer, T.; Haag, R.; Huck, W. T. S., Effect of Polymer Brush Architecture on Antibiofouling Properties. *Biomacromolecules* **2011,** *12* (11), 4169-4172.

134. Toy, A. A.; Reinicke, S.; Müller, A. H. E.; Schmalz, H., One-Pot Synthesis of Polyglycidol-Containing Block Copolymers with Alkyllithium Initiators Using the Phosphazene Base t-BuP4. *Macromolecules* **2007,** *40* (15), 5241-5244.

135. Dimitrov, I.; Tsvetanov, C., 4.21—High-Molecular-Weight Poly (ethylene oxide). *Polymer Science: A Comprehensive Reference* **2012**, 551-569.

136. Brocas, A.-L.; Mantzaridis, C.; Tunc, D.; Carlotti, S., Polyether synthesis: From activated or metal-free anionic ring-opening polymerization of epoxides to functionalization. *Progress in Polymer Science* **2013,** *38* (6), 845-873.

137. Sunder, A.; Hanselmann, R.; Frey, H.; Mülhaupt, R., Controlled Synthesis of Hyperbranched Polyglycerols by Ring-Opening Multibranching Polymerization. *Macromolecules* **1999,** *32* (13), 4240-4246.

138. Dworak, A.; Walach, W.; Trzebicka, B., Cationic polymerization of glycidol. Polymer structure and polymerization mechanism. *Macromol. Chem. Phys.* **1995,** *196* (6), 1963-1970.

139. Tokar, R.; Kubisa, P.; Penczek, S.; Dworak, A., Cationic polymerization of glycidol: coexistence of the activated monomer and active chain end mechanism. *Macromolecules* **1994,** *27* (2), 320-322.

140. Mohammadifar, E.; Bodaghi, A.; Dadkhahtehrani, A.; Nemati Kharat, A.; Adeli, M.; Haag, R., Green Synthesis of Hyperbranched Polyglycerol at Room Temperature. *ACS Macro Lett.* **2017,** *6* (1), 35-40.

141. Kim, S. E.; Yang, H. J.; Choi, S.; Hwang, E.; Kim, M.; Paik, H.-J.; Jeong, J.-E.; Park, Y. I.; Kim, J. C.; Kim, B.-S.; Lee, S.-H., A recyclable metal-free catalytic system for the cationic ring-opening polymerization of glycidol under ambient conditions. *Green Chem.* **2022,** *24* (1), 251-258.

142. Haag, R.; Sunder, A.; Stumbé, J.-F., An Approach to Glycerol Dendrimers and Pseudo-Dendritic Polyglycerols. *J. Am. Chem. Soc.* **2000,** *122* (12), 2954-2955.

143. Schmitt, V.; Rodríguez-Rodríguez, C.; Hamilton, J. L.; Shenoi, R. A.; Schaffer, P.; Sossi, V.; Kizhakkedathu, J. N.; Saatchi, K.; Häfeli, U. O., Quantitative SPECT imaging and biodistribution point to molecular weight independent tumor uptake for some long-circulating polymer nanocarriers. *RSC Adv.* **2018,** *8* (10), 5586-5595.

144.   Kautz, H.; Sunder, A.; Frey, H., Control of the molecular weight of hyperbranched polyglycerols. *Macromol. Symp.* **2001,** *163* (1), 67-74.

145.   Wallert, M.; Plaschke, J.; Dimde, M.; Ahmadi, V.; Block, S.; Haag, R., Automated Solvent-Free Polymerization of Hyperbranched Polyglycerol with Tailored Molecular Weight by Online Torque Detection. *Macromol. Mater. Eng.* **2021,** *306* (7), 2000688.

146.   Wilms, D.; Wurm, F.; Nieberle, J.; Böhm, P.; Kemmer-Jonas, U.; Frey, H., Hyperbranched Polyglycerols with Elevated Molecular Weights: A Facile Two-Step Synthesis Protocol Based on Polyglycerol Macroinitiators. *Macromolecules* **2009,** *42* (9), 3230-3236.

147.   Moore, E.; Zill, A. T.; Anderson, C. A.; Jochem, A. R.; Zimmerman, S. C.; Bonder, C. S.; Kraus, T.; Thissen, H.; Voelcker, N. H., Synthesis and Conjugation of Alkyne-Functional Hyperbranched Polyglycerols. *Macromol. Chem. Phys.* **2016,** *217* (20), 2252-2261.

148.   Kainthan, R. K.; Muliawan, E. B.; Hatzikiriakos, S. G.; Brooks, D. E., Synthesis, Characterization, and Viscoelastic Properties of High Molecular Weight Hyperbranched Polyglycerols. *Macromolecules* **2006,** *39* (22), 7708-7717.

149.   ul-haq, M. I.; Shenoi, R. A.; Brooks, D. E.; Kizhakkedathu, J. N., Solvent-assisted anionic ring opening polymerization of glycidol: Toward medium and high molecular weight hyperbranched polyglycerols. *J. Polym. Sci., Part A: Polym. Chem.* **2013,** *51* (12), 2614-2621.

150.   Anilkumar, P.; Lawson, T. B.; Abbina, S.; Mäkelä, J. T. A.; Sabatelle, R. C.; Takeuchi, L. E.; Snyder, B. D.; Grinstaff, M. W.; Kizhakkedathu, J. N., Mega macromolecules as single molecule lubricants for hard and soft surfaces. *Nat. Commun.* **2020,** *11* (1), 2139.

151.   Hasirci, V.; Yilgor, P.; Endogan, T.; Eke, G.; Hasirci, N., 1.121 - Polymer Fundamentals: Polymer Synthesis. In *Comprehensive Biomaterials*, Ducheyne, P., Ed. Elsevier: Oxford, 2011; pp 349-371.

152.   Koltzenburg, S.; Maskos, M.; Nuyken, O., *Polymer Chemistry*. Springer: 2017.

153.   Friedrich, K.; Zaikov, G. E.; Haghi, A. K., *Materials Chemistry: A Multidisciplinary Approach to Innovative Methods*. Apple Academic Press: 2016.

154.   Ulery, B. D.; Nair, L. S.; Laurencin, C. T., Biomedical applications of biodegradable polymers. J. Polym. Sci., Part B: Polym. Phys. **2011,** *49* (12), 832-864.

155.   Zhang, Z.; Ortiz, O.; Goyal, R.; Kohn, J., Chapter 23 - Biodegradable Polymers. In *Principles of Tissue Engineering (Fourth Edition)*, Lanza, R.; Langer, R.; Vacanti, J., Eds. Academic Press: Boston, 2014; pp 441-473.

156. Elmowafy, E. M.; Tiboni, M.; Soliman, M. E., Biocompatibility, biodegradation and biomedical applications of poly(lactic acid)/poly(lactic-co-glycolic acid) micro and nanoparticles. *J. Pharm. Invest.* **2019,** *49* (4), 347-380.

157. Mohamed, R.; Yusoh, K., A Review on the Recent Research of Polycaprolactone (PCL). *Adv. Mater. Res.* **2015,** *1134*, 249-255.

158. Budak, K.; Sogut, O.; Aydemir Sezer, U., A review on synthesis and biomedical applications of polyglycolic acid. *J. Polym. Res.* **2020,** *27* (8), 208.

159. Sisson, A. L.; Ekinci, D.; Lendlein, A., The contemporary role of ε-caprolactone chemistry to create advanced polymer architectures. *Polymer* **2013,** *54* (17), 4333-4350.

160. Kainthan, R. K.; Brooks, D. E., In vivo biological evaluation of high molecular weight hyperbranched polyglycerols. *Biomaterials* **2007,** *28* (32), 4779-87.

161. Dingels, C.; Müller, S. S.; Steinbach, T.; Tonhauser, C.; Frey, H., Universal Concept for the Implementation of a Single Cleavable Unit at Tunable Position in Functional Poly(ethylene glycol)s. *Biomacromolecules* **2013,** *14* (2), 448-459.

162. Tonhauser, C.; Schüll, C.; Dingels, C.; Frey, H., Branched Acid-Degradable, Biocompatible Polyether Copolymers via Anionic Ring-Opening Polymerization Using an Epoxide Inimer. *ACS Macro Lett.* **2012,** *1* (9), 1094-1097.

163. Shenoi, R. A.; Narayanannair, J. K.; Hamilton, J. L.; Lai, B. F. L.; Horte, S.; Kainthan, R. K.; Varghese, J. P.; Rajeev, K. G.; Manoharan, M.; Kizhakkedathu, J. N., Branched Multifunctional Polyether Polyketals: Variation of Ketal Group Structure Enables Unprecedented Control over Polymer Degradation in Solution and within Cells. *J. Am. Chem. Soc.* **2012,** *134* (36), 14945-14957.

164. Mohammadifar, E.; Zabihi, F.; Tu, Z.; Hedtrich, S.; Nemati Kharat, A.; Adeli, M.; Haag, R., One-pot and gram-scale synthesis of biodegradable polyglycerols under ambient conditions: nanocarriers for intradermal drug delivery. *Polym. Chem.* **2017,** *8* (47), 7375-7383.

165. Zabihi, F.; Graff, P.; Schumacher, F.; Kleuser, B.; Hedtrich, S.; Haag, R., Synthesis of poly(lactide-co-glycerol) as a biodegradable and biocompatible polymer with high loading capacity for dermal drug delivery. *Nanoscale* **2018,** *10* (35), 16848-16856.

166. Sun, H.; Meng, F.; Cheng, R.; Deng, C.; Zhong, Z., Reduction-sensitive degradable micellar nanoparticles as smart and intuitive delivery systems for cancer chemotherapy. *Expert Opin. Drug Delivery* **2013,** *10* (8), 1109-1122.

167. Chan, N.; An, S. Y.; Oh, J. K., Dual location disulfide degradable interlayer-crosslinked micelles with extended sheddable coronas exhibiting enhanced colloidal stability and rapid release. *Polym. Chem.* **2014,** *5* (5), 1637-1649.

168. Yan, Y.; Wang, Y.; Heath, J. K.; Nice, E. C.; Caruso, F., Cellular Association and Cargo Release of Redox-Responsive Polymer Capsules Mediated by Exofacial Thiols. *Adv. Mater.* **2011,** *23* (34), 3916-3921.

169. Ou, M.; Xu, R.; Kim, S. H.; Bull, D. A.; Kim, S. W., A family of bioreducible poly(disulfide amine)s for gene delivery. *Biomaterials* **2009,** *30* (29), 5804-14.

170. Pettit, G. R.; Pettit, G. R., III, Perpetration of polysulfide rubber. *J. Chem. Educ.* **1978,** *55* (7), 472.

171. Rosenthal, E. Q.; Puskas, J. E.; Wesdemiotis, C., Green Polymer Chemistry: Living Dithiol Polymerization via Cyclic Intermediates. *Biomacromolecules* **2012,** *13* (1), 154-164.

172. Son, S.; Shin, E.; Kim, B.-S., Redox-Degradable Biocompatible Hyperbranched Polyglycerols: Synthesis, Copolymerization Kinetics, Degradation, and Biocompatibility. *Macromolecules* **2015,** *48* (3), 600-609.

173. Shenoi, R. A.; Chafeeva, I.; Lai, B. F. L.; Horte, S.; Kizhakkedathu, J. N., Bioreducible hyperbranched polyglycerols with disulfide linkages: Synthesis and biocompatibility evaluation. *J J. Polym. Sci., Part A: Polym. Chem.* **2015,** *53* (18), 2104-2115.

174. Dernedde, J.; Rausch, A.; Weinhart, M.; Enders, S.; Tauber, R.; Licha, K.; Schirner, M.; Zügel, U.; von Bonin, A.; Haag, R., Dendritic polyglycerol sulfates as multivalent inhibitors of inflammation. *Proc. Natl. Acad. Sci.* **2010,** *107* (46), 19679-19684.

175. Weinhart, M.; Gröger, D.; Enders, S.; Riese, S. B.; Dernedde, J.; Kainthan, R. K.; Brooks, D. E.; Haag, R., The Role of Dimension in Multivalent Binding Events: Structure–Activity Relationship of Dendritic Polyglycerol Sulfate Binding to L-Selectin in Correlation with Size and Surface Charge Density. *Macromol. Biosci.* **2011,** *11* (8), 1088-1098.

176. Weinhart, M.; Gröger, D.; Enders, S.; Dernedde, J.; Haag, R., Synthesis of Dendritic Polyglycerol Anions and Their Efficiency Toward L-Selectin Inhibition. *Biomacromolecules* **2011,** *12* (7), 2502-2511.

177. Ferraro, M.; Silberreis, K.; Mohammadifar, E.; Neumann, F.; Dernedde, J.; Haag, R., Biodegradable Polyglycerol Sulfates Exhibit Promising Features for Anti-inflammatory Applications. *Biomacromolecules* **2018,** *19* (12), 4524-4533.

178. Läubli, H.; Borsig, L., Selectins promote tumor metastasis. *Semin. Cancer Biol.* **2010,** *20* (3), 169-77.

179. Chung, Y. I.; Kim, J. C.; Kim, Y. H.; Tae, G.; Lee, S. Y.; Kim, K.; Kwon, I. C., The effect of surface functionalization of PLGA nanoparticles by heparin- or chitosan-conjugated Pluronic on tumor targeting. *J. Controlled Release* **2010,** *143* (3), 374-82.

180. Zhong, Y.; Dimde, M.; Stöbener, D.; Meng, F.; Deng, C.; Zhong, Z.; Haag, R., Micelles with Sheddable Dendritic Polyglycerol Sulfate Shells Show Extraordinary Tumor Targetability and Chemotherapy in Vivo. *ACS Appl. Mater. Interfaces* **2016,** *8* (41), 27530-27538.

181. Cherri, M.; Ferraro, M.; Mohammadifar, E.; Quaas, E.; Achazi, K.; Ludwig, K.; Grötzinger, C.; Schirner, M.; Haag, R., Biodegradable Dendritic Polyglycerol Sulfate for the Delivery and Tumor Accumulation of Cytostatic Anticancer Drugs. *ACS Biomater. Sci. Eng.* **2021,** *7* (6), 2569-2579.

182. Cherri, M.; Romero, J. F.; Steiner, L.; Dimde, M.; Koeppe, H.; Paulus, B.; Mohammadifar, E.; Haag, R., Power of the Disulfide Bond: An Ideal Random Copolymerization of Biodegradable Redox-Responsive Hyperbranched Polyglycerols. *Biomacromolecules* **2024,** *25* (1), 119-133.

183. Zabihi, F.; Cherri, M.; Guo, X.; Rancan, F.; Schumacher, F.; Mohammadifar, E.; Kleuser, B.; Bäumer, W.; Schirner, M.; Vogt, A.; Haag, R., Topical Delivery of Tofacitinib in Dermatology: The Promise of a Novel Therapeutic Class Using Biodegradable Dendritic Polyglycerol Sulfates. *Pharmaceuticals* **2024,** *17* (1), 77.

7 Appendix

7.1 List of abbreviations

AC	active chain
AGE	allyl glycidyl ether
AM	activated monomer
API	Active pharmaceutical ingredient
AROP	anionic ring opening polymerization
CAM	cell-adhesion molecule
CMC	critical micelle concentration
Đ	polydispersity index
DB	degree of branching
DDS	drug delivery system
DFO	desferrioxamine
DOX	Doxorubicin
dPG	dendritic polyglycerol
dPGS	dendritic polyglycerol sulfate
DP_n	degree of polymerization
EEGE	ethoxyethyl glycidyl ether
EPR	enhanced permeation and retention
GSH	glutathione
GSSG	glutathione disulfide
hPG	hyperbranched polyglycerol
IC_{50}	half maximal inhibitory concentration
Li^+/t-BuP$_4$	BuLi/phosphazene base
LPG	linear polyglycerol
MeOK	potassium methoxide
NCL	Nanotechnology Characterization Laboratory
PAMAM	poly(amidoamine)
PCL	polycaprolactone
PDC	polymeric drug conjugate
PEEGE	poly(ethoxyethyl glycidyl ether)
PEI	polyethyleneimine
PG	polyglycerol
PGA	polyglycolide

PLA	polylactide
PLL	poly-L-lysine
PO	propylene oxide
PPOK	potassium 3-phenyl propanolate
RES	reticuloendothelial system
RES	reticuloendothelial system
ROMBP	anionic ring opening multibranching polymerization
SAN	poly(styrene-co-acrylonitrile)
SBR	poly(styrene-co-butadiene)
SBS	poly(styrene-block-butadiene-block-styrene)
SC	stratum corneum
t-BuOK	potassium tert-butoxide
tBGE	tert-butyl glycidyl ether
TDDS	transdermal drug delivery system
T_g	glass transition temperature
T_m	melting temperature
TMP	tris(hydroxymethyl)propane
VDW	Van der Waals

7.2 List of publications and conference contributions

Publications

[1] **M. Cherri,** J. F. Romero, L. Steiner, M. Dimde, H. Koeppe, B. Paulus, E. Mohammadifar, R. Haag, *Biomacromolecules* **2024**, 25(1), 119-133. Power of the Disulfide Bond: An Ideal Random Copolymerization of Biodegradable Redox-Responsive Hyperbranched polyglycerols.

[2] F. Zabihi, **M. Cherri**, X.Guo, F. Rancan, F. Schumacher, E. Mohammadifar, B. Kleuser, W. Bäumer, M. Schirner, A. Vogt, R. Haag, *Pharmaceuticals* **2024**, 17(1), 77. Topical Delivery of Tofacitinib in Dermatology: the Promise of a Novel Therapeutic Class Using Biodegradable Dendritic Polyglycerol Sulfates.

[3] **M. Cherri**, M. Ferraro, E. Mohammadifar, E. Quaas, K. Achazi, K. Ludwig, C. Grötzinger, M. Schirner, R. Haag, *ACS Biomater. Sci. Eng.* **2021**, 7(6), 2569–2579. Biodegradable Dendritic Polyglycerol Sulfate for the Delivery and Tumor Accumulation of Cytostatic Anticancer Drugs.

[4] **M. Cherri**, P. Stergiou, Z. Ahmadian, T. L. Povolotsky, B. Thongrom, X. Fan, E. Mohammadifar, R. Haag **(submitted).** Redox-Responsive Hydrogels Loaded with an Antibacterial Peptide as Controlled Drug Delivery for Infectious Wound Healing.

[5] M. Witt, **M. Cherri**, M. Ferraro, C. Yapto, K. Vogel, L. Schmidt, R. Haag, K. Danker, H. Dommisch, *ACS Appl. Bio Mater.* **2023**, 6(6), 2145–2157. Anti-inflammatory IL-8 Regulation via an Advanced Drug Delivery System at the Oral Mucosa.

[6] D. Braatz, **M. Cherri**, M. Tully, M. Dimde, G. Ma, E. Mohammadifar, F. Reisbeck, V. Ahmadi, M. Schirner, R. Haag, *Angew. Chem. Int. Ed. Engl.* **2022**, 61(49). Chemical Approaches to Synthetic Drug Delivery Systems for Systemic Applications.

[7] P. Pouyan, **M. Cherri**, R. Haag, *Polymers* **2022**, 14(13), 2684. Polyglycerols as Multi-Functional Platforms: Synthesis and Biomedical Applications.

[8] J. F. Romero, S. Herziger, **M. Cherri**, M. Dimde, M. Achazi, E. Mohammadifar, R. Haag, *Pharmaceutics* **2023**, 15(10), 2452. Dendritic Glycerol-Cholesterol Amphiphiles as Drug Delivery Systems: A Comparison between Monomeric and Polymeric Structures.

[9] F. Reisbeck, A. Ozimkovski, **M. Cherri**, M. Dimde, E. Quaas, E. Mohammadifar, K. Achazi, R. Haag, *Polymers* **2021**, 13(6), 982. Gram Scale Synthesis of Dual-Responsive Dendritic Polyglycerol Sulfate as Drug Delivery System.

[10] O. Bawadkji, **M. Cherri**, A. Schäfer, S. Herziger, P. Nickl, K. Achazi, I. S. Donskyi, M. Adeli, R. Haag, *Adv. Mater. Interfaces* **2022**, 2201245. One-pot Covalent Functionalization of Two-Dimensional Black Phosphorus by Anionic Ring Opening Polymerization.

Conference Talks

[1] **M. Cherri,** R. Haag, Biodegradable Polyglycerol Sulfates: An Intrinsic Targeted Delivery System for Tumor & Inflammatory Therapy. *14th International Symposium on Frontiers in Biomedical Polymers* **2023**, Portsmouth, New Hampshire, USA.

Poster Presentations

[1] **M. Cherri**, E. Mohammadifar, R. Haag, Biodegradable Dendritic Polyglycerol Sulfate for the Delivery and Tumor Accumulation of Cytostatic Anticancer Drugs. *12th International Symposium on Polymer Therapeutics* **2022**, Valencia, Spain.

[2] **M. Cherri,** E. Mohammadifar, R. Haag, Biodegradable Dendritic Polyglycerol Sulfate for the Delivery and Tumor Accumulation of Cytostatic Anticancer Drugs. *140th BASF International Summer Course* **2023**, Ludwigshafen, Germany.

7.3   Curriculum Vitae

For reasons of data protection, the curriculum vitae is not included in the online version.